

UNIVERSITA' DELLA CALABRIA

Dipartimento di Ingegneria per l'Ambiente e il Territorio e Ingegneria Chimica

Scuola di Dottorato

Life Science

Indirizzo

Ambiente, Salute e Processi Eco-sostenibili

Con il contributo di

Commissione Europea, Fondo Sociale Europeo e Regione Calabria

CICLO

XXVII

MODEL-BASED OPTIMIZATION OF RADIAL FLOW PACKED-BED BIOREACTORS FOR TISSUE ENGINEERING

Settore Scientifico Disciplinare ING-IND/34

Direttore: Ch.mo Prof. Marcello Canonaco

Supervisore: Ch.mo Prof. Gerardo Catapano

Ch.mo Prof. Patrick Segers

Dottorando: Dott. Danilo Donato

La presente tesi è cofinanziata con il sostegno della Commissione Europea, Fondo Sociale Europeo e della Regione Calabria. L'autore è il solo responsabile di questa tesi e la Commissione Europea e la Regione Calabria declinano ogni responsabilità sull'uso che potrà essere fatto delle informazioni in essa contenute

“Da bambino volevo guarire i ciliegi

quando rossi di frutti li credevo feriti

la salute per me li aveva lasciati

coi fiori di neve che avevan perduti.

Un sogno, fu un sogno ma non durò poco

per questo giurai che avrei fatto il dottore

e non per un dio ma nemmeno per gioco:

perché i ciliegi tornassero in fiore”

F. De Andrè, “Un medico”, 1970

Dedicated to my family, my “club”

and my “old” friends

Summary

Sommario

Il danneggiamento severo o la perdita delle funzioni di un organo o di un tessuto comporta ogni anno costi socio-economici elevatissimi e porta, in buona parte dei casi, alla morte del paziente. Gli approcci che si utilizzano odiernamente per ripristinare le funzionalità di organi o tessuti consistono nella sostituzione degli stessi con tessuti prelevati da donatori (allogenici) o di origine animale (xenogenici), o ricavati dal paziente stesso (autologhi). L'utilizzo di sostitutivi di origine allogenica o xenogenica è fortemente limitato dalla mancanza di donatori e dalla difficile integrazione dell'impianto nel corpo del paziente. D'altra parte, la sostituzione dei tessuti danneggiati con impianti autologhi, sebbene eviti il rischio di rigetto da parte del paziente, comporta la morbilità del sito donatore e l'insorgenza di dolori cronici, che ne permettono l'utilizzo solo per la cura di piccoli difetti. L'ingegneria dei tessuti si propone di superare le limitazioni comportate dalle tecniche comunemente utilizzate, realizzando sostituti bioingegnerizzati che riproducano le funzioni del tessuto di origine, ne sostituiscano le funzioni e che si integrino con l'organismo ospite. Secondo tale approccio, i sostituti bioingegnerizzati sono realizzati seminando cellule autologhe isolate su supporti porosi tridimensionali, detti scaffold, e guidando la proliferazione e il differenziamento cellulare in bioreattori, che riproducono l'ambiente pericellulare fisiologico per lo sviluppo del tessuto. La maggiore problematica relativa alla realizzazione di sostituti bioingegnerizzati di rilevanza clinica è il difficile apporto di quantitativi fisiologici di ossigeno e nutrienti verso, e la rimozione degli scarti metabolici da, la regione più interna dei costrutti cellulari. In particolare, è generalmente riconosciuto che il consumo severo di ossigeno da parte delle cellule rappresenta la principale limitazione per la sopravvivenza cellulare durante lo sviluppo del tessuto. Colture statiche nelle quali ossigeno e nutrienti sono forniti alle cellule attraverso un meccanismo di trasporto puramente diffusivo si sono dimostrate adatte per garantire la sopravvivenza delle cellule unicamente in costrutti di dimensioni ridotte. Per superare le limitazioni connesse al trasporto diffusivo, è stato proposto l'utilizzo di bioreattori dinamici in cui un meccanismo di trasporto convettivo è sovrapposto alla diffusione pura per consentire il trasporto dei soluti anche nelle zone

più interne dei costrutti. Tuttavia, nonostante alcuni miglioramenti rispetto alle colture statiche, i bioreattori dinamici proposti ad oggi, come gli spinner flask, i rotating wall vessels e i bioreattori a letto impaccato a perfusione assiale diretta, risultano subottimali per la realizzazione di costrutti bioingegnerizzati di interesse clinico. Recentemente, è stato proposto di perfondere radialmente costrutti anulari tridimensionali attraverso l'utilizzo di bioreattori a letto impaccato a perfusione radiale (rPBB) per superare le limitazioni dei bioreattori dinamici sopracitati, oltre che delle colture statiche, soprattutto per bioingegnerizzazione del tessuto osseo ed epatico. Infatti, poiché la perfusione del terreno di coltura avviene radialmente verso le cellule, rispetto ai bioreattori a perfusione assiale, le distanze caratteristiche per il trasporto dei soluti risultano inferiori, mentre risultano disponibili superfici di passaggio maggiori, che permettono di sviluppare i tessuti utilizzando basse velocità superficiali, e conseguentemente differenze di pressione inferiori, e a bassi gradienti di concentrazione dei soluti in direzione della perfusione. Tuttavia, a dispetto dei vantaggi offerti dal loro utilizzo, la progettazione di bioreattori a perfusione radiale risulta più complessa rispetto a quella di bioreattori a perfusione assiale. Infatti, i rPBB necessitano di due camere (una cavità interna e uno spazio anulare periferico) adibite rispettivamente alla distribuzione e alla raccolta del terreno di coltura che fluisce attraverso lo spessore del costrutto, la fluidodinamica dei quali può influenzare significativamente la distribuzione dei flussi radiali assialmente al costrutto. Inoltre, la geometria del costrutto stesso e la direzione nella quale il terreno di coltura viene perfuso (dalla cavità interna verso la zona periferica o viceversa) possono comportare differenze importanti per il trasporto dei soluti verso, e dalle, cellule. L'entità delle portate di perfusione deve infine essere ottimizzata in modo da garantire l'apporto controllato e sufficiente di ossigeno e nutrienti senza comportare sforzi di taglio elevati per le cellule, onde evitare il loro danneggiamento o trasporto fuori dal costrutto.

Modelli matematici di trasporto in rPBB possono aiutare a ottimizzarne la progettazione per una data applicazione in modo da garantire l'apporto adeguato di ossigeno e nutrienti verso, e la

rimozione degli scarti metabolici da, costrutti tridimensionali di interesse clinico. Tuttavia, una analisi sistematica dell'influenza di tutti i parametri adimensionali geometrici e operativi sul comportamento del bioreattore, allo scopo di ottimizzarne la progettazione in modo da garantire un trasporto dei soluti controllato, non è riportato in letteratura. Ciò limita lo sfruttamento delle peculiarità dei rPBB nello sviluppo di sostitutivi bioingegnerizzati per trapianto.

Nella presente tesi, viene proposta una cornice di riferimento basata su modelli matematici per ottimizzare la progettazione di rPBB in modo da garantire le condizioni ambientali favorevoli alle cellule per la realizzazione di sostituti per trapianto tridimensionali bioingegnerizzati di rilevanza clinica. In particolare, l'attenzione è focalizzata sul trasporto di ossigeno, poiché il suo ruolo limitante rispetto a quello degli altri soluti è generalmente riconosciuto. Allo scopo di raggiungere l'obiettivo proposto, il lavoro è stato suddiviso in tre fasi successive, di seguito riassunte:

1. E' stata dapprima sviluppata una cornice di riferimento basata su un modello monodimensionale di trasporto a stato stazionario di ossigeno, il cui consumo è stato descritto attraverso una cinetica di Michaelis-Menten, con l'obiettivo di ottimizzare la geometria del costrutto e la direzione e l'entità della velocità di perfusione radiale del terreno di coltura attraverso il comparto cellulare per la realizzazione di costrutti bioingegnerizzati di rilevanza clinica, ipotizzando uniforme distribuzione dei flussi radiali assialmente al costrutto. L'analisi dimensionale è stata utilizzata per definire i gruppi adimensionali che determinano il comportamento del bioreattore in condizioni tipiche dell'ingegneria dei tessuti. In particolare, secondo tale modello, il comportamento del bioreattore è stato mostrato dipendere dai seguenti gruppi adimensionali: il parametro relativo alla distribuzione del flusso, γ; la permeabilità di Darcy del costrutto adimensionale, kL/R^3; il rapporto tra il raggio interno e lo spessore del costrutto, R/δ_C; il numero di Peclet radiale massimo, $Pe_{rad,max}$; il modulo di Thiele, ϕ_C; il parametro di saturazione, β. L'efficienza del rilascio di ossigeno verso le cellule è stato espresso in termini della frazione di volume di costrutto non ipossico. Le predizioni del

modello suggeriscono che la perfusione dalla cavità interna del costrutto verso la zona periferica di costrutti anulari tridimensionali caratterizzati da un alto R/δ_C a portate più elevate (ovvero a $Pe_{rad,max}$ maggiori) favorisce l'apporto adeguato di ossigeno alle cellule rispetto alla coltura di cellule in condizioni statiche o in bioreattori a perfusione assiale.

2. E' stato sviluppato un criterio per ottimizzare la progettazione di rPBB in modo da ottenere una distribuzione uniforme dei flussi radiali lungo la direzione assiale del costrutto, basato su un modello bidimensionale di trasporto di quantità di moto in tutti i compartimenti del bioreattore (cavità cilindrica interna, costrutto, zona anulare periferica), assumendo che il terreno di coltura fosse alimentato dalla cavità interna verso l'anulo periferico, in accordo a quanto osservato nel caso del modello di trasporto monodimensionale. In particolare, il trasporto di quantitò di moto nelle camere vuote è stato descritto con l'equazione di Navier-Stokes, mentre l'equazione di Darcy-Brinkman è stata utilizzata per descrivere il trasporto di quantità di moto nel costrutto poroso. Dall'analisi dimensionale è emerso che la distribuzione dei flussi radiali è influenzata dai seguenti gruppi adimensionali: il numero di Reynolds ridotto, Re_{in}; il fattore di forma del costrutto, L/R; il rapporto tra il raggio interno e lo spessore del costrutto, R/δ_C e quello tra il raggio interno del costrutto e lo spessore della zona periferica, R/δ_E; il rapporto di permeabilità del costrutto rispetto alla cavità interna, k/R^2. L'influenza dei gruppi adimensionali R/δ_C e R/δ_E è stata inglobata in un unico gruppo adimensionale, ovvero il rapporto tra le sezioni trasversali di passaggio della cavità interna e dell'anulo periferico, ξ, come suggerito da risultati di letteratura. Il criterio di progetto, denominato CORFU (Criterion Of Radial Flux Uniformity), dipende da tutti i gruppi adimensionali derivati dall'analisi dimensionale. Secondo tale criterio, la ditribuzione uniforme dei flussi radiali può essere ottenuta scegliendo i parametri geometrici e operativi in modo da rendere la differenza di pressione assiale totale nelle camere vuote entro ±10% della differenza di pressione radiale totale attraverso il costrutto.

3. Il modello di trasporto di quantità di moto è stato integrato con le equazioni di trasporto di massa per valutare l'effettiva influenza della distribuzione dei flussi radiali sul trasporto di ossigeno verso il comparto cellulare in modo da progettare rPBB per un dato obiettivo terapeutico. Il consumo di ossigeno è stato descritto attraverso una cinetica michaeliana. Il coefficiente di trasferimento di materia che descrive il trasporto esterno di materia dal seno della fase fluida nei pori del costrutto verso la superficie cellulare è stato stimato per un letto composto da anelli di Raschig equivalente, dal punto di vista del trasporto, a uno scaffold poroso come quelli tipicamente adottati per ingegneria dei tessuti. L'analisi dimensionale ha mostrato che il comportamento del bioreattore, espresso in termini di NHy-FCV, dipende dai seguenti gruppi adimensionali, oltre a quelli elencati in precedenza: il numero di Peclet radiale massimo, $Pe_{rad,max}$; il rapporto tra la diffusività dell'ossigeno nel costrutto e nella cavità interna e quello tra la diffusività dell'ossigeno nel costrutto e nella zona periferica, D_C/D_H e D_C/D_E, rispettivamente; il numero di Sherwood, Sh; il parametro di saturazione, β; il modulo di Thiele, ϕ_C; il rapporto tra il quadrato del modulo di Thiele di superficie e il numero di Sherwood, ϕ_s^2/Sh_p. L'effetto dei gruppi adimensionali sul comportamento del bioreattore è stato studiato a condizioni tipiche dell'ingegneria dei tessuti. Le predizioni del modello suggeriscono come ottimizzare la progettazione del bioreattore in modo da garantire un apporto fisiologico controllato di ossigeno alle cellule per differenti applicazioni. La distribuzione dei flussi radiali relativi al terreno di coltura sui profili di concentrazione di ossigeno è stata mostrata essere significativa laddove il consumo di ossigeno non è compensato adeguatamente dal suo trasporto verso le cellule. Elevati valori di Re_{in} influenzano la distribuzione spaziale di ossigeno lungo la coordinata assiale per elevati valori di CORFU, assicurando elevata uniformità nella distribuzione di ossigeno. L'entità della velocità di perfusione deve essere ottimizzata non solo per controllare la distribuzione dei flussi radiali, ma anche per permettere il rilascio controllato di ossigeno verso il comparto cellulare evitando di trasportare le cellule al di fuori del costrutto, a ogni stadio di sviluppo del tessuto. In particolare, le predizioni del modello suggeriscono di perfondere il costrutto a velocità superficiali ridotte durante le prime fasi della coltura, e di incrementarne l'entità man

mano che le cellule proliferano e differenziano per controbilanciare l'aumento delle necessità metaboliche delle cellule. In particolare, velocità superficiali più elevate permettono migliore ossigenazione del comparto cellulare per un dato valore di ϕ_C. Infine, adottando portate che minimizzano il valore del numero di Damköhler radiale minimo, $Da_{rad,min} = \phi_C^2/Pe_{rad,max}$, viene assicurata la realizzazione di un adeguato ambiente pericellulare per lo sviluppo del tessuto.

Abstract

Tissue loss or organ failure represents one of the major problems in human health care, and is responsible of impressive social and economic costs worldwide. Current approaches to restore tissues or organs functions consist in tissue replacement with allogeneic or xenogeneic grafts, taken from donors or animals, respectively, or autologous grafts, taken from the patient himself. The use of allogenic and xenogenic grafts is severely limited by the donor shortage and by the difficult integration of the donor tissue within the patient body. Tissue replacement with autografts, although avoiding the risk of immune rejection by the patient, is limited by donor-site morbidity, so that it may be adopted only for small-scale tissue losses. In recent years, tissue engineering has been proposed as a promising alternative to tissue replacement with artificial grafts. According to this approach, biological engineered substitutes for tissue replacement are realized by seeding isolated autologous cells onto three-dimensional (3D) porous supports, termed scaffolds, and by guiding cell proliferation and differentiation in bioreactors, that provide the physiological pericellular environment for tissue development. The major issue for the realization of clinical-scale bioengineered substitutes for tissue replacement is the difficult supply of physiological amounts of dissolved oxygen and nutrients to, as well as metabolic wastes removal from, the cells located in the innermost regions of the 3D constructs (i.e. cell-seeded scaffolds). In particular, it is generally acknowledged that the severe consumption of dissolved oxygen by the cells represents the major limitation for cell survival in the development of bioengineered tissues. Static cultures in which dissolved oxygen and nutrients are supplied to the cells by pure diffusive transport have been shown to enable cell survival only to small-scale constructs. In order to overcome transport limitations of static cultures, dynamic bioreactors have been proposed in which a certain degree of convection is superimposed to pure diffusion to enable solutes transport towards, or away from, the innermost region of large-scale constructs. However, although some improvements over static cultures have been evidenced, dynamic bioreactors proposed so far, such as spinner flasks, rotating wall vessels

and direct axial perfusion bioreactors, are still sub-optimal for the realization of clinical-scale bioengineered tissues. Recently, radial perfusion of hollow cylindrical 3D constructs in radial flow packed-bed bioreactors (rPBBs) has been proposed to overcome the limitations of both static and direct axial perfusion bioreactors, in particular for the development of bioengineered liver and bone tissues. In fact, since culture medium is perfused radially to the cells, shorter path lengths and larger cross-sectional areas for solutes transport are featured than those in axial flow bioreactors, that enable cell culture at small pressure drops and superficial velocities, and smoother solutes concentration gradients in the direction of the medium perfusion. Despite these promising features, design of rPBBs is more difficult than that of axial flow packed bed bioreactors. In fact, rPBBs require two void chambers (i.e. the inner hollow cavity and the peripheral annular space) to distribute and collect culture medium flowing across the construct thickness, the fluid dynamics of which may significantly influence radial flux distribution of culture medium along the construct length. Furthermore, the annular construct geometry and the direction of medium perfusion may strongly affect the transport of solutes towards, or from, the cells. The extent of the perfusion flow rates have also to be chosen in order to ensure adequate mass delivery to cells while preventing cell damage and washout. Mathematical models of transport in rPBBs may help optimize bioreactor design for a given application to enable dissolved oxygen and nutrients delivery towards, and metabolic wastes removal from, 3D clinical-scale constructs. However, a systematic analysis of the influence of all the geometrical, transport and operational dimensionless groups on bioreactor behavior aimed to design rPBBs so that solutes transport towards, or from, the cells is maximized and controlled has not been reported yet. This limits the exploitation of the peculiar features of the rPBBs in the development of bioengineered substitutes for tissue replacement.

In this thesis, a model-based reference framework is proposed to optimize rPBB design to ensure adequate environmental conditions to cells for the realization of clinical-scale 3D bioengineered substitutes for tissue replacement. In particular, the attention is paid on transport of

dissolved oxygen, since its limiting role for the realization of large-scale 3D biological constructs is generally acknowledged. In order to reach the proposed objective, the workflow was divided in three different steps, as follows:

1. A reference framework was first developed based on a one-dimensional stationary transport model, combining convective and dispersive transport of dissolved oxygen with Michaelis-Menten cellular consumption kinetics, to optimize annular construct geometry and direction and extent of the radial superficial velocity of the culture medium across the cell mass for the culture of large-scale 3D porous constructs, assuming that radial flux distribution of the culture medium was uniform along the construct length. Dimensional analysis was used to find the dimensionless groups determining bioreactor behavior, under typical conditions for tissue engineering. In particular, according to this model, bioreactor behavior was shown to depend on the perfusion flow direction parameter, γ; the dimensionless construct Darcy permeability, kL/R^3; the inner hollow cavity radius-to-construct thickness ratio, R/δ_C; the maximal radial Peclet number, $Pe_{rad,max}$; the Thiele modulus, ϕ_C; the saturation parameter, β. The effectiveness of oxygen supply to the cells was expressed in terms of the non-hypoxic fractional construct volume. Model predictions suggest that outward perfusion (i.e. form the construct inner surface towards the outer peripheral surface) of 3D annular porous constructs having small curvature (i.e., high inner hollow cavity radius-to-annular thickness ratio) at high perfusion flow rates, (i.e high maximal radial Peclet numbers) may enhance dissolved oxygen supply to the cells as compared to cell culture in static and axial flow bioreactors.

2. A design criterion to optimize rPBB design in order to achieve uniform radial flux distribution of the culture medium along the construct length was obtained, based on a two-dimensional stationary transport model of momentum in all the rPBB compartments (i.e. inner hollow cavity, porous construct, peripheral annulus), assuming that medium is perfused outwards according to the results obtained with the 1D model. In particular, momentum transport in the void spaces of the rPBB was described according to the Navier-Stokes equation, whereas Darcy-Brinkman equation was used to

describe momentum transport in the porous construct. Dimensional analysis showed that the uniformity of radial flux distribution of the culture medium along the construct length depends on: a reduced Reynolds number, Re_{in}; the construct aspect ratio, L/R; the inner hollow cavity radius-to-construct thickness ratio, R/δ_C; the inner hollow cavity radius-to-peripheral annulus thickness ratio, R/δ_E; the construct-to-hollow cavity permeability ratio, k/R^2. The influence of R/δ_C and R/δ_E was lumped in one dimensionless group (i.e. the hollow cavity-to-peripheral annulus cross-sectional area ratio, ξ), as suggested by literature results. The design criterion, termed CORFU (Criterion Of Radial Flux Uniformity), was shown to depend on all the dimensionless groups found by dimensional analysis. In particular, according to the CORFU criterion, uniform radial flux distribution of the culture medium along the construct length may be achieved by adjusting the values of the dimensionless groups determining rPBB behavior in order to ensure that the ratio between the total axial pressure drop in the void spaces is maintained within ±10% of the radial pressure drop across the construct.

3. The momentum transport model was integrated with a mass transport model to assess the actual effect of the radial flux distribution of the culture medium along the construct length on dissolved oxygen transport and to design rPBBs for a given therapeutic objective. Transport of dissolved oxygen in the construct was described in terms of the convection-diffusion-reaction equation, and dissolved oxygen consumption was described according to the Michaelis-Menten kinetics. Oxygen mass transfer coefficients accounting for the external mass transport at cell/medium interface were estimated for a bed of Raschig rings transport-equivalent to porous scaffolds adopted for tissue engineering. Dimensional analysis showed that, in addition to the dimensionless groups obtained for the momentum transport model previously listed, bioreactor behavior, which was expressed in terms of the Non-Hypoxic Fractional Construct Volume, depends on the following dimensionless groups: the maximal radial Peclet number, $Pe_{rad,max}$; the construct-to-hollow cavity diffusivity ratio, D_C/D_H (and, analogously, the construct-to-peripheral annulus diffusivity ratio, D_C/D_E); the

Sherwood number, Sh; the saturation parameter, β; the Thiele modulus, ϕ_C; the squared surface Thiele modulus-to-Sherwood number ratio, ϕ_s^2/Sh_p. The effect of the dimensionless number on bioreactor behavior was investigated under working conditions typical of tissue engineering. Model predictions suggested how to optimize bioreactor design in order to ensure controlled oxygen supply to cells for different tissue engineering applications. Medium radial flux distribution was shown to significantly influence oxygen spatial distribution inside the construct under conditions in which oxygen depletion is not properly compensated by oxygen supply to cells. The effect of medium radial flux distribution on oxygen supply becomes less important if oxygen consumption is compensated by oxygen supply. Model predictions also suggest that higher Re_{in} influences oxygen spatial distribution from the top towards the bottom of the bioreactor for non-uniform medium radial flux distribution, giving higher uniformity of oxygen distribution along bioreactor length. The radial perfusion rates have to be optimized not only to control radial flux distribution, but also to enable adequate supply of dissolved oxygen to the cells while preventing cell wash out, at any given stage of tissue development. In particular, model predictions suggest that at the beginning of the culture medium flow rates may be kept low to avoid cell damage or wash out, whereas, as cells proliferate and differentiate, the medium flow rates should be gradually increased to balance out the increasing metabolic requirements of cells. In particular, higher perfusion flow rates enable more adequate oxygen supply to cells for a given value of ϕ_C. Finally, choosing perfusion rates that cause minimal Damköhler number, $Da_{rad,min} = \phi_C^2/Pe_{rad,max}$, to be small were shown to ensure adequate pericellular oxygenation (i.e. NHy-FCV around 1) for tissue development.

Chapter 1

Tissue engineering: state-of-the-art

1.1 Introduction

Millions of surgical procedures of organ transplantation are performed every year worldwide to restore lost functions of tissues and organs as a result of injury, disease or congenital defects. Tissue loss and organ failure cause dramatic social and economical costs. For instance, only in the US, the total national health care cost to treat patients suffering from tissue loss or organ failures is higher than 400 billion US dollars, whereas it is estimated that the total cost of organs substitution worldwide is around 350 billion US dollars (Lysaght and Loughlin, 2000). The success of current therapies involving organ transplantation is severely limited by the lack of donors. For instance, it has been estimated that only in the United States around 30 thousands patients die from liver failure every year while waiting for surgery, with a scenario that is expected to worsen in the near future (Langer and Vacanti, 1993).

Current treatments to replace damaged or lacking tissues generally consist in the use of allogeneic or xenogeneic grafts taken from cadavers or animals (typically of bovine or porcine origin), respectively, or autologous grafts taken from the patient himself. Allografts and xenografts may be advantageous for the treatment of large-size tissue defects, since they are available off-the-shelf form tissue banks, but they may entail immunogenic risk, donor-to-host disease transmission, slow tissue formation, possible incomplete or delayed graft incorporation. Differently from allografts and xenografts, tissue replacement with autografts avoids the risk of immune rejection, thus avoiding the necessity of immunosuppressive drug therapy (Furth and Atala, 2007). However, the availability of autologous tissues is limited by donor-site morbidity and may thus be adopted only for small tissue lacks or damages. Other disadvantages of autografts include increasing operating time and blood loss (Meyer *et al*., 2004).

Tissue engineering has been proposed to provide an interesting alternative to tissue replacement with artificial grafts. In particular, many of the aforementioned drawbacks may be overcome by adopting biological engineered tissue substitutes. To this purpose, researchers have suggested to seed autologous cells onto a degradable scaffold or matrix providing mechanical support for, and allowing transport of biochemical cues towards, the cell region, and to culture the cell-seeded scaffolds in bioreactors, which provide the physiological environment to allow cells to re-organize in their actual tissue structure (Langer *et al*., 1995).

Examples of diseases potentially treatable with the realization of bioengineered tissue substitutes include, among the others, congestive heart failure, with around 5 million patients only in the United States (Murray-Thomas and Cowie, 2003), diabetes mellitus, osteoporosis (10 million patients only in the US), Alzheimer's and Parkinson's diseases (5.5 million patients), severe skin burns (300 thousands), spinal cord injuries (250 thousands), and birth defects (150 thousands) (Furth and Atala, 2007).

1.2 Tissue Engineering

1.2.1 Background of Tissue Engineering

Tissue engineering has been defined as a multidisciplinary field involving life science and engineering principles aimed to realize biological substitutes of damaged tissues in order to restore, maintain and/or improve tissue function (Langer and Vacanti, 1993).

The possibility of realizing engineered biological substitutes according to tissue engineering strategy is based on the following observations:

i. most tissues are subject of constant remodeling due to the attrition and renewal of their constituent cells;
ii. isolated cells tend to form actual tissue structure *in vitro* under favorable conditions;

iii. although isolated cells may organize in actual tissue structures *in vitro*, only a limited degree of organization is possible when cells are transplanted as a suspension into the middle of mature tissue;

iv. in most cases, the tissue cannot be implanted in large volumes, since the cells cannot survive without adequate vascularization.

Based on such observations, the common strategy for the realization on bioengineered tissue substitutes consist of several phases, that are listed below and summarized in Figure 1.1:

1. cells are first isolated through a biopsy from the patient or a donor
2. isolated cells are expanded *in vitro*
3. expanded cells are seeded onto three-dimensional (3D) scaffolds under conditions allowing their attachment and maintenance of functions.
4. the resulting cell-scaffold system (that will be referred to as construct) is then cultured *in vitro* to produce a bioengineered tissue substitute for implantation. The *in vitro* culture conditions, provided by bioreactors, must be optimal for a given cell type and scaffold material in terms of culture parameters (e.g. concentration of oxygen and nutrients, temperature, pH), mass transfer requirements (e.g. specific oxygen and nutrients consumption rates) and sensitivity to mechanical stress (e.g. shear stresses) (Langer et al., 1995).
5. the bioengineered tissue substitute is finally implanted in the specific site of patient's body.

Several studies have demonstrated the success of the implantation of constructs in the *in vivo* tissue regeneration. In such studies, different parameters have been varied: donor cell type, time of *in vitro* cultivation, target species, implantation site and method, *in vivo* healing time (Freed et al., 1993 and 1994; Vacanti et al., 1991 and 1993; Cao et al., 1994; Uyama et al., 1993, Organ et al., 1993; Atala et al., 1992).

Although significant progress has occurred since tissue engineering strategy has been proposed, so far only few products incorporating cells and scaffolds have been approved (Furth and Atala, 2007). However, many researchers believe that in the long terms with tissue engineering it will be possible to create vital organs, such as the kidney, the liver and the pancreas, or even an entire heart (Nerem, 2007).

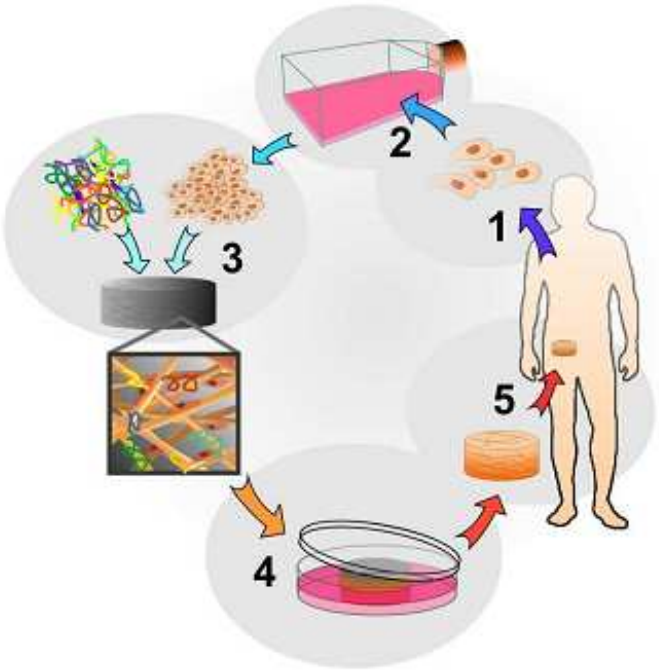

Figure 1.1 Phases of realization of a bioengineered tissue substitute (Adapted from van Blitterswijk et al., 2008)

1.2.2 Key factors of Tissue Engineering

The successful realization of a bioengineered tissue substitute depends on the possibility of reproducing *in vitro* the complex interactions occurring between cells and extracellular environment *in vivo*. For this reason, it is fundamental to understand the complex biological and molecular mechanisms occurring inside the tissue and those occurring during tissue formation and restoring. The reproduction of such mechanisms is limited by the complexity of the molecular composition of cells and extracellular environment and by the interactions among cells and between cells and extracellular environment in the biological tissues. As outlined in paragraph 1.2.1, the strategy to

overcome these limitations entails the combinations of four key elements: 1. cells; 2. scaffold; 3. biochemical and biomechanical cues; 4. bioreactors.

1.2.2.1 Cells

The first step in the realization of bioengineered tissues is the choice of the type of cells. This choice is based on the ability of cells to proliferate, differentiate, undergo cell-to-cell interaction, produce biomolecules and extracellular matrix. Ideally, the cells chosen for the realization of bioengineered tissues should have some important properties, including availability, high proliferative activity, maintenance of the adult phenotype, absence of immunogenicity. These properties strongly depend on the sources of appropriate stem or progenitor cells. The former seem to have unlimited capacity for self-renewal and the ability to differentiate in different mature cell types (pluri or multi –potency), whereas the latter are proliferative cells with limited capacity of self-renewal and are often unipotent (i.e. they can differentiate in only one mature cell type) (Seaberg and Van der Kooy, 2003). Three major sources of cells have been investigated by researchers: 1. embryonic stem (ES) cells derived from the inner cell mass of embryonic blastocysts (which later forms the embryo); 2. ES cells created by therapeutic cloning; 3. “adult” stem cells derived from fetal, neonatal, or adult tissue, either autologous or allogeneic (Furth and Atala, 2007). The ES cells have excellent ability of proliferation and differentiation. In particular, they have been shown to be capable of undifferentiated proliferation *in vitro* for 4-5 months and differentiation in all the three embryonic germ layers (i.e. endoderm, mesoderm, ectoderm), so that they can induce the subsequent differentiation in the desired cell phenotype. As a result, they may be classified as pluripotent (Amit et al., 2000; Thomson et al., 1998). However, although showing attractive features, ES cells may be tumorigenic (G. R. Martin, 1981; Thomson et al., 1995) and give rise to important ethical issues, since their use involves the discard of the human embryo or cloning (Khademhosseini et al, 2007; Tuan et al., 2003). For this reasons, adult stem (AS) cells are generally preferred and represent the only cell type used so far for therapeutic applications. The AS

cells have high capacity of self-renewal in culture and are normally classified as multipotent, that is they can differentiate only in certain types of mature phenotypes. Even if their ability to proliferate is lower than ES cells, in some cases AS cells do not result to be subject to replicative senescence. Furthermore, AS cells do not appear to be tumorigenic. AS cells may be classified based on their originating embryonic germ layer. An important class of AS cells, derived from the mesodermic embryonic germ layer, for its great potential in tissue engineering is represented by the mesenchymal stem cells (MSC), that were first isolated from bone marrow (Friedenstein and Petrakova, 1966). Even if they are present only in very small fraction of the total population of nucleated cells in marrow, they may be isolated and expanded with high efficiency and may differentiate into cells phenotypes of connective tissue lineages, including bone, cartilage, muscle, tendon, and fat. For this reasons, the MSC are subject of enormous interest for musculoskeletal and vascular tissue engineering (Barry and Murphy, 2004; Gao and Caplan, 2003; Riha et al., 2005; Tuan et al., 2003). Although AS cells have been considered to maintain a certain tissue specificity, recent experiments suggest that under particular circumstances, AS cells may “transdifferentiate”, that is they can convert into cells of distinct lineages from their originating one, thus losing the tissue-specific markers and functions of the original cell type and acquiring markers and functions of the transdifferentiated cell type. Such phenomenon has given rise to the concept of “cell plasticity”, indicating that AS cells may differentiate in adult phenotypes different from those typical of their originating embryonic germ layer (Blau et al., 2001; Wagers and Weissman, 2004). Examples of cell plasticity have been suggested for neuronal stem cells (Bjornson et al, 1999), bone marrow-derived stem cells (Ferrari et al., 1998), muscular (Jackson et al., 1999) and skin –derived stem cells (Liang et al., 2002).

1.2.2.2 Scaffold

Isolated cells cultured *in vitro* cannot reorganize spontaneously in tissues if they are not provided with 3D structures guiding and stimulating their activity (Schugens et al., 1996). In human

tissues, such 3D structure is provided by the extracellular matrix (ECM). The characteristics of the ECM strongly depend on the composition of the related specific tissue. In general, the functions of the ECM may be listed as follows: 1. ECM provides tissue-specific structural support and physical environment to allow cell adhesion, proliferation, migration and response to biochemical and biomechanical signals; 2. ECM contributes to mechanical properties of the specific tissue, e.g. rigidity and elasticity; 3. ECM may actively provide bioactive cues for the residing cells to respond to their microenvironment 4. ECM may act as reservoir of growth factors; 5. ECM provides a degradable environment to allow neovascularization and tissue formation resulting from tissue dynamic processes such as morphogenesis and wound healing (Chan and Leong, 2008). In the realization of bioengineered substitutes for tissue replacement, the 3D structure for cell support and activity guidance is provided by the scaffold. Ideally, the scaffold should be able to mimic all the functions provided *in vivo* by the ECM. However, due to the complex composition and the high number of functions of the ECM, this requirement results to be very difficult to satisfy. As a result, the functions of scaffolds are defined in analogy with those of the ECM in the natural tissues. In particular, for a given tissue type, the fundamental requirements for scaffolds are associated to:

1. Architecture: The scaffold should provide a sufficient void volume to allow tissue vascularization and expansion. High porosity and a structure with interconnected pores are required for the scaffold to ensure cell penetration and ECM formation, as well as adequate transport of oxygen and nutrients to, and metabolic wastes from, the cells, without compromising its mechanical stability. The pore size of the scaffold should be optimized to foster cell migration, while ensuring a high specific surface for cell adhesion
2. Biocompatibility: the scaffold biomaterial has to ensure the absence of immunogenicity in order to prevent inflammatory response by the body that may cause the rejection of the implant.

3. Biodegradability: The scaffold must be biodegradable in order to permit cells to produce the ECM, showing a kinetics of degradation comparable to that of tissue regeneration, and does not have to cause the formation of toxic metabolic wastes during its biodegradation.

4. Bioactivity: Scaffolds may provide biological cues to cells in order to help them regulate their activity, as well as to guide their morphology and alignment, and foster the delivery of growth factors to the cells.

5. Mechanical properties (e.g. strength, Young modulus, toughness, ductility): Scaffolds must provide mechanical stability to the tissue. Its mechanical properties should be as comparable as possible to those of the native tissue and ensure, at the same time, adequate mechanical resistance during culture.

Finally, scaffolds should be easy to sterilize and its production should be easy and cost effective. (O'Brien, 2011; Chan and Leong, 2008, Muschler et al., 2004).

A wide range of biomaterials have been used for scaffold realization depending on the specific application. Based on their origin, the biomaterials for scaffold realization may be classified as natural or synthetic. Natural biomaterials, such as collagen, fibrin, silk, agarose, alginate and chitosan, are obtained by extraction from living organisms. They are mainly attractive for tissue engineering applications due to their high biocompatibility and bioactivity. Some of the disadvantages of natural biomaterials include the limited range of mechanical properties and the possible impurity of the protein or polysaccharides they are composed of (Willerth et al., 2008). Natural biomaterials applications include the regeneration of bone (Chan et al., 2007; Hofmann et al., 2007; Kim et al., 2005; Meinel et al., 2005; Sumanasinghe et al., 2006), cartilage (Worster et al., 2001; Wang et al., 2005; Awad et al., 2004; PP et al., 2005; Hofman et al., 2006), ligaments (Altman et al., 2002; Noth et al., 2005), nerve (Ma et al., 2004; O'Connor et al., 2000; Watanbe et al., 2007; Willerth et al, 2006), vasculature (Gerecht-Nir et al., 2003), liver (Maguire et al., 2006), adipose tissue (Flynn et al., 2007) and skin (Myers et al., 2007).

Synthetic biomaterials provide a valid alternative to natural biomaterials in the culture of cells. The advantages related to the use of synthetic biomaterials include reproducibility and good mechanical properties, good workability and high versatility. As compared to natural biomaterials, synthetic biomaterials offer the possibility of tailoring scaffolds with a specific degradation rate. Drawbacks concerning the use of synthetic biomaterials include possible low biocompatibility, reduced bioactivity and, in some cases, the necessity of surface modifications to optimize cell adhesion and delivery of biomechanical cues (Willerth et al., 2008). Synthetic biomaterials may be generally classified as polymeric-based and ceramic-based (and composite biomaterials). Examples of polymeric-based synthetic biomaterials include PLGA, PLLA, PGA, PCL and PEG, that have been used for the regeneration of adipose tissue (Choi et al., 2005; Neubauer et al., 2005), nerves (Bhang et al., 2007; Mahooney and Anseth, 2005), bone (Chastain et al., 2006; Benoit et al., 2005; Kim et al., 2006), cartilage (Uematsu et al., 2005; Buxton et al., 2007) and liver (Underhill et al., 2007), whereas ceramic biomaterials, such as Hydroxiapatite and tri-calcium phosphate (TCP), have been used mainly for bone tissue engineering, due to their good mechanical properties and biocompatibility with bone tissue (Arinzeh et al., 2005; Bruder et al., 1998; Dennis and Caplan, 1993; Kotobuki et al., 2005; Marcacci et al., 2007; Shimaoka et al., 2004).

1.2.2.3 Growth factors

In order to promote tissue development, it is fundamental to control the environment in which cells grow. Beyond adequate oxygen and nutrient supply and metabolic waste removal, it is necessary to deliver the appropriate concentration of growth factors to the cells. Growth factors (GF) may be defined as soluble signaling polypeptides capable to guide specific cellular response (cell survival, migration, proliferation, differentiation) during tissue development in a given biological environment. The first step in signal transmission is the GF secretion by a producer cell. Once secreted, the GF binds specific cell transmembrane receptors of the target cell (different from the producer cell) and activates the signal transduction into the cell. The transduction mechanism

involves a complex system of events and results in a specific cell response (Figure 1.2). The ability of a GF to deliver a specific instruction to a given cell population is not only modulated by the identity of the GF itself and by its ability of diffusing through the ECM of the target cells, but also on the type and number of target cells, the type of receptors expressed by the target cell and the path of signal transduction, that may be different from one cell type to another, so that a growth factor may fulfill a variety of functions under different conditions. Finally, the specific cellular response of a target cell to a given GF also depends on other external factors, such as the ability of the GF to bind the ECM of the target cell, the degradation rate of the ECM, the GF amount and the position of the cell target (Lee et al., 2001; Cross and Dexter, 1991; Lamalice et al., 2007).

Examples of common GF and their functions encountered in tissue regeneration are listed in Table 1.1.

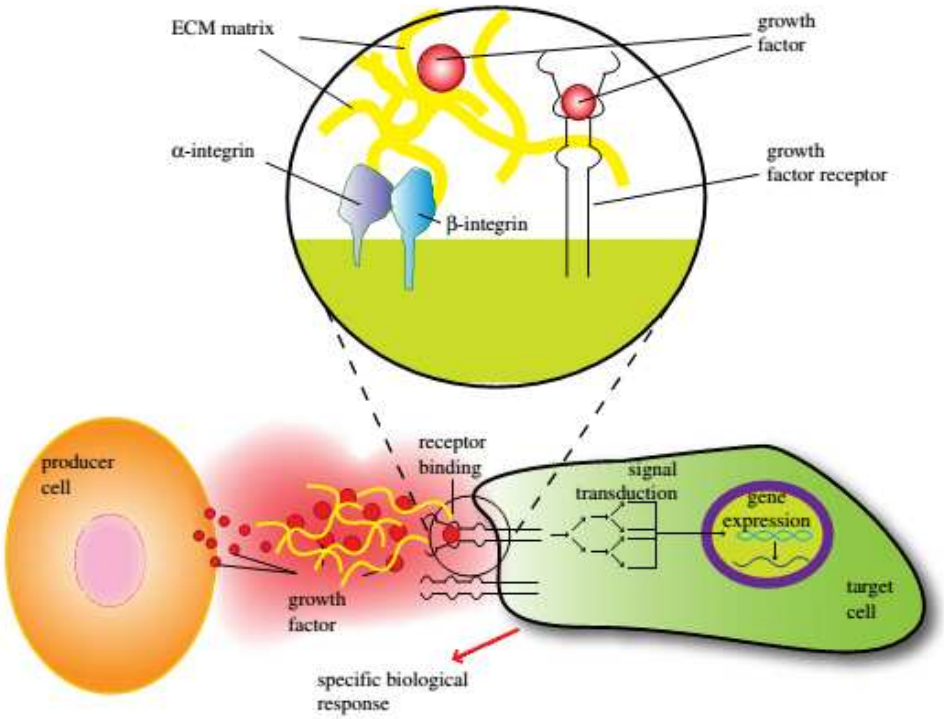

Figure 1.2 Mechanism of action of a growth factor (image from Lee et al., 2011)

abbreviation	tissues treated	representative function
Ang-1	blood vessel, heart, muscle	blood vessel maturation and stability
Ang-2	blood vessel	destabilize, regress and disassociate endothelial cells from surrounding tissues
FGF-2	blood vessel, bone, skin, nerve, spine, muscle	migration, proliferation and survival of endothelial cells, inhibition of differentiation of embryonic stem cells
BMP-2	bone, cartilage	differentiation and migration of osteoblasts
BMP-7	bone, cartilage, kidney	differentiation and migration of osteoblasts, renal development
EGF	skin, nerve	regulation of epithelial cell growth, proliferation and differentiation
EPO	nerve, spine, wound healing	promoting the survival of red blood cells and development of precursors to red blood cells.
HGF	bone, liver, muscle	proliferation, migration and differentiation of mesenchymal stem cells
IGF-1	muscle, bone, cartilage, bone liver, lung, kidney, nerve, skin	cell proliferation and inhibition of cell apoptosis
NGF	nerve, spine, brain	survival and proliferation of neural cells
PDGF-AB (or -BB)	blood vessel, muscle, bone, cartilage, skin	embryonic development, proliferation, migration, growth of endothelial cells
TGF-α	brain, skin	proliferation of basal cells or neural cells
TGF-β	bone, cartilage	proliferation and differentiation of bone-forming cells, anti-proliferative factor for epithelial cells
VEGF	blood vessel	migration, proliferation and survival of endothelial cells.

Table 1.1 Common growth factors in tissue regeneration. Ang, angiopoietin; bFGF, basic fibroblast growth factor; BMP, bone morphogenetic protein; EGF, epidermal growth factor; FGF, fibroblast growth factor; HGF, hepatocyte growth factor; IGF, insulin-like growth factor; NGF, nerve growth factor, PDGF, platelet-derived growth factor; TFG, transforming growth factor; VEGF, vascular endothelial growth factor (table from Lee et al., 2011).

1.2.2.4 Bioreactors

Critical for the development of a bioengineered tissue *in vitro*, is an adequate culture environment promoting cells survival and activity. The environmental conditions (i.e. temperature, pH, oxygen and nutrients concentration, biomechanical and biochemical cues) allowing the culture of 3D bioengineered constructs are provided by bioreactors. Bioreactors have been defined as "devices in which biological and/or biochemical processes develop under closely monitored and tightly controlled environmental and operating conditions (e.g. pH, temperature, pressure, nutrient supply and waste removal)" (Martin et al., 2004). Usually, a bioreactor consists of a sterile culture chamber in which 3D cellular constructs are contained and supplied with culture medium through a pump, that collects the culture medium from a reservoir and discharge it in the culture chamber in monitored fashion. The culture medium contains oxygen, nutrients and the growth factors necessary to foster cell activities. The bioreactors are usually provided of detecting systems to monitor the environmental conditions and may be successfully used not only for the *in vitro* development of

functional tissues, but also as models to study the mechanisms of cell function under physiological conditions (e.g. *in vitro* drug screening) (Wendt et al., 2009).

In the design of a bioreactor for a specific tissue engineering application several key factors have to be taken into account. The detailed requirements of a bioreactor generally depend on the specific type of tissue to develop. However, there are some general principles that may be applied in the development of a bioreactor. First of all, the material selection is fundamental to avoid adverse reactions by the cells. As a result, all the bioreactor components that are in contact with cells and culture medium must be bioinert and biocompatible. Furthermore, all the bioreactor components should be chosen so that they can be used in wet environment and at a constant temperature of 37 °C. In order to reduce economical costs, all the bioreactor components have to be easily sterilized by autoclaving (i.e. they have to be resistant to high temperatures), except those disposable. The bioreactor design should also permit simple assembly and disassembly, in order to minimize the exposition of cells to an undesired environment. Finally, bioreactors should permit easy control of operational conditions and scale-up (Plunkett and O'Brien, 2011).

The primary function of a bioreactor is that of ensuring cell survival and proliferation by providing uniform transfer of oxygen and nutrients to the cells and biochemical and biomechanical cues to yield their differentiation towards the natural tissue during their *in vitro* cultivation. Furthermore, bioreactors are adopted to provide uniform cell seeding at the beginning of the culture by perfusing cells into the construct pores (Freed and Guilak, 2007; Fournier, 2012). The obtainment of adequate cell seeding uniformity and the controlled supply of oxygen, nutrients and biochemical and biomechanical cues to the cells is a major issue in tissue engineering and depends on the bioreactor geometry and operational conditions, on mass transport inside and outside the construct and on the cell type under culture (i.e. cell metabolism) (Martin et al., 2004; Catapano and Gerlach, 2007).

1.3 Bioreactors for Tissue Engineering

1.3.1 Bioreactor design issues

1.3.1.1 Cell seeding onto 3D scaffolds

The dissemination of isolated cells onto a 3D porous scaffold represents the first step for the culture of bioengineered tissues and plays a critical role in the progression of tissue maturation (Martin et al., 2004). Cells should be seeded onto the scaffolds with the highest possible efficiency to maximize the utilization of the small number of cells that may be isolated from a biopsy (Portner et al., 2005; Martin et al., 2004). High initial cell densities have been associated to enhanced tissue formation in 3D porous constructs, as in the cases of cartilage (Freed et al., 2007), bone (Holy et al., 2000) and cardiac (Carrier et al., 1999) tissues. In particular, a uniform initial seeding distribution of cells in the construct have been associated to a better cell distribution in the tissue once it has formed, in different applications (Holy et al., 2000; Freed et al., 1998; Kim et al., 1998). On the other hand, inhomogeneous cell distribution within the scaffold may severely alter the final properties of the tissues (Portner et al., 2005).

However, the obtainment of uniform seeding distribution of a high number of cells (i.e. high cell density) is a challenging issue, particularly when large and complex 3D scaffolds are used (Martin et al., 2004). The degree of uniformity of cell distribution depends on the balance between the rate at which cells are transported from the medium bulk towards the external surface of the scaffold (i.e. external transport) and from the surface of the scaffold into its pores (i.e. internal transport), as well as on the rate at which cells adhere to the scaffold surface and bind the other cells in their vicinity and form cell clusters, that further influence internal transport. For instance, the penetration of suspended cells into the scaffold pores depends on the cell/cluster-to-pore diameter ratio, high values of which may hinder cell penetration (Catapano and Gerlach, 2007).

Due to its simplicity, the most common seeding technique is the static seeding, which consists in pipetting a concentrated cell suspension in the scaffold and relies on gravity as the

leading principle for cell settlement and adhesion within the scaffold pores. However, static loading generally cause low seeding efficiency and non-uniform cell distribution within the scaffold, due to the lack of control and to the operator-dependent nature of the process (Holy et al., 2000; Kim et al., 1998; Wendt et al., 2009; Martin et al., 2004). As a result, dynamic techniques according to which bioreactors are used to enhance cell seeding by means of convective transport rather than gravitational effects, which may reduce external and internal resistance to cell penetration, have been proposed to overcome the limitations resulting from conventional static seeding (Vunjak-Novakovic et al., 1999; Bueno et al., 2007; Freed and Vunjak-Novakovic, 1997). In particular, the most promising approach seems to be represented by the perfusion seeding, which consists in the direct perfusion of a cell suspension into the pores of the scaffold. This method has been shown to be particularly successful for the seeding of cells into large-size scaffolds of low porosity, due to the active driving forces involved that enhance fluid penetration into the scaffold pores (Wendt et al., 2003).

1.3.1.2 Transport of oxygen, nutrients and metabolites

In vivo, the efficient supply of oxygen and nutrients to, and the removal of the waste metabolites from, the cells is ensured by a complex vascular network, which is difficult to reproduce *in vitro*. In fact, cells continuously consume oxygen and nutrients and produce waste metabolites. This causes the solutes concentration at cell surface to significantly differ from that in the bulk medium. Steep solutes concentration gradients may induce cells to behave differently depending on their spatial distribution inside the scaffold and cause cell starvation. To reach the cells anywhere in the construct, solutes have to be transported external to the construct across a relatively stagnant layer of medium (i.e., from the medium bulk to the construct outer surface) and inside the construct (i.e., from its outer surface to the innermost regions) across the cell mass, where they are consumed (or produced). As a result, the spatial profile of such solutes depend on the overall resistance determined by each bioreactor compartment (Catapano and Gerlach, 2007).

The external resistance to solutes transport, and the consequent solutes concentration gradients establishing from the medium bulk to the cell surface, increases with decreasing solute diffusion coefficient in the medium, and increasing cell-specific solute consumption rate as well as increasing thickness of the stagnating layer of medium. External mass transport resistance mainly depend on the hydrodynamic conditions of the bioreactor and may be reduced by increasing the intensity of culture medium mixing by superimposing a certain degree of convection over pure diffusive transport. Internal solute transport and solutes consumption (or production) occur simultaneously inside the construct. Under steady conditions, the solute concentration profiles balance out the rate of internal transport with the rate of solute consumption (or production). As cells proliferate and produce ECM, the pores of the construct become smaller, and the diffusion ability of the solutes decreases as a result of a decreased construct porosity and increased construct tortuosity. At the same time, since the cell concentration increases, the metabolic requirements of the cells increase. These simultaneous phenomena contribute to increase the solutes concentration gradients across the cell mass (Catapano and Gerlach, 2007; Martin et al., 2004; Fogler et al., 2006). Since tissue constructs should have larger size, mass-transfer limitations represent a major issue in tissue engineering (Portner et al., 2005).

1.3.2 Bioreactor systems used in Tissue Engineering

In general, bioreactors may be classified based on the mechanism through which solutes are transported into (or out of) the cell compartment in static and dynamic. In particular, in static cultures transport only occurs by diffusion, whereas in dynamic bioreactors solutes transport and consequent tissue formation is enhanced by mechanical, hydraulic or pneumatic control of the cell environment.

1.5.2.1 Static bioreactors

Examples of bioreactors used for static cultures are the Petri dish, the multi-well plates and the T-flask. They are generally suitable for the *in vitro* expansion of anchorage-dependent cells and very easy to use. An important advantage related to the use of these systems is that cells are subject to small shear stresses, that avoids cell wash out and damage. However, these devices only permit an increase of the cell number by a factor of 10, so that several subcultivations are required to obtain adequate cell expansion, that may cause cell dedifferentiation (Portner, 2005). Furthermore, pure diffusive transport in static bioreactors ensures dissolved oxygen and nutrients supply only to a distance about 100 μm away from the construct outer surface, it subjects cells to oxygen and nutrients concentrations largely varying in space (e.g., across the construct), and ultimately limits the realization of clinical-scale 3D cell constructs (Griffith et al., 2005; Gaspar et al., 2012; Muschler et al., 2004).

1.5.2.2 Dynamic bioreactors

To overcome the transport limitations resulting from static cultures, bioreactors have been proposed in which cells are cultivated in a dynamic environment. In fact, several studies have shown that a dynamic environment may have a positive impact on tissue formation (Portner et al., 2005).

Spinner flaks- In the spinner flask bioreactor, cell-seeded 3D scaffolds are attached to needles hanging from the bioreactor lid, and the dynamic environment is provided by a magnetic stirrer bar inducing the continuous mixing of oxygen and nutrients throughout the culture medium. During seeding, cells are transported into the construct pores by convection, whereas during culture stirring minimizes the thickness of the stagnant layer of medium at the construct surface (i.e. reduces external resistance to mass transport) and provides a well-mixed environment around cells throughout the culture chamber (Martin et al., 2004). Spinner flasks have been shown to enhance

cell proliferation and differentiation in bone tissue engineering as compared to static culture (Carrier et al., 1999; Gooch et al., 2001). However, while enhancing external mass transport, medium stirring generates turbulent eddies which cause shear stress that may be detrimental for cells (Freed and Vunjak-Novakovic, 1995). Furthermore, it has been shown that, despite a certain improvement of cell proliferation and differentiation of osteogenic cells as compared to static culture, spinner flasks are not suitable to enhance uniform cell and ECM distribution in the innermost construct (Sikavitsas et al., 2002). Finally, spinner flask have been shown to yield low seeding efficiency in different applications (Carrier et al., 1999; Vunjac-Novakovic et al., 1998).

Rotating Wall Vessels - Rotating wall vessels consist of a cylindrical chamber in which cell-seeded 3D scaffolds are suspended within the culture medium, as a result of the rotation of the vessel wall at a rate enabling the balance of drag force, centrifugal force and net gravitational force, and in which it is coaxially located a cylindrical chamber from which oxygen and nutrients are provided to the culture medium. This device can provide a dynamic culture environment for the cells with low shear stress and high external mass transfer rate (Martin et al., 2004), that makes them suitable for the culture of chondrocytes (Vunjak-Novakovic et al., 1999) and cardiac (Carrier et al., 1999) and osteogenic (Granet et al., 1998) cells, among the others. However, the micro-gravity environment to which cells are subject has been shown to be potentially inhibitory for osteoblast proliferation and differentiation (Ontiveros and McCabe, 2003), whereas, likely due to the single axial rotation, cell distribution may result to be non-uniform (Sikavitsas et al., 2002; Freed and Vunjak-Novakovic, 1997). Furthermore, the imperfect balance of centrifugal, gravitational and drag forces could lead to the collision of the construct with the bioreactor wall, which causes cell damage (Goldstein et al., 2001; Sikavitsas et al., 2002; Chen and Hu 2006). Finally, medium convection around 3D porous constructs in rotating wall vessels has not been shown to permit adequate oxygen and nutrients supply to cells deep into the construct and adequate expression of cell differentiation markers,

although it has been reported to improve cell distribution and viability with respect to static bioreactors (Granet et al., 1998; Sikavitsas et al., 2002; Catapano et al., 2007).

Axial flow packed-bed bioreactors - In order to overcome the transport limitations resulting from the use of spinner flasks and rotating wall vessels, direct axial perfusion of 3D porous constructs with medium in axial-flow packed bed bioreactors (aPBBs) has been proposed in which the enhancement of oxygen and nutrients transport to cells internal to the construct is provided by convection (Kim et al., 2000; Bancroft et al., 2002; Warnock et al., 2005). In particular, aPBBs have been shown to be suitable for the enhancement of proliferation and differentiation of bone cells (Goldstein et al., 2001), growth of human keratinocytes for skin tissue engineering (Navarro et al., 2001), albumin synthesis by hepatocytes (Kim et al., 2000) and differentiation of cardiomyocytes (Carrier et al., 2002). Furthermore, aPBBs are used to enhance cell seeding into 3D porous scaffolds by transporting cells directly into the pores of the scaffold, which yields uniform cell distribution (Martin et al., 2004). However, direct perfusion may cause undesired effects dependent on the extent of the medium flow rate and the maturation stage of the constructs (Davisson et al., 2002). For instance, at low axial superficial velocity the dissolved oxygen and nutrients concentrations may steeply decrease towards the end of the construct leading to poor cell nourishment and causing the formation of a necrotic end zone in constructs of high cell concentration (Piret et al., 1991; Fassnacht and Portner, 1999), whereas cell perfusion at high axial superficial velocity to keep cells viable and differentiated anywhere in the construct may cause cell wash-out (Singh et al., 2007; Martin et al., 2004). As a result, the optimization of aPBBs for the engineering of clinical-size 3D tissues is limited by the difficult balance among the mass transfer of nutrients towards, and waste products from, the cells, the retention of ECM components within the construct pores, and the shear stresses to which cells may be subject as a result of the extent of the medium flow rate (Martin et al., 2004).

1.5.3 Radial flow packed-bed bioreactors

Radial perfusion with medium of cells seeded in 3D cylindrical porous scaffolds with a coaxial hollow cavity has first been proposed to overcome the transport limitations of pure diffusive operation and direct axial perfusion for the culture of hybridoma cells seeded onto porous glass spheres (Kurosawa et al., 1991). Similar to axial perfusion, superimposition of convection to pure diffusion should enhance solute transport to cells. Radially perfused hollow constructs would also feature a larger cross-sectional area for solute transport and shorter solute transport path-length than axially perfused constructs. Hence, cell constructs could be cultured in radial-flow packed-bed bioreactors (rPBBs) at lower pressure drop and lower superficial velocity (hence lower shear stresses) than aPBBs and still enable cell culture under smoother and more controllable dissolved oxygen and nutrients concentration gradients in the direction of medium perfusion (Kino-Oka and Taya, 2005). This is a very interesting feature to control pericellular environment and to guide cell differentiation when realizing biological tissue substitutes for implantation or for the *in vitro* toxicity screening of new drugs (Guillozo et al., 2008). In spite of these interesting features, only a few reports have been published on the culture of human cells seeded in 3D porous scaffolds in radial-flow packed-bed bioreactors for therapeutic applications. Radial perfusion of 3D constructs in rPBBs has been shown to promote cell proliferation and differentiation to a greater extent than static culture and conventional perfusion systems in different applications, especially for bone and liver tissue engineering.

Xie et al. have shown the effectiveness of the radial perfusion in the culture of sheep mesenchymal stem cells seeded onto large-size β-tricalcium phosphate porous scaffolds as compared to static culture. In particular, the authors have reported an about 4-fold higher glucose concentration and uniform cell proliferation through the whole scaffold under conditions of radial flow perfusion of the constructs, whereas non uniform cell proliferation has been reported under static culture (Xie et al., 2006). Similar results have been reported by Olivier et al. for the culture of

MG63 osteoblast-like cells seeded onto large-size β-tricalcium phosphate porous scaffolds in rPBBs. In particular, the authors have reported a more uniform cell distribution throughout the construct under dynamic conditions, independent of the direction of medium perfusion, as compared to static conditions (Olivier et al., 2007). The advantages of radial perfusion of cell constructs over static cultures have been also shown by Arano et al. (Arano et al., 2010) and Katayama et al. (Katayama et al., 2013) in the culture of MC3T3-E1 mouse osteoblastic cells and human mesenchymal stem cells, respectively, seeded onto type 1 collagen sheets for bone tissue engineering. In particular, the cell number has been reported to undergo up to a fivefold increase (Arano et al., 2010) or a 60% increase (Katayama et al., 2013) with uniform cell distribution throughout the construct under dynamic conditions as compared to static culture. Furthermore, radial flow perfusion has been reported to be successful as compared to static systems in the culture of goat bone marrow stromal cells seeded onto clinical-scale starch–polycaprolactone scaffolds. In particular, it has been shown that radial flow perfusion enables cell proliferation up to 21 days of cultures (Gardel et al., 2013). The usefulness of the radial flow type bioreactor for a three-dimensional culture system was confirmed by the results reported for inward radial perfusion culture in rPBBs of high concentrations of human liver cancer cells FLC-7 cultured onto porous glass bead microcarriers (Kawada et al., 1998), and human squamous cell carcinoma A431 (Shibata et al., 2009) and FLC-5 (Iwahori et al., 2011) seeded onto hydroxyapatite beads. In the development of a bioartificial liver, inward radial perfusion culture in rPBBs has been reported to maintain in an active metabolic state high concentrations of HepG2 cells seeded onto hydroxyapatite beads (Hongo et al., 2005), porcine hepatocytes (Miskon et al., 2007) in small-scale constructs, and porcine primary hepatocytes in clinical-scale constructs (Morsiani et al., 2000 and 2001). The co-culture in rPBBs of immortalized (Saito et al., 2006) and primary fetal hepatocytes and non-parenchymal cells (Ishii et al., 2008) in a 3D porous scaffold perfused inwards has been reported to promote the partial organization of cells in a liver-like architecture with sinusoid-like lumen structures and sustained liver-specific functions for a week. Finally, Kitagawa et al. have shown the effectiveness of the

radial perfusion in the seeding and culture of NIH/3T3 cells in poly(L)lactic acid porous scaffolds as compared to cell seeding in static systems and culture in spinner flasks, and have reported that an optimal value of medium flow rate exists that balances out the oxygen and nutrients supply to the cells and the extent of shear stress that washes cells out (Kitagawa et al., 2006).

1.4 Limitations in the realization of bioengineered tissue substitutes

Although considerable interest and effort has been paid on the possibility of realizing engineered substitutes for the replacement of different types of tissues, so far the success of tissue engineering has been only limited to the development of thin avascular tissues, such as epidermis and nasal septum cartilage (Bryant et al., 2001; Martin et al., 1999; Obradovic et al., 1999). It is generally acknowledged that the realization of 3D large-size tissue substitutes is limited by the difficult supply of adequate amounts of dissolved oxygen and nutrients to cells located in the innermost regions of 3D constructs, as well as the difficult removal of metabolic wastes (Malda et al., 2007). Within the human body, oxygen and nutrients supply towards, and metabolic wastes removal from, the cells are provided through a complex vasculature. In particular, in order to ensure the adequate supply of oxygen and nutrients to the cells *in vivo*, each cell is located close to a blood vessel. Such organized vasculature is lacking in implants formed *in vitro*. In *in vitro* static cultures, oxygen, nutrients and metabolic wastes are supplied to, or removed from, the constructs only by diffusion. Within the grafts *in vitro,* diffusion distances for oxygen and nutrients supply may be of the order of multiple millimeters or even centimeters (Godia and Cairò, 2006; Malda et al., 2009; Hassel et al., 1991), whereas diffusive transport may ensure oxygen and nutrients supply only to constructs having thickness around 100 μm (Chauduri et al., 2005). As a result, oxygen and nutrients limitations and waste products accumulation can occur, especially when high cell metabolic requirements and high cell concentrations are involved (Muschler et al., 2004).

In particular, the severe consumption of dissolved oxygen has been acknowledged to represent the major limiting factor for cell survival in the development of bioengineered tissues, due

to its low diffusion capacity, high cell-specific consumption rate and low solubility in acqueous media, as compared to those of the other solutes (Malda et al., 2007). As a result, maintenance of controlled oxygen concentration profiles throughout the constructs seems to be the most challenging issue to overcome (Griffith and George, 2009).

1.5 Effect of oxygen concentration on mammalian cell behavior

Oxygen is mainly required by mammalian cells for energy production through aerobic cellular respiration. In the development of a tissue *in vitro*, local oxygen concentration also regulates cell differentiation to a given phenotype, as in the case of bone (Bassett and Herman, 1961; Utting et al., 2006; Malda et al., 2003; Robins et al., 2005).

Cell behavior strongly depends on the amount of available dissolved oxygen concentration in the culture environment. Studies on different cell types in static 3D cultures have shown that dissolved oxygen concentration gradients form from the periphery to the core of the constructs, and they are directly related to the alteration of cell viability (Radisic et al., 2006; Malda et al., 2004) and differentiation ability (Tuncay et al., 2006; Salim et al., 2004). These gradients become steeper as cells grow, due not only to the higher cell concentrations, and thus to the increased metabolic requirements of the tissue, but also on the construct pore obstruction caused by ECM formation that limits oxygen convective transport (Malda et al., 2007). The inadequate dissolved oxygen supply results in the formation of hypoxic (i.e. dissolved oxygen concentration is lower than the physiologic values) or anoxic (no dissolved oxygen) regions in the innermost part of tissue-engineered constructs. If the exposition of cells to such conditions is restrained in times (up to 12-24 h), in many cases cells are able to adapt their metabolism so that their viability is not compromised. For instance, hypoxia can enhance ECM production and increase angiogenesis and cell proliferation. However, prolonged exposition to hypoxic or anoxic conditions overcomes the adaptive capacity of cells and results in cell death (Malda et al., 2007; Catapano et al., 1996; Muschler et al., 2004).

Cell growth may also be inhibited under hyperoxic conditions. Reactive oxidative intermediates formed under cell exposition to higher-than-physiologic dissolved oxygen concentrations have been shown to damage cells and contribute to cell ageing. As a result, dissolved oxygen concentration should range within physiologic values throughout the constructs to ensure cell survival (Balin et al., 1984).

The dependence of cell behavior on dissolved oxygen concentration *in vitro* is related to the degree of vascularization of the specific tissue *in vivo*. For instance, highly vascularized tissues, such as liver (Catapano et al., 1996), bone (Volkmer et al., 2008) and cardiac muscle (Carrier et al., 2002), require higher dissolved oxygen concentration for their survival and activity, whereas tissue with low vascularization *in vivo*, such as cartilage (Malda et al., 2003) or fibroblasts (Balin et al., 1984), may perform their function under low dissolved oxygen concentrations.

1.6 Importance of mathematical modeling in Tissue Engineering

In order to understand the complex mechanisms involved in tissue development, experimental results represent the most important way to validate theoretical assumptions so that all the different parameters may be chosen to ensure optimal culture conditions for given cell requirements. However, experiments require high consumption of time and economic costs, that may be limiting in several cases. Furthermore, experimental results are often not reliable, due to non-optimal conditions under which experiments are performed. To minimize the number of experiments, and the related time consumption and economic costs, mathematical models integrated in an iterative framework with experimental results may be adopted to simulate the effect of the different parameters involved in cell culture on tissue development, so that the environmental conditions required for cell survival and activity may be more easily optimized. (Sidoli et al., 2004). The integration of mathematical modeling with experimental results may also help couple different fields of expertise towards a common aim (MacArthur and Oreffo, 2005).

1.7 Objectives of thesis and structure

The realization of engineered biological human tissue substitutes has been indicated as a promising alternative to synthetic grafts for the replacement of large-size tissue or organ defects. The successful obtainment of bioengineered tissue substitutes able to reproduce the specific functions of a given tissue *in vivo* and integrating within the body environment once implanted is based on the combination of four key elements: isolated human autologous adult or stem cells (1) are seeded onto a 3D porous support, termed scaffold (2), and cultivated in the presence of biochemical and biomechanical cues (3) in bioreactors (4), that reproduce the adequate environmental conditions guiding cells to re-organize and differentiate as in natural tissues and organs. The major limitation for the development of bioengineered substitutes for tissue replacement is the difficult supply of adequate amounts of dissolved oxygen and nutrients towards the cells located in the innermost part of large-size 3D porous constructs. Static cell cultures have been shown to ensure cell survival only in regions of the constructs close to their external surface, since dissolved oxygen and nutrients are provided to the cells through pure diffusion. To overcome the diffusion limitations of static cultures, bioreactors have been proposed in which some degree of convection is superimposed to pure diffusion in order to reproduce more adequate environmental conditions for cell survival and activity. However, several issues are involved in bioreactor design. In particular, bioreactors proposed and used so far are suboptimal for geometry and operational conditions to allow effective transport of dissolved oxygen and nutrients to, and metabolic wastes removal from, the cell compartment.

Recently, radial flow bioreactors packed with annular porous constructs have been proposed to overcome the transport limitations of static and axial perfusion bioreactors for the development of clinical-scale substitutes for tissue replacement. In fact, radial perfusion of the porous construct allows tissue development under perfusion rates ensuring adequate delivery of dissolved oxygen and nutrients towards, and metabolic wastes removal from, the cells, under small shear stress and

pressure, due to the shorter transport path-length and higher cross-sectional area for solutes transport, as compared to axial construct perfusion. However, the design of radial flow packed bed bioreactors is more difficult than that of axial flow bioreactors. First of all, for a given construct thickness and length, the annular construct geometry influences mass distribution across the cell compartment. Second, two void chambers are required to distribute and collect the culture medium (i.e. the hollow cavity and the peripheral annulus), the fluid dynamics of which influences the uniformity of radial flux distribution of culture medium along the construct length. Furthermore, different flow configurations can be chosen for culture perfusion, that influence bioreactor behavior to different extent. In fact, medium may be perfused inwards (*i.e.* from the peripheral annulus towards the hollow cavity) or outwards (*i.e.* from the hollow cavity towards the peripheral annulus) across the cell mass, and with same or opposite axial directions in the void spaces (z or π-configuration, respectively). Third, the extent of the perfusion rates has to be chosen in order to avoid cell damage or washout while ensuring adequate oxygen and nutrients delivery to cells during tissue development.

In the optimization of bioreactor design, thorough experimental information should be available to understand how the geometrical and operational parameters influence bioreactor performance, and thus to optimize bioreactor design. However, such information may be provided with a wide range of experiments, which are not cost and time effective. In the absence of such experimental results, mathematical models may be useful to investigate how the different parameters influence bioreactor performance and to optimize bioreactor geometry and operations for a given application. However, as it will be discussed in the next chapters, a systematic analysis of the influence of all the geometrical, transport and operational parameters on bioreactor performance aimed to optimize the design of radial flow packed-bed bioreactors for tissue engineering is still lacking. This limits the recognition of the most relevant parameters, and the understanding of their interplay, determining rPBB behavior, and makes it difficult to optimize bioreactor design for a given therapeutic objective.

The aim of this work is to develop a model-based reference framework to optimize bioreactor design so that transport of dissolved oxygen, nutrients and biochemical and biomechanical cues towards, and metabolic wastes removal from, the cells is maximized and controlled, in order to prevent cell starvation and to guide cell differentiation towards a given phenotype in the development of clinical-scale bioengineered substitutes for tissue replacement. Particular attention will be paid on dissolved oxygen transport, since its limiting role is generally acknowledged for the realization of large-scale 3D constructs. In order to reach the proposed objective, the present work is divided in three different steps, that will be correspondingly discussed in the following three chapters. In particular:

1. In the second chapter, a reference framework based on a one-dimensional stationary transport model is presented aimed to optimize scaffold geometry and direction and extent of radial superficial velocity of the culture medium across the cell mass for the culture of clinical-size bioengineered tissues in rPBBs, under the assumption that radial fluxes of culture medium are uniformly distributed along the construct length.

2. In the third chapter, a criterion to optimize radial flux distribution of culture medium along the construct length is presented based on a two-dimensional stationary momentum transport model accounting for the fluid dynamics of the void spaces and time-changing construct properties.

3. In the fourth chapter, a two-dimensional steady-state model is presented describing mass and momentum transport in the rPBB to determine the actual influence of medium radial flux distribution on mass transport towards the cells during tissue reconstruction and to design rPBBs providing controlled physiological supply of oxygen to cells depending on their metabolic requirements for a given therapeutic objective.

Chapter 2[1]

Model-based optimization of scaffold geometry and operating conditions of radial flow packed-bed bioreactors for therapeutic applications

2.1 Introduction

In recent years, the scarcity of donor tissue to replace the mechanical or metabolic functions of missing or failing tissue has prompted the search for alternative treatments (Langer et al., 1995). An interesting alternative to tissue replacement with artificial grafts and to animal models for *in vitro* drug screening is to engineer biological substitutes of human tissue by seeding isolated autologous cells in three-dimensional (3D) porous scaffolds and by guiding cell re-organization and differentiation in bioreactors in which cells are subject to physiological mechanical and biochemical cues. In the repair of large bone defects, the presence of autologous cells could eliminate rejection of allo- or xenografts and could enhance graft osteointegration as compared to artificial bone grafts (VandeVord et al., 2005). In the extracorporeal assist to liver failure patients, treatments based on bioreactors using engineered liver tissue could provide the patient with more liver-specific functions (virtually all of them) than non-specific artificial treatments and bioreactors using immortalized cell lines or enzymes (Zeilinger et al., 2004).

An important step in the realization of clinical-scale engineered tissue is the construct culture in bioreactors designed and operated in such a way to guide cell re-organization and differentiation as in the natural tissue. Cell culture in the presence of controlled physiological concentrations and supply of nutrients and dissolved oxygen is a basic bioreactor requirement to ensure cell survival and to make cells differentiate to a given phenotype. Pure diffusive transport in static bioreactors has been shown to subject cells to oxygen and nutrients concentrations steeply varying across the

[1] This chapter is adapted from Donato, D; De Napoli, I.E.; Catapano, G. Model-Based Optimization of Scaffold Geometry and Operating Conditions of Radial Flow Packed-Bed Bioreactors for Therapeutic Applications. *Processes* **2014**, 2, 34-57.

construct and to limit the realization of clinical-scale 3D cell constructs (Wendt et al., 2003; Glicklis et al., 2000; Gaspar et al., 2012; Muschler et al., 2004; Griffith and George, 2005). To minimize the diffusive limitations to external solute transport, bioreactors have been proposed in which some degree of external convection is superimposed over pure diffusion by perfusing the medium around or along the construct. Radial medium perfusion along two-dimensional (2D) cultures of liver cells in a gel sandwich adherent to glass discs (Jaesung et al., 2008) or constrained between microporous membranes encased in a rigid frame (Niu et al., 2009) permits the design of more compact bioreactors than the typical flasks or dishes. Medium convection around 3D porous constructs in spinner flasks and rotating wall vessel bioreactors has been reported to improve cell distribution and viability with respect to static bioreactors but has not been shown to permit adequate oxygen and nutrients supply to cells deep into the construct and adequate expression of cell differentiation markers (Granet et al., 1998; Sikavitsas et al., 2002; Catapano and Gerlach, 2007). Medium supplementation with carriers reversibly binding oxygen (e.g., cross-linked hemoglobins or perfluorocarbons) has also been proposed to mimic the oxygen storage function of hemoglobin in the red blood cells and overcome the low solubility of oxygen in aqueous media (Radisic et al., 2005; Sullivan and Palmer, 2006). The inclusion of porous hydrophobic microspheres in 3D collagen gel constructs has been shown to enhance oxygen diffusive transport, and increase the oxygen penetration depth, into the construct and hepatocyte functions by promoting some degree of local natural convection at the gel interface with the microspheres (McClelland and Coger, 2000, 2004). Direct axial perfusion of 3D porous constructs with medium in axial-flow packed bed bioreactors (aPBBs) has been shown to enhance oxygen and nutrients transport to cells internal to the construct as compared to static culture (Kim et al., 2000; Bancroft et al., 2002; Warnock et al., 2005; Frolich et al., 2010), but also to possibly cause poor cell nourishment (Piret et al., 1991; Fassnacht and Portner, 1999) or cell wash out when medium is perfused at axial superficial velocity low enough to avoid cell detachment or high enough to ensure cell survival, respectively (Singh et al., 2007).

Radial perfusion with medium of cells seeded onto 3D annular porous scaffolds has been shown to be advantageous over pure diffusive operation and direct axial perfusion to realize biological tissue substitutes for tissue replacement or for the *in vitro* toxicity screening of new drugs (Kurosawa et al., 1991; Kino-Oka and Taya, 2005; Guillouzo and Guguen-Guillouzo, 2008). However, only a few reports have been published on the culture of human cells seeded in 3D porous scaffolds in radial-flow packed-bed bioreactors for therapeutic applications, which suggest the successful use of this bioreactor configuration particularly for the development of bioengineered bone (Xie et al., 2006; Olivier et al., 2007; Arano et al., 2010; Katayama et al., 2013) and liver (Hongo et al., 2005; Miskon et al., 2007; Morsiani et al., 2000 and 2001; Ishii et al., 2008; Kawada et al., 1998; Saito et al., 2006).

In the absence of thorough experimental information, the peculiar features of rPBBs could be exploited with the help of mathematical models of momentum and solute transport across the construct. In this chapter reference is mainly made to the few models proposed for mammalian cell culture in rPBBs because they account for some typical cell features, such as the sensitivity of their metabolism to the culture environment (e.g., pericellular dissolved oxygen and nutrients concentration, shear stress, pressure), and the fact that some cell types proliferate during culture thus changing both the geometry of the flow channel and the conditions under which the bioreactor is operated, among others. All models propose a pseudo-homogeneous description of transport across the construct, and neglect transport in the inner hollow cavity and the peripheral annular space. Tharakan and Chau (Tharakan and Chau, 1987) proposed a steady-state transport model of the limiting metabolic substrate and the products across an annular bed of mammalian cells perfused outwards with medium for the production of monoclonal antibody. The model accounts for dispersive and convective solute radial transport across the cell construct, for substrate consumption in terms of the Monod kinetics and for the possible presence of semipermeable membranes in the cell mass, albeit in lumped fashion. The model was used to investigate the effect of the dimensionless radial superficial velocity, the dimensionless construct thickness, and the cell

metabolic activity on the substrate conversion to products and their distribution across the cell construct. Cima *et al*. (Cima et al., 1990) described the steady-state transport by diffusion and convection of dissolved oxygen and nutrients across an annular bed of cells seeded in the thin gap between two concentric thick-walled microporous hollow fiber membranes. Dimensionless analytic expressions for the dissolved oxygen and nutrients concentrations across the cell mass have been reported for zero-th order cellular consumption kinetics and for uniform solute concentrations in the inner fiber lumen and outside the outer fiber wall, equal to each other. The model was used to investigate the effect of the dimensionless radial superficial velocity and solute consumption rate on the dissolved oxygen and nutrients concentrations across the cell mass for a given hollow fiber membranes geometry, outward medium perfusion flow, and cells with low metabolic requirements. Böhmann *et al*. (Bohmann et al., 1992) developed and experimentally validated a lumped parameter model describing radial perfusion and metabolic consumption of dissolved oxygen across a 35 mm thick annular bed of SIRAN® macroporous beads wrapped in a dialysis membrane in which hybridoma cells were cultured. The model was used to investigate the influence of the concentration of low-molecular weight solutes, freely permeable across the membrane, and high molecular weight solutes, retained in the bed, on long-term monoclonal antibody production. The model enabled the bioreactor scale-up from a 0.1 L to a 5 L bed volume (Pörtner et al., 2007).

A systematic analysis of the influence of all the dimensionless parameters accounting for geometrical, transport and operational parameters on bioreactor performance to enable culture of clinical-scale substitutes for tissue replacement under controlled pericellular environment has not been reported yet. Assuming that uniform radial flux distribution of culture medium along the construct length may be achieved for a given construct geometry, the first step in the optimization of rPBB design is the optimization of construct geometry and shape and of the medium flow configuration (*i.e*. direction and extent of the radial superficial velocity of the culture medium) enabling survival of cells, which have a concentration-dependent solute consumption kinetics, with a given radial perfusion rate to avoid cell damage or wash out.

In this chapter, it is proposed a model-based reference framework aimed to optimize scaffold geometry and operating conditions (*i.e.*, direction and superficial velocity of the perfusing medium) of convection-enhanced rPBBs for therapeutic applications. The framework relies on a one-dimensional pseudo-homogeneous model based on the Darcy and the convection-dispersion-reaction equation to describe the pseudo steady-state transport of momentum and dissolved oxygen in annular porous constructs of varying geometry, which are perfused with medium flowing in different directions, under the assumption that uniform radial flux of culture medium is ensured along the construct length, and in which human cells consuming oxygen according to Michaelis-Menten kinetics are cultured at varying concentrations. Dimensional analysis is used to identify the dimensionless groups determining the bioreactor performance expressed in terms of a more apt parameter to therapeutic applications.

2.2 Materials and Methods

2.2.1 Model Development

2.2.1.1 Convection-enhanced transport model of rPBB

A model was developed to describe the transport of momentum and low molecular weight solutes in convection-enhanced radial packed-bed bioreactors. The attention was focused on oxygen for its importance to cell metabolism (Rotem et al., 2004; Catapano et al., 1996; Allen et al., 2005; Volkmer et al., 2008; Griffith et al., 2009). Schemes of an rPBB with opposite perfusion flows are reported in Figure 2.1. The bioreactor consists of a cylindrical chamber equipped with inlet and outlet fittings in which it is located a 3D cylindrical porous scaffold of length L, outer radius R_o, and porosity ε, with a coaxial hollow cavity of radius R. Human cells are seeded and cultured at a concentration C_{cell} in the pores of the construct annular wall of thickness δ_C. Medium of viscosity μ carrying oxygen at a concentration C_o is fed to the bioreactor at a flow rate Q and continuously flows radially across the construct from the outer peripheral annular space towards the inner hollow

cavity (*i.e.*, inwards), as shown in Figure 2.1a, or from the inner hollow cavity towards the outer peripheral annular space (*i.e.*, outwards), as shown in Figure 2.1b, at a maximal superficial velocity v_o at the inner construct surface (*i.e.*, $r = R$). In the inner hollow cavity and the peripheral annular space medium is assumed to flow axially in opposite directions and is assumed well-mixed (*i.e.*, solute concentration is uniform throughout). The flow configurations considered are often referred to as CP-π flow (or centripetal) (Figure 2.1a) or CF-π flow (or centrifugal) (Figure 2.1b) (Chang et al., 1983). The term π-flow indicates that medium flow directions in the inner hollow cavity and the peripheral annular space are opposite. Dissolved oxygen is carried by the medium into the construct where it is transported to the cells by convection (*i.e.*, associated to the net medium flow) and dispersion with a dispersion coefficient D_C (*i.e.*, transport is promoted by a concentration gradient in the presence of the flowing medium), and it is metabolized by the cells. At low medium superficial velocity across the construct, the concentration gradient-driven oxygen transport occurs mainly by diffusion (Delgado, 2006). At high medium superficial velocity, the mixing generated by the medium flowing across the porous scaffold becomes important and the concentration gradient-driven oxygen transport is mainly dispersive (Delgado, 2006). The conservation equations governing the rPBB performance were obtained under the following assumptions:

1. axial symmetry;
2. steady-state conditions;
3. incompressible fluid;
4. isothermal conditions;
5. transport in the construct is described according to a pseudo-homogeneous approach;
6. construct is described as an isotropic porous medium with Darcy permeability k;
7. uniform cell distribution C_{cell};
8. no cell lysis or apoptosis;

9. solute concentration in the construct does not vary along the axial and angular coordinates;
10. momentum transport in the construct is described according to the Darcy equation;
11. dissolved oxygen is transported across the construct by convection and dispersion;
12. cells consume oxygen according to Michaelis-Menten kinetics, with a maximal cell-specific consumption rate G and a Michaelis constant K_M.

Under these assumptions, upon introducing the following non-dimensional coordinates and variables

$$r^* = \frac{r}{R};\ v_C{}^* = \frac{v_C}{v_o};\quad P_C^* = \frac{P_C}{v_o \mu L/R^2};\ C_C{}^* = \frac{C_C}{C_o};\ \beta = \frac{K_M}{C_o} \tag{2.1}$$

the governing conservation equations in the construct may be re-arranged in dimensionless form to give:

continuity equation

$$v_C{}^* = \frac{1}{r^*} \tag{2.2}$$

momentum conservation (Darcy equation)

$$v_C{}^* = -\gamma \frac{kL}{R^3} \frac{dP_C{}^*}{dr^*} \tag{2.3}$$

mass conservation

$$Pe_{rad,\max} \frac{R}{\delta_C} \left(v_C{}^* \frac{dC_C{}^*}{dr^*} \right) = \frac{1}{r^*} \frac{d}{dr^*} \left(r^* \frac{dC_C{}^*}{dr^*} \right) - \gamma \phi_C{}^2 \frac{R^2}{\delta_C{}^2} \frac{C_C{}^*}{\beta + C_C{}^*} \tag{2.3}$$

where $\gamma = 1$ in the case of outward flow, and $\gamma = -1$ in the case of inward flow. Equation 2.3 is subject to the boundary condition stating that the outlet pressure equals atmospheric pressure, as follows:

B.C. 1a $\quad outward\,flow(\gamma=1) \quad r^* = 1+\frac{\delta_C}{R} \quad P_C{}^* = 0$ (2.4a)

B.C. 1b $\quad inward\ flow(\gamma=-1) \quad r^* = 1 \quad P_C{}^* = 0$ (2.5b)

Equation 2.4 is subject to two boundary conditions, of which B.C.2 states the continuity of solute flux at the entrance to the construct in terms of Danckwert's condition, and B.C.3 states the continuity of fluxes across the outer construct surface when solute concentration does not change any further once the medium leaves the construct, as follows:

B.C. 2a $\quad outward\ flow(\gamma=1) \quad r^* = 1 \quad 1 = C_C{}^* - \frac{1}{Pe_{rad,\max}} \frac{\delta_C}{R} \frac{dC_C{}^*}{dr^*} = 0$ (2.5a)

B.C. 2b $\quad inward\ flow(\gamma=-1) \quad r^* = 1+\frac{\delta_C}{R} \quad 1 = C_C{}^* - \frac{1}{Pe_{rad,\max}} \frac{\delta_C}{R}\left(1+\frac{\delta_C}{R}\right) \frac{dC_C{}^*}{dr^*} = 0$ (2.6b)

B. B.C. 3a $\quad outward\ flow\,(\gamma=1) \quad r^* = 1+\frac{\delta_C}{R} \quad \frac{dC_C^*}{dr^*} = 0$ (2.6a)

B.C. 3b $\quad inward\ flow\,(\gamma=-1) \quad r^* = 1 \quad \frac{dC_C^*}{dr^*} = 0$ (2.7b)

When $Pe_{rad,\max} >> 1$, Equations 2.6a,b state that solute concentration in the stream entering the construct equals that in the feed.

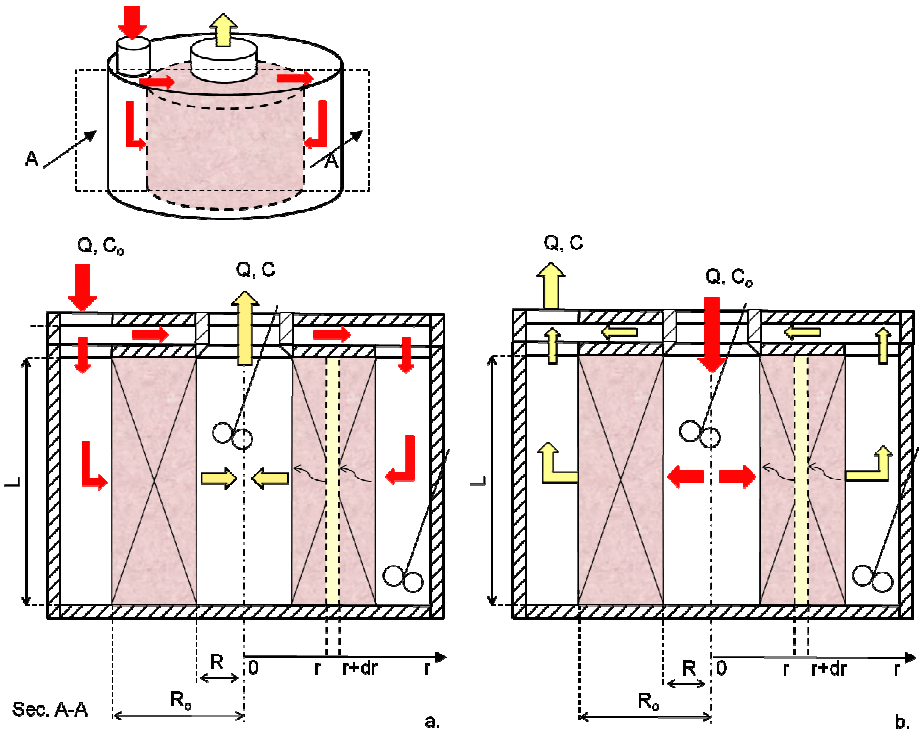

Figure 2.1. Scheme of radial flow packed-bed bioreactors (rPBBs) with opposite perfusion flows across the annular construct wall: (**a**) inward flow; (**b**) outward flow.

2.2.1.2. Diffusion-limited transport model of rPBB

For the sake of comparison, a diffusion-limited model of solute transport in the rPBB was also developed. In this case, the construct is assumed to be dipped and held suspended in medium carrying oxygen at a concentration C_o in a reservoir and medium has unhindered access to the hollow cavity. Under the same assumptions as in the convection-enhanced transport model, but for the fact that oxygen transport occurs only by diffusion with an effective diffusion coefficient D_{eff}, and for the same non-dimensional coordinates and variables as in Equation 2.1, the governing mass conservation equation in the construct may be re-arranged in dimensionless form to give:

$$\frac{1}{r^*}\frac{d}{dr^*}\left(r^*\frac{dC_C{}^*}{dr^*}\right)=\phi_D{}^2\frac{R^2}{\delta_C{}^2}\frac{C_C{}^*}{\beta+C_C{}^*} \tag{2.7}$$

which is subject to two boundary conditions stating that both the inner and the outer construct surfaces are exposed to the same dissolved oxygen concentration in medium C_o (*i.e.*, well mixed reservoir):

B.C. 1 $$r^* = 1 \qquad C_C^* = 1 \tag{2.8a}$$

B.C. 2 $$r^* = 1 + \frac{\delta_C}{R} \qquad C_C^* = 1 \tag{2.9b}$$

2.2.1.3. Convection-enhanced transport model of aPBB

To compare the rPBB performance to that of an aPBB, reference was made to the dimensionless design equations of aPBBs in which medium carrying oxygen at a concentration C_o perfuses at an axial superficial velocity u_o a cylindrical construct of length L and radius R, as in (Fogler, 2006). Under the same assumptions as in the convection-enhanced transport model of rPBB, and for the same non-dimensional coordinates and variables as in Equation 2.1 but for $z^* = z/L$, the governing mass conservation equation in the construct may be re-arranged in dimensionless form to give:

momentum conservation (Darcy equation)

$$u_C{}^* = -\frac{k}{R^2}\frac{dP_C{}^*}{dz^*} \tag{2.9}$$

mass conservation

$$Pe_{ax} u_C{}^* \frac{dC_C{}^*}{dz^*} = \frac{d^2 C_C{}^*}{dz^{*2}} - \phi_C{}^2 \frac{C_C{}^*}{\beta + C_C{}^*} \tag{2.10}$$

Equation 2.10 is subject to the boundary condition stating that the outlet pressure equals atmospheric pressure, as follows:

B.C. 1 $$z^* = 1 \qquad P_C^* = 0 \tag{2.11}$$

Equation 2.11 is subject to two boundary conditions of which B.C. 2 states the continuity of solute flux at the entrance to the construct in terms of Danckwert's condition, and B.C. 3 the continuity of

fluxes across the outer construct surface when solute concentration does not change any further once the medium leaves the construct, as follows:

B.C. 2 $$z^* = 0 \qquad 1 = C_C{}^* - \frac{1}{Pe_{ax}} \frac{dC_C{}^*}{dz^*} \tag{2.12a}$$

B.C. 3 $$z^* = 1 \qquad \frac{dC_C{}^*}{dz^*} = 0 \tag{2.13b}$$

2.2.2. Dimensionless Groups

2.2.2.1. Convection-enhanced transport model of rPBB

Analysis of dimensionless Equations 2.1–2.7 shows that the rPBB performance is determined by the six dimensionless groups reported in Table 2.1. The physical interpretation of most of these dimensionless groups is well established (Bird et al., 2007). The dimensionless group $k\,L/R^3$ may be interpreted as the dimensionless Darcy permeability of the construct and provides information about the radial pressure drop across the construct at a given flow rate. The higher its value, the lower the radial pressure drop across the construct. The construct inner radius-to-wall thickness ratio, R/δ_C, accounts for the construct curvature. The higher the inner radius or the thinner the thickness of the annular wall, the more negligible the construct curvature. The maximal radial Peclet number, $Pe_{rad,\max}$, compares the maximal rate of solute transport in the construct by convection to dispersion. The higher its value, the higher the importance of convection to solute transport as compared to dispersion. The Thiele modulus compares the maximal zero-th order solute consumption rate, $V_{\max} = C_{cell} \cdot G$, to the maximal rate of dispersive solute transport, $C_o\,D_C/\delta_C{}^2$. High Thiele moduli may be associated with high cell concentrations, C_{cell}, or high cell-specific metabolic consumption rates, G. The saturation parameter β provides information on the extent to which the consumption kinetics differs from the zero-th order. The higher its value, the closer the kinetics to the first order.

Group Definition	Description
1. γ	perfusion flow direction parameter
2. $k\,L/R^3$	dimensionless Darcy permeability of construct
3. R/δ_C	inner radius-to-thickness ratio of the construct
4. $v_o\,\delta_C/D_C$	maximal radial Peclet number, $Pe_{rad,max}$
5. $\sqrt{(V_{max}\delta_C^2/(D_C\,C_o))}$	Thiele modulus, φ_C
6. K_M/C_o	saturation parameter, β

Table 2.1. Dimensionless groups determining the rPBB performance.

2.2.2.2 Diffusion-limited transport model of rPBB

Analysis of dimensionless Equations 2.8 and 2.9 shows that under diffusion-limited operation, the performance of the rPBB is determined only by the construct curvature, R/δ_C, the Thiele modulus $\varphi_D = \sqrt{(V_{max}\,\delta_C^2/(D_{eff}\,C_o))}$ and the saturation parameter $\beta = K_M/C_o$.

2.2.2.3 Convection-enhanced transport model of aPBB

Analysis of dimensionless Equations 2.10–2.13 shows that the dimensionless groups determining the performance of an axial-flow packed bed bioreactor are the dimensionless Darcy permeability of the construct, k/R^2, the axial Peclet number, $Pe_{ax} = u_o\,L/D_C$, the Thiele modulus $\varphi_C = \sqrt{(V_{max}\,L^2/(D_C\,C_o))}$ and the saturation parameter $\beta = K_M/C_o$.

2.2.3. Computational Methods

The resulting set of governing equations for a convection-enhanced or a diffusion-limited rPBB, and for an aPBB, was integrated numerically with the commercial Finite Element Method (FEM) code Comsol Multiphysics (Comsol Inc., Burlington, MA, USA). An optimal non-uniform mesh with more than 20,000 rectangular elements, finer at the construct inner and outer surfaces, was

generally used to describe the spatial domain. Model-predicted spatial profiles of superficial velocity, pressure and dissolved oxygen concentration were obtained for values of the model parameters and dimensionless groups representative of those used in experiments in which rPBBs were used, or typically reported or of interest for therapeutic applications, as reported in Tables 2.2 and 2.3 unless otherwise stated. In particular, the effective diffusivity of oxygen, D_{eff}, was estimated according to (Fogler, 2006) by multiplying that in water at 37 °C (Han and Bartels, 1996) by a construct porosity $\varepsilon = 0.7$, typical of the 3D porous scaffolds used in rPBBs (Xie et al., 2006; Olivier et al., 2007). The dispersion coefficient for oxygen in the construct was estimated by adjusting the diffusivity according to the correlations for liquids in (Delgado, 2006) for the value of the maximal radial superficial velocity, v_o. The value of v_o was set equal to 1.98×10^{-4} m/s throughout, consistent with the values used in the few culture experiments reported for rPBBs with small-scale constructs seeded with human cells (Xie et al., 2006; Olivier et al., 2007).

Group Definition	Description
1. perfusion flow direction parameter, γ	−1 (inwards), 1 (outwards)
2. dimensionless Darcy permeability of construct, $k\,L/R^3$	2.24×10^{-10}–2.24×10^{-4}
3. construct curvature, R/δ_C	0.1–10
4. maximal radial Peclet number, $Pe_{rad,max}$	49
5. Thiele modulus, φ_C or φ_D	1–20
6. saturation parameter, β	0.019

Table 2.2. Dimensionless group values used for model predictions, unless otherwise stated.

Symbol	Model Parameter	Value	Units	Reference
C_o	oxygen inlet concentration	0.216	mol/m^3	(Abdullah et al., 2006)
D	oxygen diffusivity in water	2.64×10^{-9}	m^2/s	(Han and Bartels, 1996)
D_{eff}	effective oxygen diffusivity in the construct	1.85×10^{-9}	m^2/s	(Fogler, 2006)
D_C	oxygen dispersivity in the construct	2×10^{-8}	m^2/s	(Delgado, 2006)
K_M	oxygen Michaelis constant	4.05×10^{-3}	mol/m^3	(Zahm et al., 2010)
k	Darcy permeability of construct	1.4×10^{-13}	m^2	(Chen and Palmer, 2009)
L	scaffold length	0.2	m	
v_o	maximal inlet superficial velocity	1.98×10^{-4}	m/s	(Olivier et al., 2007)
δ_C	scaffold thickness	0.005	m	(Olivier et al., 2007)
μ	medium viscosity	6.92×10^{-4}	Pa s	(Abdullah et al., 2006)

Table 2.3. Model parameter values used for model predictions, unless otherwise stated.

Although the spatial dissolved oxygen concentration profiles are essential to assess the actual pericellular culture conditions, a more helpful approach to the first decisional phases of design is to condense bioreactor performance in one parameter only, and to analyze the influence of the most relevant dimensionless groups on this performance parameter. With respect to oxygen, the basic requirement for cell survival is that cells should be supplied with physiological amounts of oxygen and should be cultured at physiological dissolved oxygen concentrations anywhere in the construct. To this purpose, an alternative performance parameter was introduced that was deemed more significant to bioreactor designers for therapeutic applications. It provides information on the volume fraction of the construct in which cells are exposed to physiological dissolved oxygen concentrations, and was termed the non-hypoxic fractional construct volume (NHy-FCV). In this

work, the minimal value for physiological oxygen concentrations was set equal to 2×10^{-2} mM, a typical threshold for mammalian cells (Loiacono and Shapiro, 2010).

2.3 Results and Discussion

Radial-flow packed bed bioreactors have distinctive features that make them interesting for therapeutic applications. Their structure resembles the architecture of long bones (e.g., the femur shaft) (Clarke, 2008) and the medium perfusion pattern is similar to blood in the liver lobule (Tortora and Derrickson, 2006), when the construct is perfused inwards. Radial perfusion enhances solute transport to cells with respect to pure diffusion. Radially perfused hollow cylindrical constructs feature also a larger cross-sectional area and a shorter path-length for solute transport than axially perfused constructs. In this chapter, a model reference framework is presented to help designers of rPBBs optimize their geometry and operation to meet given therapeutic requirements. The framework is based on the model described by Equations 2.1–2.9 in which the pseudo steady-state transport of momentum and dissolved oxygen across an annular cell-seeded construct is described according to the Darcy and the dispersion-convection-reaction equation, respectively. The dimensionless groups determining the actual dissolved oxygen concentration profile in the construct and the performance of the rPBB were obtained by dimensional analysis of Equations 2.1–2.9 and are shown in Table 2.1. The pseudo steady-state assumption is not a limitation to the use of the model. In fact, the large difference in the time scale typical of bioreactor dynamics (of the order of the minute) and of the kinetics of cell growth (of the order of the day), makes it possible to use the model for investigating bioreactor performance as cells proliferate and/or secrete an own ECM by adjusting the dimensionless groups values to the maturation of the cell construct. Another important assumption in the model development is that medium flows at uniform superficial radial velocity along the bioreactor length. In fact, maldistribution of radial velocity has been reported to have more influence on the performance of radial-flow packed bed reactors for industrial applications than other parameters, such as the flow direction (Ponzi and Kaye, 1979). In the use of rPBBs for

human cell culture, a non-uniform superficial radial velocity would cause a non-uniform supply of dissolved oxygen, nutrients and biochemical cues to cells that, during culture, might yield a non-uniform cell distribution in the construct as an effect of poor cell proliferation or cell necrosis in the poorly perfused regions of the construct. As tissue matures, this would cause the Darcy permeability of the construct to decrease non-uniformly thus worsening even further the radial flow maldistribution and its effects. As Figure 2.1 shows, in the model development reference was made to rPBBs in which the directions of axial flow in the inner hollow cavity and the outer peripheral annular space are opposite, *i.e.*, a π-flow type bioreactor configuration, to make it more likely that the actual radial superficial velocity be uniformly distributed along the bioreactor length under actual operation. In fact, if the frictional pressure drop is negligible in the inner hollow cavity and the outer peripheral annular space, independent of the flow direction, the axial pressure profiles in these regions develop in such a way to maintain a constant radial pressure drop across the construct (Chang et al., 1983).

2.3.1 Model validation

The scarcity of experimental data for human cell culture in convection-enhanced rPBBs and the difficult procurement of detailed information on the conditions and geometry used made it awkward to validate the model. For these reasons, model goodness was assessed by comparing the model-predicted dissolved oxygen concentration profiles across the annular constructs to those predicted by Cima *et al*. (Cima et al., 1990) and the model-predicted glucose consumption, to that reported by Olivier *et al*. (Olivier et al., 2007) for the culture of osteosarcoma cells in an rPBB perfused with medium both inwards and outwards, as shown in Figure 2.2. In the latter case, the rPBB was assumed to be connected in closed loop to a completely mixed reservoir, and its dynamics was neglected with respect to the reservoir on the account of its small volume. Glucose consumption was estimated from the model-predicted decrease of glucose concentration in the reservoir after 24 h. Figure 2.2a shows that the predictions of the model presented in this paper were

in good agreement with those reported by Cima *et al*., for the geometry and the operating conditions used therein, *i.e.*, zero-th order consumption kinetics, Thiele moduli typical of cells with low metabolic requirements, and exposure of the construct inner and outer surfaces to equal dissolved oxygen concentrations (Cima et al., 1990). Figure 2.2b shows that the model effectively predicted also the experimental results reported by Olivier *et al*., for the culture of osteosarcoma cells in an rPBB (Olivier et al., 2007). In this case, the cell-specific glucose consumption rate was estimated with the diffusion-limited transport model as that best fitting the experimental data reported for static culture in the rPBB. When medium was perfused outwards, the decreased cell concentrations that were observed by Olivier *et al*. in the construct, likely as an effect of cell wash-out, were taken into account.

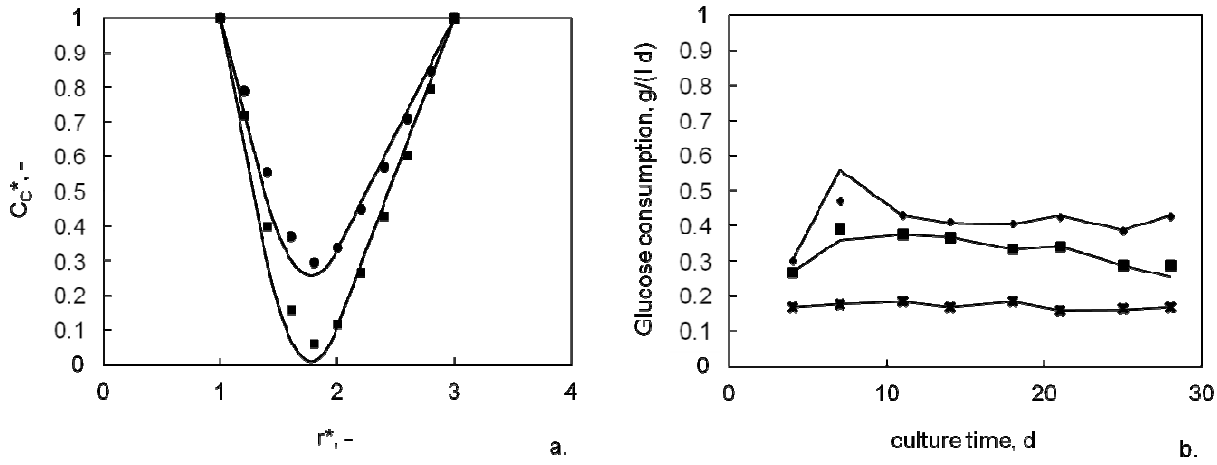

Figure 2.2. Comparison of model-predicted low molecular weight substrate concentrations to: (**a**) the theoretical predictions for dissolved oxygen of Cima *et al*. (Cima et al., 1990); (**b**) the experimental data for glucose consumption of Olivier *et al*. (Olivier et al., 2007). Predictions obtained for the following parameter values: (**a**) $\gamma = 1$, $R/\delta_C = 1.49$, $Pe_{rad,max} = 0.67$, $k\,L/R^3 = 1.5 \times 10^{-2}$, $\varphi_C = 1.16$ (●) and 1.34 (■); (**b**) $R/\delta_C = 0.4$, $Pe_{rad,max} = 1071$, $kL/R^3 = 2.5 \times 10^{-7}$, $\varphi_C = 0.82-0.93$, $\beta = 0.02$, for perfusion inwards $\gamma = 1$ (♦), outwards $\gamma = -1$ (■), or static operation (x).

2.3.2 Convection-enahced vs. diffusion-limited rPBBs

Model predictions show the convenient characteristics of radial-flow packed bed bioreactors as compared to static operation and axial-flow packed bed bioreactors in the culture of cell-seeded constructs. Figure 2.3 shows that radial perfusion in an rPBB may yield better oxygen supply to

cells anywhere in the construct and more uniform pericellular dissolved oxygen concentrations than static operation. In spite of the fact that under static operation oxygen is supplied to cells through both the inner and the outer construct surfaces, when transport is diffusion-limited the dissolved oxygen concentration steeply decreases towards the innermost regions of the annular construct. Oxygen depletion gets worse when highly concentrated cells with high metabolic requirements are cultured, *i.e.*, as the Thiele modulus increases. Figures 2.3a,b show that under static operation for $V_{max} = 1.76 \times 10^{-9}$ mol/(mL s) cells would be cultured under anoxic conditions in about 65% of the construct volume. This could be the case of osteoblasts consuming oxygen at $G = 5.5 \times 10^{-17}$ mol/(s cell) (Komarova et al., 2000) cultured in a 3D porous hollow cylindrical scaffold at a concentration of $C_{cell} = 3.2 \times 10^{7}$ cells/mL (Warnock et al., 2005). When the same construct is radially perfused with medium at $Pe_{rad,max} = 49$, independent of the direction of the perfusion flow, the radial dissolved oxygen concentration profile is about uniform across the construct at the same value as in the feed as long as the cell-specific oxygen consumption rate and cell concentration yields V_{max} up to *ca*. 1.8×10^{-10} mol/(s mL). Independent of the flow direction, at higher Thiele moduli the dissolved oxygen concentration smoothly decreases along the direction of medium perfusion. Figures 2.3a,b show that for $V_{max} = 1.76 \times 10^{-9}$ mol/(s mL) the minimal dissolved oxygen concentration nowhere gets below ca. 50% of that in the feed. Such a remarkable transport enhancement may be attributed directly to convection, but also to the convection-related increase of the dispersion coefficient.

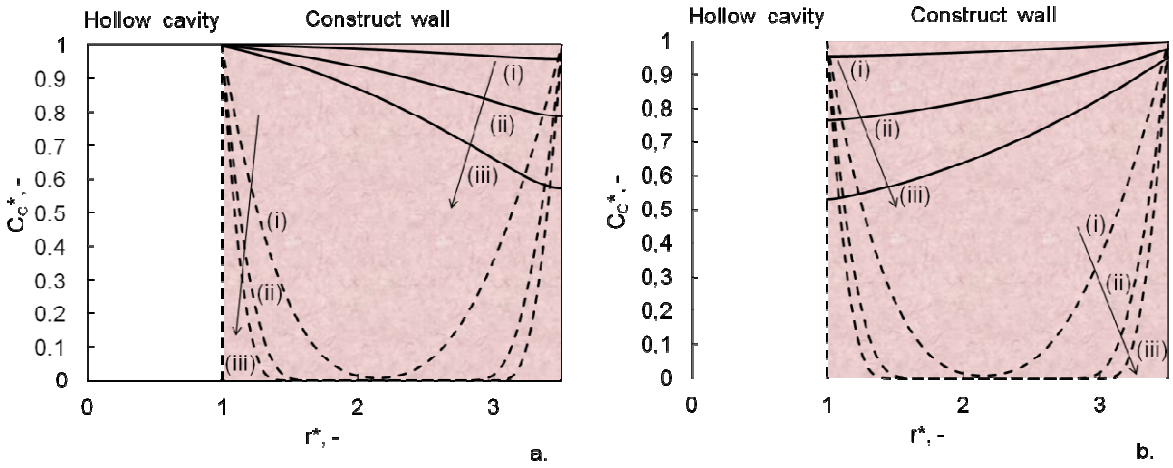

Figure 2.3. Dimensionless radial oxygen radial concentration profiles at varying maximal oxygen consumption rates V_{max}: (i) 1.76 × 10^{-10} mol/(s mL); (ii) 8.8 × 10^{-10} mol/(s mL); (iii) 1.76 × 10^{-9} mol/(s mL) for cells cultured in a hollow cylindrical construct in an rPBB radially perfused with medium (solid lines) (**a**) outward or (**b**) inwards, or (dashed lines) statically operated. Parameter values: R/δ_C = 0.4, $Pe_{rad,max}$ = 49. Other parameters are as in Tables 2.2 and 2.3.

2.3.3 Radial vs. axial PBBs

The performance of an rPBB was compared to that of an aPBB for the case of the bioengineering of a clinical-scale long bone graft (e.g., a femur shaft) or of a bioreactor for a bioartificial liver (BAL), under the constraint that the construct length and volume, and the maximal superficial velocity be equal to the aPBB. For the superficial velocity this means that $v_o = u_o$. In the case of the aPBB, the bioengineered femur shaft was approximated with a cylindrical porous construct 40 cm long and 3.5 cm in diameter, similar in size to the human femur shaft (Clarke, 2008), and the bioreactor for BAL was assumed to be based on a cylindrical porous construct 20 cm long and 3 cm in diameter so as to be easily fitted in the housing of some clinical-scale BAL bioreactors proposed in the last years (Catapano and Gerlach, 2007). In either case, the rPBB was assumed to be equipped with a cylindrical construct of equal length and volume with an inner hollow cavity of radius R = 5 mm. For the bone graft, the constructs were assumed to be seeded with 10^7 osteoblasts/mL consuming oxygen at 5.5 × 10^{-17} mol/(cell s) (Komarova et al., 2000). For the liver graft, it was considered the possibility that the constructs are seeded with either hepatocytes or HepG2 cells, consuming oxygen at 9 × 10^{-16} mol/(cell s) (Balis et al., 1999) or 6.62 × 10^{-17}

mol/(cell s) (Mehta et al., 2009), respectively. Radial medium perfusion across the construct generally yields dissolved oxygen concentration profiles, which decrease more smoothly in the direction of medium perfusion than in aPBBs. In the case of the bioengineered long bone graft, Figure 2.4a shows that in an aPBB the dissolved oxygen concentration steeply decreases away from the entrance. This results in a non-hypoxic fractional construct volume of only NHy-FCV = 0.18 and causes cells to be cultured under anoxic conditions in about 78% of the construct volume. Figure 2.4b shows that in an rPBB the dissolved oxygen concentration in the construct decreases more smoothly in the direction of the perfusion flow and it is nowhere below 62% of the feed, largely exceeding the set physiological threshold value. Similar results were obtained in the case of bioreactors for BAL seeded with the HepG2 immortalized cell line (data not shown). Oxygen depletion was much more severe in bioreactors seeded with primary hepatocytes causing cells to be cultured under anoxic conditions in more than 60% of the construct volume. However, in the rPBB the well oxygenated fractional construct volume was about fifteen fold higher than in the aPBB (31% *vs*. 2%, respectively). The transport enhancement in the rPBB may be attributed to the shorter oxygen transport path-length than the aPBB (*i.e.*, the construct annular thickness *vs*. length) that apparently more than compensates for the fact that the axial Peclet number in the aPBB is more than one order of magnitude higher than the maximal radial Peclet number in the rPBB. Bioreactor performance was compared at $v_o = u_o = 1.98 \times 10^{-4}$ m/s because this would guarantee that cells are not damaged by shear stresses. In fact, if the average shear stress acting on cells for medium perfusion in the construct is estimated according to (Wang and Tarbell, 2000), as follows:

$$\tau = \frac{\mu \ v_o}{\sqrt{k}} \tag{2.14}$$

it may be estimated that $\tau = 0.35$ Pa in both bioreactors. This is below the reported range of laminar shear stress at which adherent cells are removed from surfaces (Christi, 2001). However, the maximal pressure drop across the axially perfused construct is about two orders of magnitude higher than in the radially perfused construct which may compress or even crush soft scaffolds and

cause mechanical damage to cells or cell wash-out. Increasing u_o in the aPBB to obtain a smoother axial dissolved oxygen concentration profile would cause an even greater increase of the axial pressure drop that may worsen these effects.

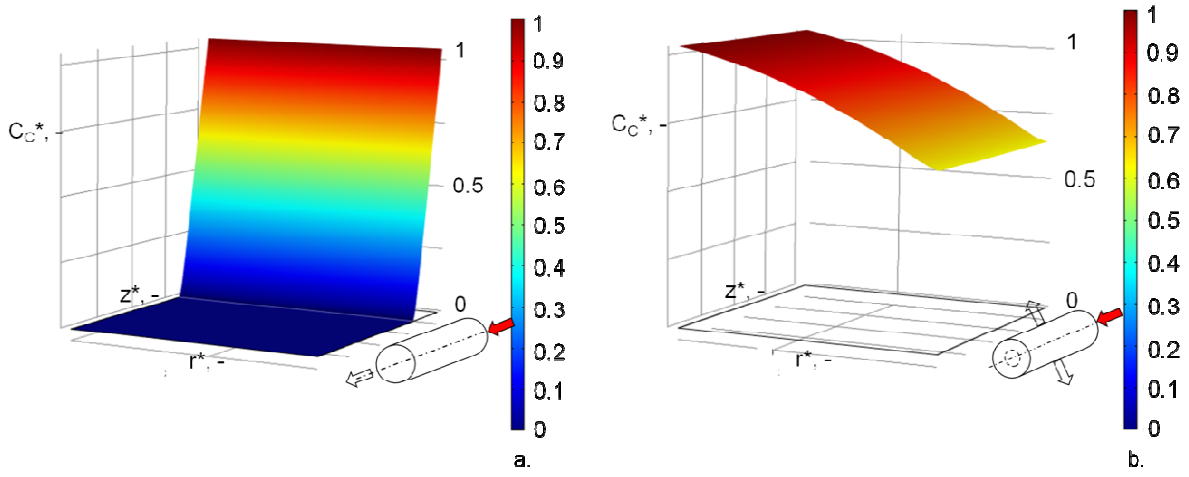

Figure 2.4. Dimensionless oxygen concentrations in a 3D porous bone construct perfused with medium: (**a**) axially (Pe_{ax} = 3910); (**b**) radially outwards ($Pe_{rad,max}$ = 129, R/δ_C = 0.38, γ = 1). Parameter values: $C_{cell} = 10^7$ cell/mL, $G = 5.5 \times 10^{-17}$ mol/(s·cell), L = 40 cm. Other parameters are as in Tables 2.2 and 2.3.

2.3.4 Effect of dimensionless groups on rPBB behavior

In the reports published on convection-enhanced rPBBs, it has not been paid much attention to the effect of the construct curvature on rPBB performance. In the model proposed in this chapter, the construct curvature is accounted for by the ratio of the inner hollow cavity radius to the construct annular thickness, R/δ_C. Model-predicted dissolved oxygen concentration profiles were obtained at varying values of this dimensionless group by keeping δ_C constant and by varying the construct inner radius R to avoid changes of the other dimensionless groups. This way, dimensionless groups such as the $Pe_{rad,max}$ and φ_C, as well as the oxygen transport path-length and medium residence time, were kept constant. Figure 2.5 shows the dissolved oxygen concentration profiles across the annular wall of constructs featuring two values of R/δ_C an order of magnitude different, at increasing Thiele moduli. At any given R/δ_C, the dissolved oxygen concentration decreases in the direction of medium perfusion with a steeper slope as the Thiele modulus increases. Figure 2.5 shows that in constructs with greater curvature, *i.e.*, lower R/δ_C, increasing Thiele moduli

cause a greater oxygen concentration decay along the direction of medium perfusion than in constructs with smaller curvature, *i.e.*, higher R/δ_C. Figure 2.5a shows that for $R/\delta_C = 0.1$ and $\varphi_C = 4$ cells are cultured under hypoxic conditions in about 32% of the construct volume. Figure 2.5b shows that at $R/\delta_C = 1$ and $\varphi_C = 4$ the dissolved oxygen concentration profile is much smoother and oxygen concentration is above 50% of the feed almost everywhere in the construct. This suggests that constructs of smaller curvature, *i.e.*, higher R/δ_C, may help obtain more uniform dissolved oxygen concentration profiles throughout the construct in all those applications in which the control of the pericellular environment is important (e.g., in the *in vitro* toxicity test of drugs).

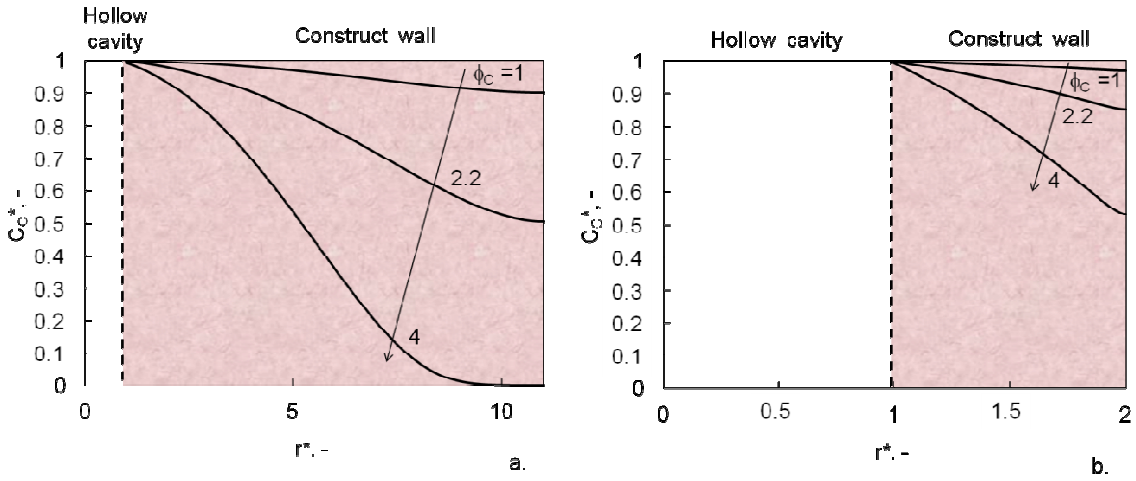

Figure 2.5. Model-predicted dimensionless oxygen concentrations along the annular wall of constructs, cultured in an rPBB and perfused outwards with medium (*i.e.*, $\gamma = 1$), featuring different curvature: (**a**) $R/\delta_C = 0.1$; (**b**) $R/\delta_C = 1$. Other parameters as in Tables 2.2 and 2.3.

In the first decisional phases of the design of rPBBs it may be convenient to condense the bioreactor performance in one parameter only, and to analyze the influence of the most relevant dimensionless groups on this performance parameter. The basic requirement for human cell culture for therapeutic treatments (as well as for the *in vitro* drug testing) is that cells are viable and express differentiated tissue-specific functions for the duration of the treatment (or the *in vitro* test). Culturing cells at controlled pericellular dissolved oxygen concentrations within the physiological range of the specific cell niche seems a reasonable approach to avert cell death by anoxia or by hyperoxic poisoning (Navdeep et al., 2007). In this work, the performance of the rPBB was

condensed in the non-hypoxic fractional construct volume (NHy-FCV). When oxygen convective transport becomes important, the balance between the rate of physical transport and metabolic consumption is better evaluated in terms of the Damköhler number rather than the Thiele modulus. In rPBBs, the radial superficial velocity varies along the construct radius. A minimal radial Damköhler number $Da_{rad,min}$ may be defined as the ratio of the squared Thiele modulus to the maximal radial Peclet number, $Da_{rad,min} = \varphi_C^2/Pe_{rad,max}$. Figure 2.6 shows how the NHy-FCV varies with increasing $Da_{rad,min}$ at values of the curvature, R/δ_C, varying by three orders of magnitude, for both inward and outward medium perfusion. Independent of the direction of medium perfusion and R/δ_C, at sufficiently low $Da_{rad,min}$ the bioreactor is operated under kinetic control, *i.e.*, the dissolved oxygen concentration profile is nearly uniform in the construct, and NHy-FCV approaches unity. At high $Da_{rad,min}$ the bioreactor is operated under transport control, *i.e.*, winning the transport resistance requires significant amounts of the oxygen supplied, and NHy-FCV is lower than unity. Faster consumption rates worsen the scenario, and NHy-FCV linearly decreases with increasing $Da_{rad,min}$ in the log-log plot shown in Figure 2.6. Figure 2.6 shows that the transition between kinetic and transport control occurs at a value of $Da_{rad,min}$ which increases as the curvature of the construct decreases. At any given R/δ_C, the negative slope of the NHy-FCV dependence on $Da_{rad,min}$ under transport-limited conditions is lower when medium is perfused outwards across the construct. Figure 2.6 shows that for $Da_{rad,min} = 0.2$ and $R/\delta_C = 0.1$ cells are well oxygenated in about 90% of the construct volume when medium is perfused outwards, whereas the well oxygenated construct volume decreases to only about 40% when medium is perfused inwards. rPBBs in which constructs with smaller curvature are used, *i.e.*, higher R/δ_C, are generally more robust. In fact, inward medium perfusion or the increase of $Da_{rad,min}$ as tissue matures (e.g., cells proliferate or differentiate to a phenotype with higher metabolic requirements) causes a smaller decrease of NHy-FCV than in the radial perfusion culture of constructs with greater curvature, *i.e.*, lower R/δ_C. Figure 2.6 shows that for $Da_{rad,min} = 1$ and $R/\delta_C = 1$ the NHy-FCV decreases ca. 28% from 0.7 to 0.5 upon switching from outward to inward medium perfusion, respectively. At the same $Da_{rad,min}$ and for $R/\delta_C = 10$, the

NHy-FCV is independent of the direction of medium perfusion. The smaller NHy-FCV for inward medium perfusion may be blamed on the fact that the oxygen-rich feed enters the construct through its outer surface at the minimal superficial radial velocity. Under such conditions, the cells located in the construct periphery consume oxygen at the highest metabolic rate and have time enough to deplete the medium of oxygen and establish steep dissolved oxygen concentration gradients. When medium is perfused outwards, the oxygen-rich feed enters the construct through its inner surface at the maximal radial superficial velocity. Under such conditions, the cells located in the construct close to the inner hollow cavity consume oxygen at the highest metabolic rate but are not given time enough to deplete the medium of oxygen, which will be more available to cells located in the construct periphery where medium flows at the minimal superficial radial velocity. This leads to the establishment of smoother dissolved oxygen concentration profiles along the direction of medium perfusion. The NHy-FCV dependence on the minimal radial Damköhler number $Da_{rad,min}$ shown in Figure 2.6 is consistent with that reported by Moustafa *et al*. (Moustafa et al., 2012), who showed that higher substrate conversions (*i.e.*, lower substrate concentrations) are obtained in rPBRs for industrial applications if the bed of porous inorganic catalyst is perfused inwards when gas-phase reactions with Langmuir-Hinshelwood kinetics take place. The model-predicted effect of the direction of flow perfusion is in apparent contrast to the general use of inward perfusion in published reports on rPBBs and to Olivier *et al*. (Olivier et al., 2007), who reported experiments showing that inward medium perfusion enhances osteoblastic cell proliferation to a greater extent than outward perfusion. In their paper, Olivier *et al*., raised an important practical issue influencing the decision as to whether an rPBB should be perfused with medium outwards or inwards. In fact, many cylindrical scaffolds have pores of increasing size towards their periphery (Kitagawa et al., 2006), causing significant reduction of the local specific surface area. If cells attach weakly to the scaffold surface, for its chemical nature or for the little surface area available for adhesion, outward medium perfusion may exert high enough mechanical stresses to remove the adherent cells and wash them out. When medium is perfused inwards, the finer pores in the construct inner regions

may act as a sieve and may retain the removed cells, thus avoiding cell wash-out. In addition to this, upon assuming that the MG63 osteoblastic cells used in (Olivier et al., 2007) consume oxygen at 1.33×10^{-18} mol/(s cell), as other immortalized cell lines (Rowley et al., 2002), and for a cell concentration of 2.8×10^{6} cell/mL, the minimal radial Damköhler number of the construct may be estimated to be about $Da_{rad,min} = 4.5 \times 10^{-4}$. Figure 2.6 shows that at such a low value of $Da_{rad,min}$ the rPBB is operated under kinetic control and the bioreactor performance is independent of the direction of medium perfusion. This suggests that cell wash-out may indeed have played an important role in making inward medium perfusion enhance the number of cells found in the construct after 7 and 28 days of culture to a greater extent than outward perfusion. This effect should be seriously considered when the conditions are chosen under which an rPBB is operated. Figure 2.6 suggests that, during cell culture in rPBBs, a low $Da_{rad,min}$ should be maintained to minimize oxygen concentration gradients across the construct. This could be achieved by perfusing thin constructs at high maximal radial superficial velocities, v_o, for as much as is permitted by cell resistance to shear damage. It suggests also that, as tissue matures, increasing v_o may balance out the increase of cell metabolic activity caused by cell proliferation and differentiation.

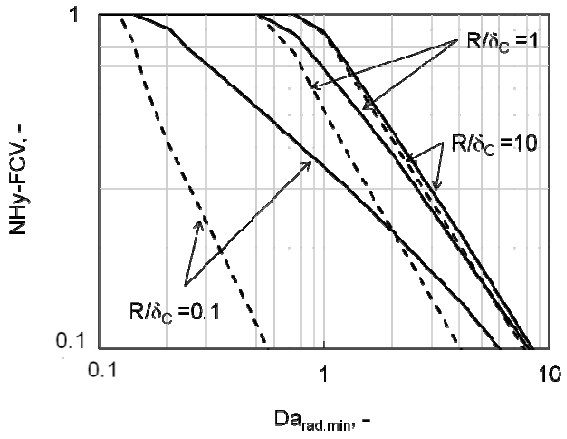

Figure 2.6. Model-predicted dependence on $Da_{rad,min}$ of the NHy-FCV of 3D porous hollow cylindrical constructs featuring varying wall curvature, R/δ_C, in an rPBB when radially perfused with medium outwards ($\gamma = 1$, solid lines), or inwards ($\gamma = -1$, dashed lines).

It is important to recall that model predictions are as good as the assumptions upon which the model is based. An important assumption on transport is that medium perfuses the construct at a

uniform superficial velocity along its length. Axial variations of the porous structure of the scaffold may make its Darcy permeability significantly vary along the construct length and may cause superficial radial velocity maldistribution. In the use of rPBBs for human cell culture, the flow maldistribution would cause a non-uniform supply of dissolved oxygen, nutrients and biochemical cues to cells that, in time, might yield a non-uniform distribution of cells and cell activities. This way, cells would synthesize and deposit the own extracellular matrix non-uniformly in the construct worsening even further the radial flow maldistribution and its effects. Additional phenomena possibly affecting the transport and the actual concentration of larger solutes (e.g., the physical adsorption of proteins to the scaffold) have also been neglected on the account of the low molecular weight and high mobility of oxygen. A word of caution is also in order concerning the fact that the value of condensed performance parameters such as NHy-FCV and the shape of diagrams such as that shown in Figure 2.6 strongly depend on the threshold value set for the dissolved oxygen concentration below which cells become apoptotic or die.

2.4 Conclusions

The use of radial flow packed-bed bioreactors (rPBBs) for therapeutic applications may be advantageous to overcome the typical limitations of static and axial perfusion bioreactors. In this chapter, a reference model framework is proposed to help bioreactor designers optimize geometry and operation of rPBBs to meet given therapeutic requirements. The framework is based on a model in which transport across an annular cell-seeded construct is described according to the Darcy and the dispersion-convection-reaction equations. Dimensional analysis was used to combine more effectively geometric and operational variables in the dimensionless groups determining the rPBB performance. Their effect was investigated on bioreactor performance. The effectiveness of cell oxygenation was also expressed in terms of the non-hypoxic fractional construct volume (NHy-FCV), which was deemed more apt than other integral performance parameters used in technical applications. Model predictions suggest that outward radial perfusion of a 3D porous hollow

cylindrical construct with small curvature (*i.e.*, high inner hollow cavity radius-to-annular thickness ratio) at high perfusion flow rates (*i.e.*, high maximal radial Peclet numbers) may be more convenient than culture in static or axial perfusion bioreactors. In fact, this would enable effective oxygenation of human cells also in large-scale constructs and culture at more controllable (e.g., more uniform) concentration profiles of dissolved oxygen and biochemical cues, at tolerable pressure drops. In conclusion, culture of human cell-seeded constructs in perfused rPBBs may permit robust control of the pericellular environment, and guidance of cell proliferation and differentiation in the engineering of biological substitutes. These features make rPBBs suitable for therapeutic treatments as well as for the *in vitro* toxicity screening of drugs. However, model predictions are as good as the assumptions upon which the model is based. In designing an rPBB with the model proposed, care should be taken to use model parameters estimated from culture experiments and to verify that the model assumptions hold true for the specific case considered. For instance, it was assumed that radial flux uniformity of culture medium may be achieved along the construct length, although radial flux maldistribution has been shown to possibly occur in radial flow reactors for industrial applications and to severly limit reactor beahavior. It should also be noted that the value of integral performance parameters, such as NHy-FCV, and diagrams such as that shown in Figure 2.6 strongly depend on the threshold value set for the dissolved oxygen concentration below which cells become apoptotic or die.

In the next chapter, a criterion to optimize radial flux distribution of culture medium along the construct length will be presented, based on a two-dimensional stationary model of momentum transport accounting for the effect of fluid dynamics of the rPBB void spaces, the time-changing construct transport properties and the construct geometry on the degree of radial flux uniformity.

Chapter 3[2]

Optimization of construct perfusion in radial packed-bed bioreactors for tissue engineering with a 2D stationary fluid dynamic model

3.1 Introduction

In the previous chapters, radial flow perfusion of cell-seeded 3D construct was shown to be advantageous over static culture and axial flow perfusion in the realization of clinical-scale bioengineered substitutes for tissue replacement. One of the major advantages of rPBBs as compared to aPBBs consists in the fact that rPPBs can be easily scaled-up by increasing the construct length rather than the diameter, which permits to maintain relatively short path-lengths for solute transport inside the construct. This also allows to better preserve the graft shape (e.g. in long bone replacement). However, the design of rPBBs is more complicated than aPBBs. In fact, rPBBs require additional void spaces for distributing (and collecting) medium flow along the length of the bioreactor (i.e. the inner hollow cavity and the outer peripheral annulus), the fluid dynamics of which may significantly influence the bioreactor behavior. Radial medium flux must also be uniformly distributed along the length of the bioreactor to enable the uniform utilization of the catalyst bed (Ponzi and Kaye, 1979) for tissue reconstruction. In fact, radial flux maldistribution would yield an uneven supply of dissolved oxygen, nutrients and biochemical cues to cells that could cause non-uniform cell proliferation and differentiation and even cell starvation in poorly perfused zones of the construct. Flux maldistribution may even worsen during culture as an effect of the non–uniform decrease of the construct Darcy permeability as cells proliferate and produce extracellular matrix in non-uniform fashion.

[2] This chapter is adapted from: Donato, D.; Falvo D'Urso Labate, G.; Debbaut, C.; Segers, P.; Catapano, G. Optimization of construct perfusion in radial packed-bed bioreactors for tissue engineering with a 2D stationary fluid dynamic model. **2015**. *Under revision*

Mathematical models of momentum transport may help optimize the design of void spaces and scaffolds, and prevent radial flux maldistribution in rPBBs under the conditions typical of tissue engineering. Models of momentum transport have been mainly proposed for industrial radial flow packed-bed reactors treating gaseous streams flowing under turbulent conditions. For such reactors, a criterion to prevent radial flux maldistribution has been proposed by Genkin et al. (Genkin et al., 1973), limited to the optimization of the hollow cavity-to-peripheral annulus cross-sectional flow area ratio. The effects of the direction of turbulent flow perfusion and reactor configuration on radial flux maldistribution have been discussed by Chang et al. (Chang et al., 1983), Heggs et al. (Heggs et al., 1995) and Kareeri et al. (Kareeri et al., 2006). Analytical, simplified mathematical descriptions of momentum transport have been generally preferred for large industrial reactors, which assume gaseous turbulent flow in void spaces and seldom account for the transport properties of the catalytic bed. Only a few transport models of rPBBs have been proposed for the small scale and medium flow rates, and the scaffold properties typical of tissue engineering (Tharakan and Chau, 1987; Cima et al., 1990; Kurosawa et al., 1991). They account only for transport and consumption of soluble nutrients across the construct, and assume that the radial flux of medium is uniformly distributed along the construct length and that medium flows as a plug across the construct.

In this chapter, a two-dimensional axisymmetric model is proposed for steady-state momentum transport in radial flow packed-bed bioreactors for tissue engineering which accounts for all bioreactor compartments. Momentum transport in the inner hollow cavity and the outer peripheral annulus was described according to the Navier-Stokes equation, and that across the construct according to the Darcy-Brinkman equation. The dimensionless groups, which lump geometric and operating parameters and effectively determine radial flux distribution in the bioreactor, were obtained by dimensional analysis. Values of the main dimensionless groups that may prevent radial flux maldistribution were sought by integrating the resulting momentum balance equations with a commercial finite elements package. A criterion was developed to design and

operate rPBBs in which radial fluxes are uniformly distributed along the bioreactor length under the conditions typical of tissue engineering.

3.2 Materials and methods

3.2.1 Model development

Momentum transfer across the three compartments of an rPBB operated at steady-state was described according to a two-dimensional axisymmetric model. The rPBB is schematically shown in Figure 3.1. A cell-seeded annular porous scaffold is coaxially positioned at the bottom of a cylindrical housing forming a cylindrical culture chamber. Medium is fed axially into the inner hollow cavity, radially perfuses the construct, flows along the outer peripheral annulus in centrifugal (CF), counter-current (π) configuration, and leaves the rPBB through a 3-zone outlet port. Such configurations were chosen because the π-configuration has been shown to reduce the extent of radial flux maldistribution in radial flow reactors treating gaseous streams (Kareeri et al., 2006), and the CF-configuration has been shown to provide a more effective supply of dissolved oxygen and nutrients to cells in the case of uniform radial fluxes. The momentum conservation equations governing the rPBB behavior were obtained under the following assumptions:

i. axial symmetry;

ii. steady-state isothermal conditions;

iii. incompressible Newtonian fluid;

iv. isotropic porous construct;

v. transport in the construct described according to the Darcy-Brinkman equation;

vi. transport in the inner hollow cavity and the outer peripheral annulus described according to the Navier-Stokes equation (Perry et al., 1999).

Axial and radial spatial coordinates, z and r, pressure P_i and axial and radial velocity components, u_i and v_i, in the i-th rPBB compartment were obtained in non-dimensional form as follows:

$$r^* = \frac{r}{R}\ ;\ \ z^* = \frac{z}{L};\quad u_i^* = \frac{u_i}{u_{in}};\quad v_i^* = \frac{v_i}{u_{in}}\frac{L}{R};\quad P_i^* = \frac{P_i}{u_{in}\,\mu\, L/R^2} \tag{3.1}$$

where R and L are the scaffold inner radius and length, respectively, u_{in} is the axial velocity at the rPBB inlet, and μ is the medium dynamic viscosity. Consistently, the conservation equations were re-arranged in non-dimensional form to give:

continuity equations (for i=H, inner hollow cavity; C, construct; or E, external or outer peripheral annulus)

$$\frac{1}{r^*}\frac{\partial}{\partial r^*}\left(r^* v_i^*\right) + \frac{\partial u_i^*}{\partial z^*} = 0 \tag{3.2}$$

momentum balance equations

inner hollow cavity, H:

$$r)\qquad \mathrm{Re}_{in}\left(v_H^*\frac{\partial v_H^*}{\partial r^*} + u_H^*\frac{\partial v_H^*}{\partial z^*}\right) = -\left(\frac{L}{R}\right)^2\frac{\partial P_H^*}{\partial r^*} + \frac{\partial}{\partial r^*}\left(\frac{1}{r^*}\frac{\partial}{\partial r^*}\left(r^* v_H^*\right)\right) + \left(\frac{R}{L}\right)^2\frac{\partial^2 v_H^*}{\partial z^{*2}} \tag{3.3}$$

$$z)\qquad \mathrm{Re}_{in}\left(v_H^*\frac{\partial u_H^*}{\partial r^*} + u_H^*\frac{\partial u_H^*}{\partial z^*}\right) = -\frac{\partial P_H^*}{\partial z^*} + \frac{1}{r^*}\frac{\partial}{\partial r^*}\left(r^*\frac{\partial u_H^*}{\partial r^*}\right) + \left(\frac{R}{L}\right)^2\frac{\partial^2 u_H^*}{\partial z^{*2}} \tag{3.4}$$

construct, C:

$$r)\qquad v_C^* = -\frac{k}{R^2}\frac{L^2}{R^2}\frac{dP_C^*}{dr^*} + \frac{k}{R^2}\frac{1}{\varepsilon}\frac{\partial}{\partial r^*}\left(\frac{1}{r^*}\frac{\partial}{\partial r^*}\left(r^* v_C^*\right)\right) \tag{3.5}$$

$$z)\qquad u_C^* = -\frac{k}{R^2}\frac{dP_C^*}{dz^*} + \frac{k}{R^2}\frac{1}{\varepsilon}\left(\frac{1}{r^*}\frac{\partial}{\partial r^*}\left(r^*\frac{\partial u_C^*}{\partial r^*}\right)\right) + \frac{k}{R^2}\frac{1}{\varepsilon}\frac{R^2}{L^2}\frac{\partial^2 u_C^*}{\partial z^{*2}} \tag{3.6}$$

outer peripheral annulus, E:

$$r)\qquad \mathrm{Re}_{in}\left(v_E^*\frac{\partial v_E^*}{\partial r^*} + u_E^*\frac{\partial v_E^*}{\partial z^*}\right) = -\left(\frac{L}{R}\right)^2\frac{\partial P_E^*}{\partial r^*} + \frac{\partial}{\partial r^*}\left(\frac{1}{r^*}\frac{\partial}{\partial r^*}\left(r^* v_E^*\right)\right) + \left(\frac{R}{L}\right)^2\frac{\partial^2 v_E^*}{\partial z^{*2}} \tag{3.7}$$

$$z)\qquad \mathrm{Re}_{in}\left(v_E^*\frac{\partial u_E^*}{\partial r^*} + u_E^*\frac{\partial u_E^*}{\partial z^*}\right) = -\frac{\partial P_E^*}{\partial z^*} + \frac{1}{r^*}\frac{\partial}{\partial r^*}\left(r^*\frac{\partial u_E^*}{\partial r^*}\right) + \left(\frac{R}{L}\right)^2\frac{\partial^2 u_E^*}{\partial z^{*2}} \tag{3.8}$$

where $Re_{in}=(\rho\ u_{in}\ R/\mu)\ R/L$ is a reduced inlet Reynolds number. Other variables are defined in Figure 3.1 and Table 3.1.

Equations 3.2-3.8 are subject to the following boundary conditions: fully developed axial velocity profile at the bioreactor entrance; bioreactor axis is impervious to momentum and fluid (*i.e.* $\forall z^*$, for $r^*=0$, $v_H^*=0$, $\partial u_H^*/\partial r^*=0$); continuity of pressure and velocity at the interface between inner hollow cavity and construct, and between construct and outer peripheral annulus; the walls of the housing are impervious to momentum and adherent for the fluid; the pressure of the stream leaving the outer peripheral annulus differs from atmospheric pressure by an amount ΔP_{out}^* equal to the sum of the local pressure drops in the three zones at the bioreactor outlet (zones 1-3 in Figure 3.1) where the cross-sectional area for flow changes. The non-dimensional total pressure drop caused by the local cross-sectional surface area expansion and constrictions was estimated as follows:

$$\Delta P_{out}^* = \sum_{j=1}^{3} \frac{k_j}{2} \mathrm{Re}_{in}\ g_j \tag{3.9a}$$

where k_j and g_j are the loss coefficients and characteristic functions dependent on the geometry of the j-th zone, respectively (Appendix A). Exemplary values of k_j and g_j were estimated from the charts reported in Idelchik (Idelchik, 1960), Munson et al. (Munson et al., 2013), and Perry et al. (Perry et al., 1999) for a sudden cross-sectional area expansion (zone 1) as a function of the actual value of R/δ_C and R/δ_E (i.e. k_1 and g_1), followed by a gradual contraction of 60% with a 75 degree contraction angle (zone 2) and a sudden contraction of 35% at the bioreactor outlet (zone 3) (i.e. k_2, g_2 and k_3, g_3 respectively)

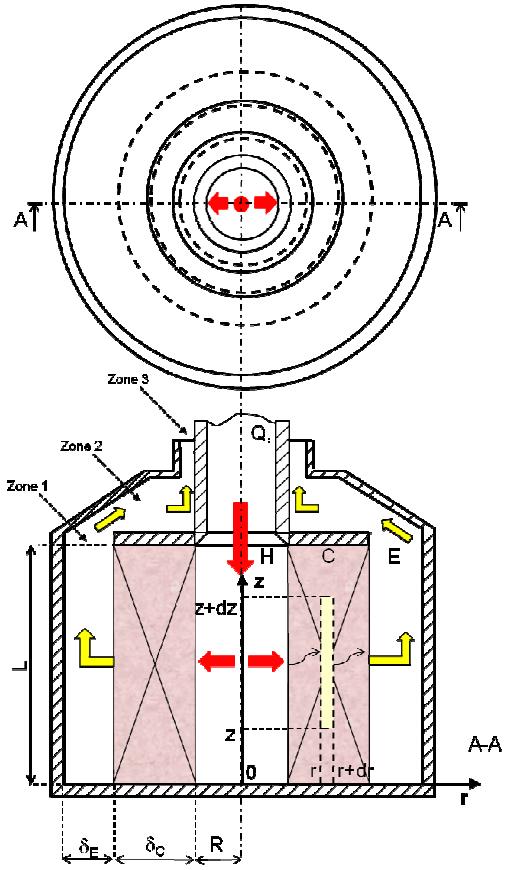

Figure 3.1 Scheme of an rPBB showing the three compartments (i.e. inner hollow cavity, H; construct, C; outer peripheral annulus, E), three exemplary zones of the bioreactor outlet, and an exemplary differential control volume.

Parameter	Value	Units	Description
L	0.015-0.15	m	construct length (Hongo et al., 2005; Noble et al., 1988)
R	$4\ 10^{-3}$	m	construct inner radius (Melchels et al., 2011)
δ_C	$5\ 10^{-3}$	m	construct thickness (Olivier et al., 2007; Xie et al., 2006)
δ_E	10^{-3}-$8\ 10^{-3}$	m	thickness of outer peripheral annulus (Arano et al., 2010)
ρ	993.37	kg/m^3	medium density (Ma et al., 2009)
μ	$6.94\ 10^{-4}$	kg/(m s)	medium viscosity
ε	0.9	-	construct porosity (Karageorgiou and Kaplan, 2005)
k	10^{-10}-10^{-8}	m^2	construct Darcy permeability (Li et al., 2003; Dias et al., 2012; Grimm et al., 1997; Nauman et al., 1999)

Table 3.1 Dimensional parameter values used for model predictions, unless otherwise stated

3.2.2 Dimensionless groups

The dimensionless conservation Equations 3.2-3.8 and related boundary conditions suggest that the bioreactor behavior is mainly determined by the independent dimensionless groups reported in Table 3.2. The physical interpretation of some of these dimensionless groups is known and may be found in literature (Perry et al., 1999). In this investigation, scaffold geometries were used typically proposed for bone tissue engineering (Xie et al., 2006; Olivier et al., 2007). Higher reduced inlet Reynolds numbers, Re_{in}, are generally associated with higher inlet medium flow rates at any given construct geometry. In the simulations, Re_{in} was kept in the range typically reported in *in vitro* experiments to enable laminar flow and prevent cell wash-out, which justifies the use of Navier-Stokes and Darcy-Brinkman equations.

Dimensionless groups	**Values**	**Description**	**Application**
1. $(\rho\, u_{in}\, R/\mu)R/L$	0.067-6	reduced Reynolds number at inlet of inner hollow cavity, Re_{in}	BTE, LTE, CTE (Hongo et al., 2005; Melchels et al., 2011; Shao, 2009)
2. L/R	3.75-37.5	construct aspect ratio	BTE, HP, LTE, TE (Hongo et al., 2005; Olivier et al., 2007; Kitagawa et al., 2006; Noble et al., 1988)
3. R/δ_C	0.8	construct inner radius-to-thickness ratio	HP (Noble et al., 1988)
4. R/δ_E	0.19-4	construct inner radius-to-peripheral annulus width ratio	BTE, LTE (Arano et al., 2010; Park et al., 2008)
5. k/R^2	$6.25\,10^{-6}$-$6.25\,10^{-4}$	construct-to-hollow cavity permeability ratio	BTE, TE, HP (Li et al., 2003; Grimm et al., 1997; Gardel et al., 2013)

Table 3.2 Independent dimensionless groups determining rPBB performance and values used for model predictions, unless otherwise stated. *Applications: BTE – bone tissue engineering; CTE – cartilage tissue engineering; HP – human physiology; LTE –liver tissue enginering; TE – generic tissue engineering.

3.2.3 Computational methods

Equations 3.2-3.8 with the related boundary conditions were solved numerically according to the finite element method with the Comsol Multiphysics (Comsol Inc., Burlington, MA, USA). Two-dimensional steady-state profiles of dimensionless axial and radial velocity components, u_i^* and v_i^*, and pressures P_i^* were predicted for the values of model parameters and dimensionless groups representative of those typical of tissue engineering reported in Tables 3.1 and 3.2, unless otherwise specified. The construct Darcy permeability was varied in the range typical of scaffolds and constructs for bone tissue engineering (Li et al., 2003; Dias et al., 2012). The bioreactor geometry was meshed with rectangular elements. Their number and distribution was optimized to keep the relative error on the predicted average axial and radial velocity components at the outlet of the peripheral annulus below 0.005% for every set of dimensionless groups values (Figure 3.2).

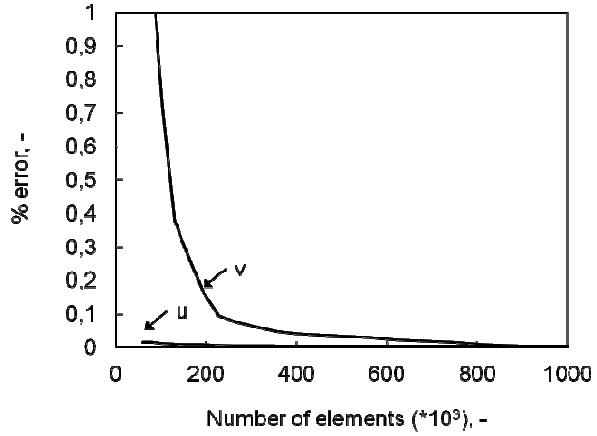

Figure 3.2 Relative error on the predicted average axial and radial velocity at the outlet of the peripheral annulus. L/R= 25, Re_{in} = 0.04, $R/\delta_C = R/\delta_E$ = 0.8, $k/R^2 = 6.25 \times 10^{-4}$.

The uniformity of radial flux (i.e. the radial velocity component at $r^* = 1$) distribution along the bioreactor length was characterized in terms of the average distance of the actual fluxes from their length-averaged value, as proposed by Mu et al. (Mu et al., 2003)

$$\eta = 1 - \sqrt{\int_0^1 \left(\frac{v_C^*|_{r^*=1}}{v_{C,avg}^*|_{r^*=1}} - 1 \right)^2 dz^*} \qquad (3.10)$$

Values of η=1 (i.e. 1-η=0) characterize an ideally uniform radial flux distribution.

Along that proposed in Celik and Ackley (Celik and Ackley, 2012), a criterion is proposed herein to optimize rPBB design and operation based on the assumption that, to ensure radial flux uniformity, the total axial pressure drop in the void spaces has to be negligible with respect to the radial pressure drop across the construct. The design criterion, termed the criterion of radial flux uniformity (CORFU), may be expressed as a function of the dimensionless groups in Table 3.1, as follows (Appendix B):

$$CORFU = \frac{\Delta P_{z,H} + \Delta P_{z,E}}{\Delta P_{r,C}} = \frac{\left\{\left(8\,\frac{1}{\mathrm{Re}_{in}} - \frac{1}{\alpha_H}\right)\right\} + \left\{\xi^2\left[\frac{1}{\alpha_E} + 8\,\frac{1}{\mathrm{Re}_{in}}\left(2\left(\frac{1+\frac{\delta_C}{R}}{\frac{\delta_E}{R}}\right)+1\right)\right]\right\}}{\left(\frac{R^2}{k}\left(\frac{R}{L}\right)^2 \ln\left(1+\frac{\delta_C}{R}\right)\frac{1}{\mathrm{Re}_{in}}\right)} = f_1\left(\mathrm{Re}_{in}, \frac{L}{R}, \frac{\delta_C}{R}, \frac{\delta_E}{R}, \frac{k}{R^2}\right) \to 0 \quad (3.11)$$

where α_H and α_E are the kinetic energy correction factors which account for the variation of the xial velocity over the cross section of the entrance or outlet bioreactor section normalized with respect to the average axial velocity in the same section, respectively.

3.3 Results and discussion

The model proposed in this chapter aims to investigate how geometric, transport and operating parameters influence the distribution of medium radial flux along an rPBB, and to provide the designer with a criterion to design and operate rPBBs so that radial flux is uniformly distributed along the bioreactor length. In fact, no model has been proposed yet that provides a comprehensive analysis of the dimensionless groups determining the actual radial flux distribution along the length of rPBBs, and that accounts for the fluid dynamics of the inner hollow cavity and the outer peripheral annulus and for construct permeability, under the conditions typical of tissue engineering. Nor is any optimal design criterion available, yet.

3.3.1 Model validation

The lack of experimental velocity and pressure profiles in the compartments of an rPBB and the difficult procurement of detailed information on the bioreactor geometry and operation used in literature made it difficult to quantitatively validate the model. For these reasons, the goodness of model predictions was assessed qualitatively in terms of the agreement of the model-predicted axial distribution of radial velocity (i.e. flux) to that predicted by the criterion for radial flux uniformity proposed for very permeable catalyst beds by Genkin et al. (Genkin et al., 1973) and by comparison to the experimental data of Xie et al. (Xie et al., 2006) and Olivier et al. (Olivier et al., 2007). For industrial radial packed-bed reactors treating gaseous streams, Genkin et al. (Genkin et al., 1973) showed that the actual radial flux distribution along the reactor length depends on the ratio of the inner hollow cavity cross-sectional flow area to that of the outer peripheral annulus, ξ, which may be expressed as a function of the dimensionless groups in Table 3.2 as follows (Appendix C):

$$\xi = \frac{\left(\frac{R}{\delta_E}\right)^2}{1+2\frac{R}{\delta_E}\left(1+\frac{\delta_C}{R}\right)} = f_2\left(\frac{R}{\delta_C}, \frac{R}{\delta_E}\right) \tag{3.12}$$

Kareeri et al. (Kareeri et al., 2006) reported that an optimum value of ξ exists of about ξ=0.21 which ensures radial flux uniformity in radial flow reactors in the CF-π configuration, such as the one used in this study. Indeed, Figures 3.3a-b show that the model soundly predicts a non-uniform distribution of radial flux along constructs cultured in rPBBs featuring a thin inner hollow cavity, with R/δ_E=0.19 and ξ=0.011 (Figure 3.3a), or a thin outer peripheral annulus, with R/δ_E=3.62 and ξ=0.85 (Figure 3.3b). This is an effect of the non-uniform axial profile of pressure difference between the inner hollow cavity and the outer peripheral annulus caused by friction in the thin compartment with high resistance to flow, as shown in Figure 3.3c for the same conditions as in Figure 3.3a. The poor radial flux distribution in the two cases shown in Figures 3.3a-b is characterized by η=0.16 and 0.53, respectively, in good agreement with that expected from

Genkin's criteria for reactors featuring ξ=0.011 and ξ=0.85, respectively. Figure 3.3d shows that the model soundly predicts a uniform radial flux distribution along the bioreactor length, with η=0.93, when the flow resistance of the inner hollow cavity and outer peripheral annulus is reduced and ξ=0.21, equal to the optimal value suggested by Kareeri et al. (Kareeri et al., 2006). Xie et al. (Xie et al., 2006) and Olivier et al. (Olivier et al., 2007) reported that mesenchymal sheep cells (MSCs) or MG63 cells, respectively, could be seeded and cultured in an annular β-tricalcium phosphate porous scaffold in an rPBB without significant differences in cell number among the upper, intermediate and bottom parts of the scaffold. Model predictions for the scaffold and bioreactor geometry and operating conditions reported therein, and $k = 0.3\ 10^{-9}\ m^2$ (Li et al., 2003), showed that cells were seeded at uniform radial flux distribution (with η=0.971 and η=0.976 for MSCs and MG63 cells, respectively). The resulting uniform drag exerted on cells during seeding likely contributed to the observed uniform axial cell distribution (Alvarez-Barreto et al., 2007).

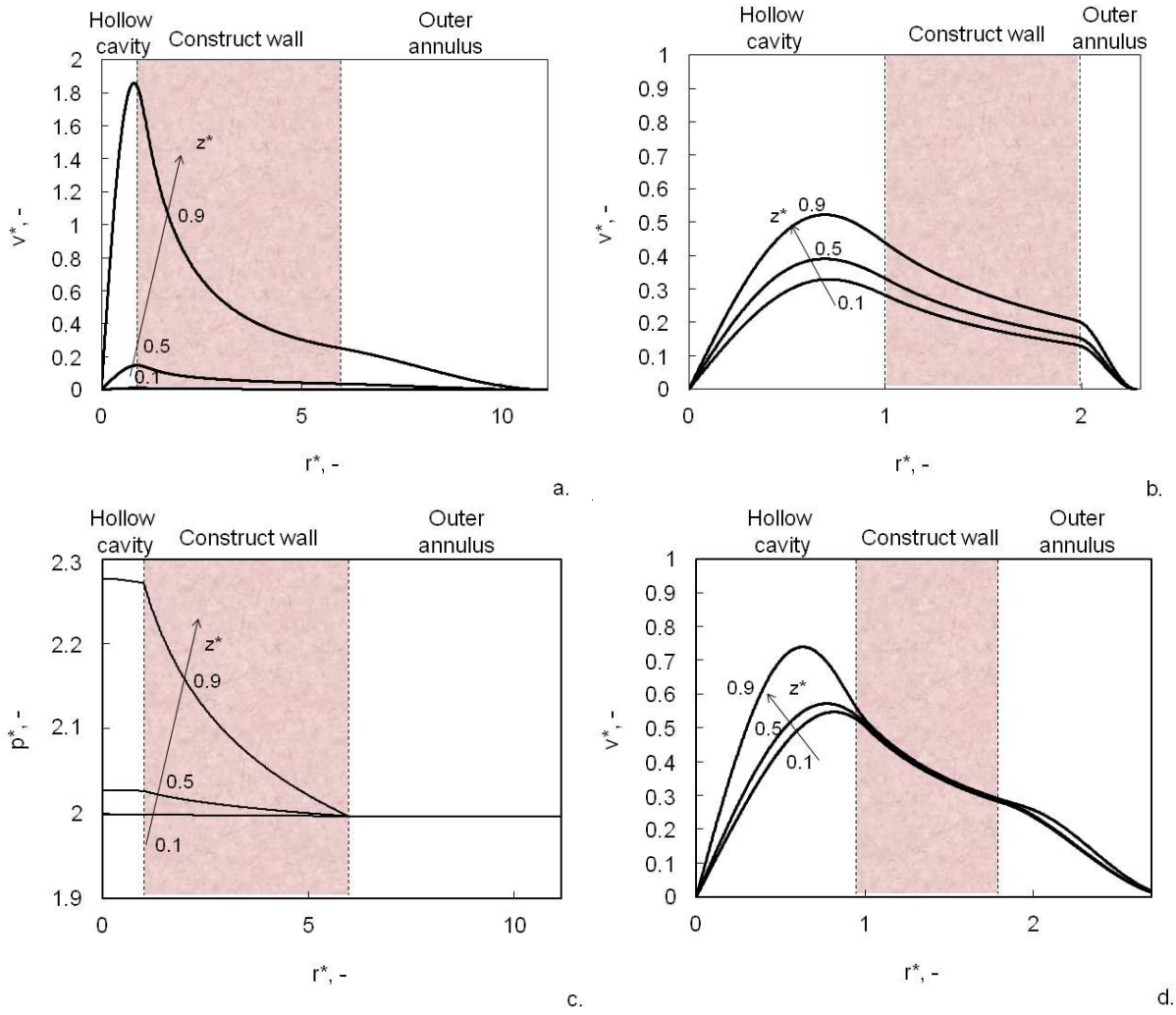

Figure 3.3 Model-predicted dimensionless radial flux (a,b,d) or pressure (c) profiles at varying dimensionless distance from bioreactor bottom, z^*: **a)** k/R^2= 8.46 10^{-3}, Re_{in}=0.54, L/R= 33, R/δ_C= 0.2, R/δ_E= 0.19, ξ=0.011; **b)** k/R^2= 3.38 10^{-4}, Re_{in}= 4.54, L/R= 6.6, R/δ_C= 1, R/δ_E= 3.62, ξ=0.85; **c)** same as in a; **d)** k/R^2= 2.35 10^{-4}, Re_{in}=6, L/R= 5.5, R/δ_C= 1.2, R/δ_E= 0.98, ξ=0.21;

3.3.2 Effect of dimensionless groups on radial flux distribution

Table 3.2 shows that the bioreactor behavior is mainly determined by five independent dimensionless groups. Accordingly, the actual pressure and velocity profiles anywhere in the bioreactor are determined by: k/R^2, accounting for construct transport properties; Re_{in}, mainly accounting for feed flow rate; and L/R, R/δ_C, and R/δ_E, accounting for construct and bioreactor geometry. Equation 3.12 shows that the analysis proposed in this study is more comprehensive than Genkin's criterion, which accounts only for the last two dimensionless groups.

3.3.2.1 Effect of k/R^2 and Re_{in}

The effect of the construct Darcy permeability (i.e. k/R^2) on radial flux distribution has been generally neglected. Only Kareeri et al. (Kareeri et al., 2006) showed that using tightly packed beds, or poorly porous perforated plates to hold the beads in the bed, may yield more uniform radial flux distributions in industrial radial flow packed-bed reactors. Figures 3.4a-b show the importance of k/R^2 for radial flux distribution. Under similar geometry and operating conditions to Figure 3.4a, Figure 3.4a shows that, even when the inner hollow cavity exhibits a high resistance to flow, using a construct with a Darcy permeability two orders of magnitude lower than in Figure 3.3a yields a rather uniform radial flux distribution in the construct, with η=0.9, in spite of ξ=0.011. Similarly, when the outer peripheral annulus exhibits a high resistance to flow, Figure 3.4b shows that using a construct with Darcy permeability two orders of magnitude lower than in Figure 3.3b yields a uniform radial flux distribution, with η=0.95, in spite of ξ=0.85.

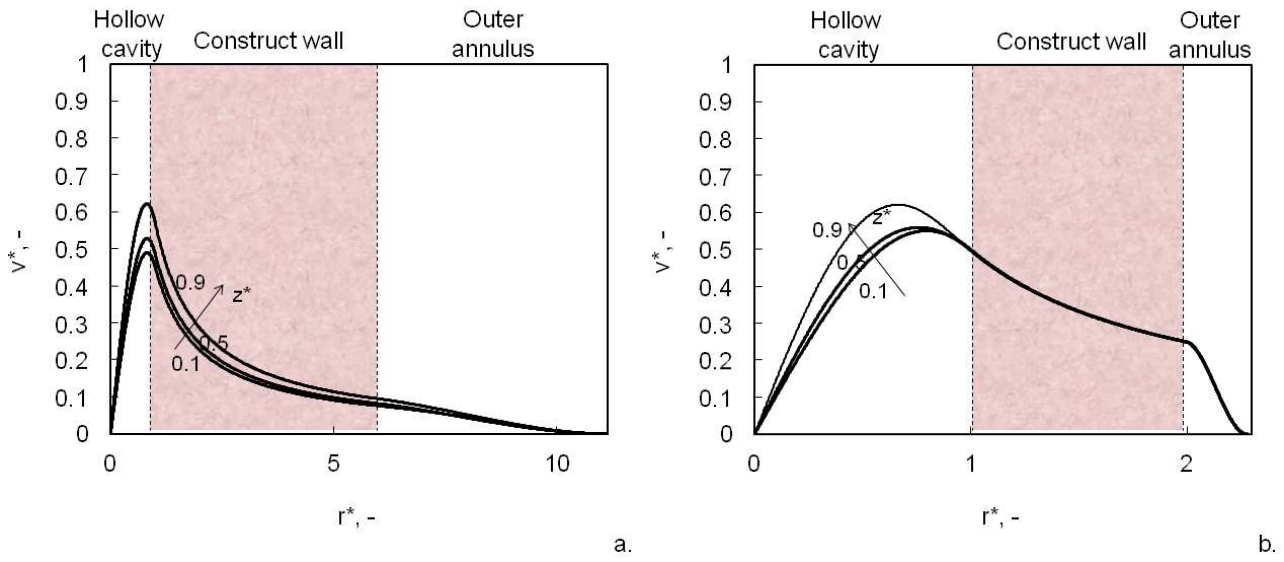

Figure 3.4 Model-predicted dimensionless radial flux (a,b,d) or pressure (c) profiles at varying dimensionless distance from bioreactor bottom, z^*: **a)** k/R^2= 8.46 10^{-5}, Re_{in}=0.54, L/R= 33, R/δ_C= 0.2, R/δ_E= 0.19, ξ=0.011; **b)** k/R^2= 3.38 10^{-6}, Re_{in}= 4.54, L/R= 6.6, R_i/δ_C= 1, R/δ_E= 3.62, ξ=0.85..

Figure 3.5a shows that for constructs of very low k/R^2 the radial flux distribution along the rPBB length is uniform, with η>0.9, and independent of Re_{in}. For constructs with high k/R^2,

increasing Re_{in} makes η (hence the radial flux uniformity) increase up to an optimal $Re_{in,opt} \approx 2.8$ for the conditions used. Further increases of Re_{in} make radial flux maldistribution progressively increase (hence η decrease). The existence of the optimal Re_{in} may be explained by considering that fluid pressure in the inner hollow cavity and the outer peripheral annulus is determined by the balance between friction at the wall surface, which makes pressure decrease in the direction of flow, and momentum recovery caused by the axial flow rate variation induced by suction, which makes pressure increase in the direction of decreasing flow. For the conditions used in Figure 3.5a and high k/R^2, at lower Re_{in} than the optimum, friction in the inner hollow cavity prevails over that in the outer peripheral annulus. This makes the radial pressure drop decrease along the bioreactor length and causes poor perfusion of the bottom of the construct. At higher Re_{in} than the optimum, momentum recovery in the inner hollow cavity prevails over friction in the outer peripheral annulus. This makes radial pressure drop increase along bioreactor length and causes poor perfusion of the upper part of the construct. The influence of k/R^2 on the dependence of η on Re_{in} suggests that the choice of the medium feed flow rate to rPBBs influences radial flux distribution to a larger extent at the beginning of culture, when construct Darcy permeability is the highest. As cells proliferate and produce extracellular matrix, construct Darcy permeability decreases and Re_{in} may be increased to match the increased cell metabolic demand without causing significant radial flux maldistribution. Figures 3.5b-c show that, with very permeable constructs, the dependence of the uniformity of radial flux distribution, η, on Re_{in} is strongly influenced by the construct aspect ratio, L/R, and ξ. Figure 3.5b shows that the extent of radial flux maldistribution significantly increases with increasing L/R at any given Re_{in}, but close to $Re_{in,opt}$. At the conditions used, Figure 3.5c shows that, at $Re_{in} < Re_{in,opt}$, rPBB designs featuring increasing ξ increase the extent of radial flux maldistribution by causing increasingly poorer perfusion of bioreactor bottom, less so as Re_{in} increases. Increasing Re_{in} beyond $Re_{in,opt}$ makes η decrease for increasingly poorer perfusion of bioreactor inlet, less so as ξ increases. The optimal Re_{in} value increases also from 2.8 to ca. 5.3 as ξ

increases from 0.14 to 0.31, respectively. Figure 3.6a shows that, when very permeable and slender constructs are operated at low inlet flow rates (i.e. high k/R^2 and L/R, and low Re_{in}), zones may form at the bioreactor bottom in which the average axial velocity of medium is only a few percent of that entering the bioreactor (less than 2% up to a distance from the bioreactor bottom of ca. 15% of its length, at the conditions of Figure 3.6a) and much lower than in the presence of a uniform radial flux distribution at the same position. Medium stagnation in such zones contributes to further worsening the radial flux maldistribution. Similar behavior may be predicted for the outer peripheral annulus (Figure 3.6b).

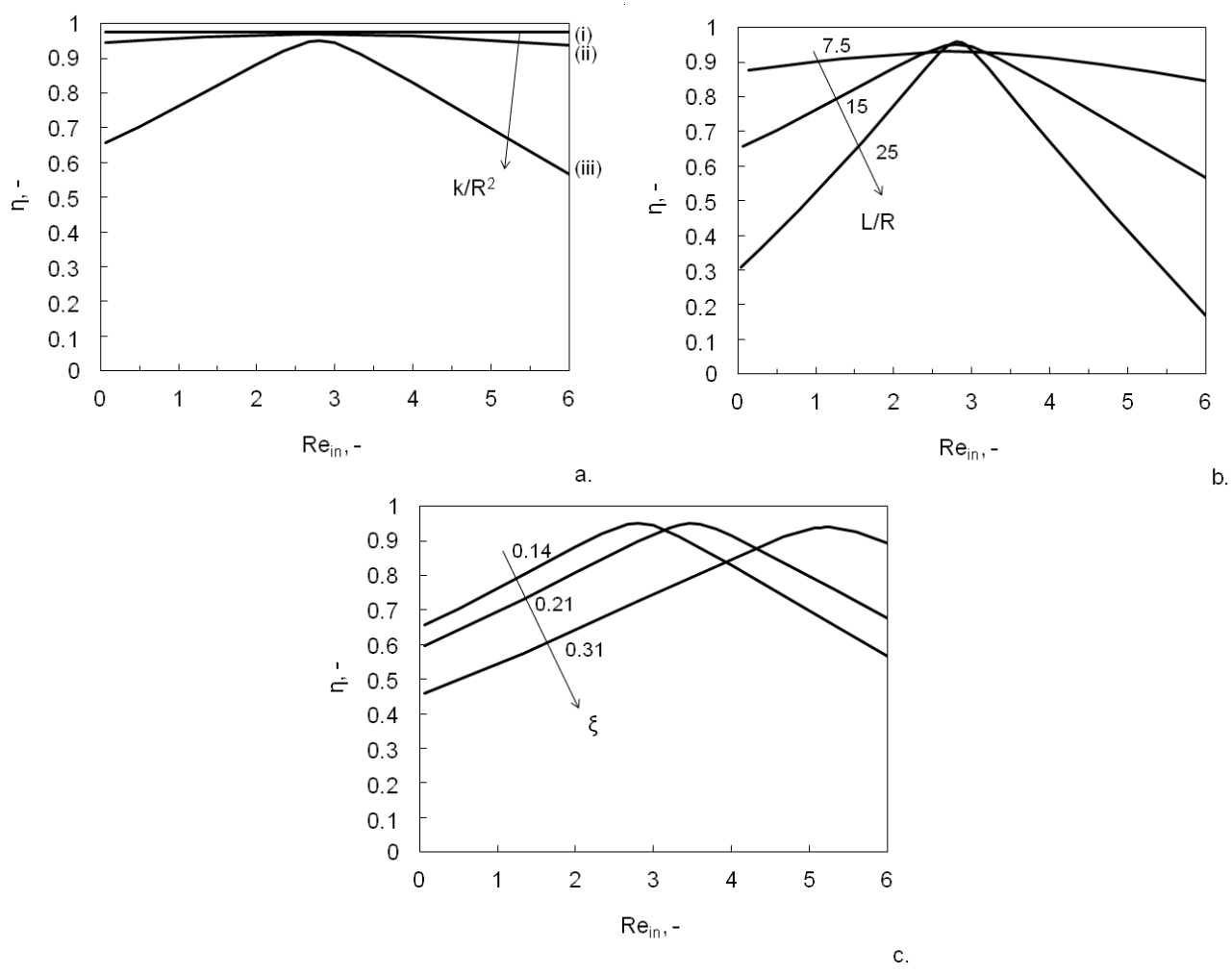

Figure 3.5 Model-predicted effect of Re_{in} on the uniformity of radial flux distribution, η: **a)** at varying dimensionless construct permeability, k/R^2: (i) 6.25 10^{-6}, (ii) 6.25 10^{-5}, (iii) 6.25 10^{-4}. Other dimensionless groups values: L/R= 15, R/δ_C=0.8, R/δ_E=0.8; **b)** at varying construct aspect ratio, L/R: 7.5, 15, 25. Other dimensionless groups values: k/R^2= 6.25 10^{-4}, R/δ_C=0.8, R/δ_E=0.8; **c)** at varying ξ: 0.14, 0.21, 0.31. Other dimensionless groups values: k/R^2= 6.25 10^{-4}, L/R =15, R/δ_C=0.8.

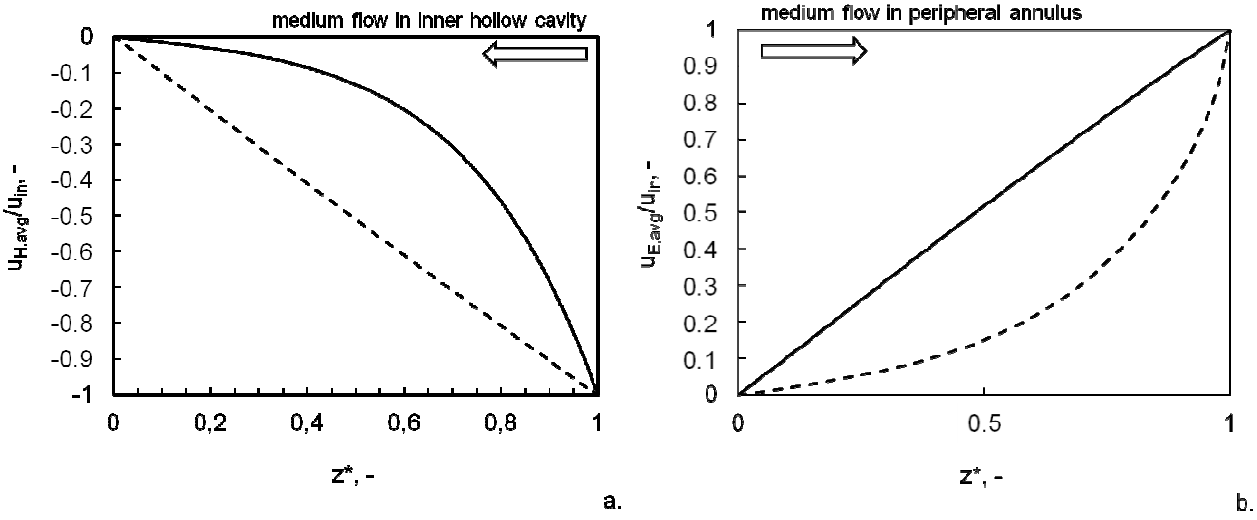

Figure 3.6 Model-predicted space-average axial velocity profile in the inner hollow cavity, $u_{H,avg}$, and peripheral annulus, uE,avg, along bioreactor length normalized with respect to the average axial velocity at inlet of the inner hollow cavity, u_{in}, for: (a) (dashed line) - uniform radial flux distribution, L/R = 11, Re_{in} = 3, R/δ_E= 0.8; (solid line) - non-uniform radial flux distribution, L/R = 37.5, Re_{in} = 0.27, R/δ_E= 0.8; (b) (dashed line) - uniform radial flux distribution, R/δ_E= 0.8, L/R = 11, Re_{in} = 2.72; (solid line) - non-uniform radial flux distribution, R/δ_E= 4, L/R = 11, Re_{in} = 0.1; In all cases: R/δ_C =0.8, $k/R^2 = 6.25\ 10^{-4}$.

3.3.2.2 Effect of L/R

Figure 3.7 shows that, for constructs of very low k/R^2, radial flux distribution is uniform (with η>0.9) and almost independent of L/R. As k/R^2 increases, using more slender constructs (i.e. constructs with higher L/R) yields progressively more uniform radial fluxes up to L/R≈8 (where η>0.9) for the conditions used. Further increases of L/R make radial flux maldistribution increase (i.e. η decrease) as an effect of the decrease of the intercompartmental radial pressure drop towards the bioreactor bottom caused by friction in the outer peripheral annulus.

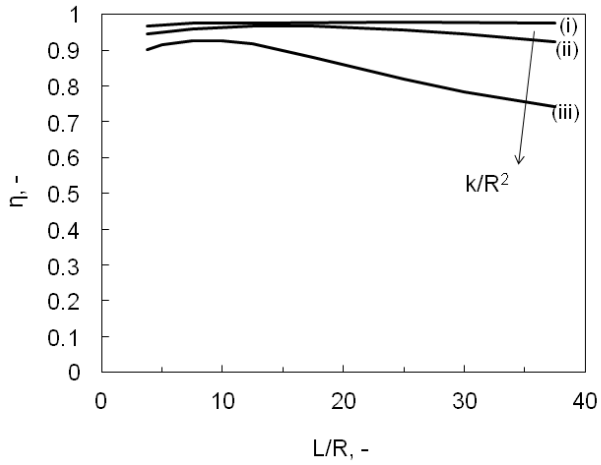

Figure 3.7 Model-predicted effect of L/R on the uniformity of radial flux distribution, η, at varying dimensionless construct permeability: i) k/R^2= 6.25 10^{-6}; ii) k/R^2= 6.25 10^{-5}; iii) k/R^2= 6.25 10^{-4}. In all cases: Re_{in}=2.8, R/δ_C =0.8, R/δ_E= 0.8.

3.3.2.3 Effect of R/δ_C and R/δ_E

After Genkin et al. (Genkin et al., 1973), the effect of R/δ_C and R/δ_E on radial flux distribution is better evaluated in terms of ξ, as defined in equation #3.12. Figure 3.8 shows that in rPBBs equipped with constructs of low k/R^2, ξ has no significant effect on radial flux distribution. However, at high k/R^2, rPBB geometries characterized by increasing values of ξ progressively increase radial flux maldistribution (and make η decrease). Radial flux is practically uniform along the bioreactor length and features η≥0.9 up to a value of ξ which decreases with increasing k/R^2, e.g. from ξ=0.6 to 0.28 as k/R^2 increases from $6.25 \cdot 10^{-5}$ to $6.25 \cdot 10^{-4}$ at the conditions used. Above such value of ξ, friction in the outer peripheral annulus prevails and makes radial pressure drop decrease towards bioreactor bottom. This causes poor perfusion of the bottom of very permeable constructs. At any ξ, the degree of maldistribution (i.e. 1-η) is higher the higher k/R^2.

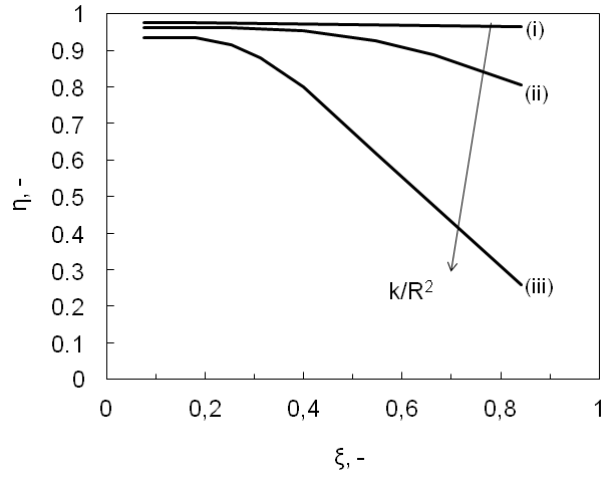

Figure 3.8 Model-predicted effect of ξ on the uniformity of radial flux distribution, η, at varying dimensionless construct permeability: i) $k/R^2 = 6.25\ 10^{-6}$; ii) $k/R^2 = 6.25\ 10^{-5}$; iii) $k/R^2 = 6.25\ 10^{-4}$. In all cases: Re_{in}=2.8; L/R=8.25; R/δ_C= 0.8

3.3.2.4 The CORFU criterion

The CORFU criterion defined in Equation 3.11 correlates well with the model-predicted ratio between the total axial pressure drop in the void spaces and the radial pressure drop across the construct, for α_H=0.32 and α_E=0.5 (Figure 3.9a). This suggests that the CORFU is a good predictor of the actual pressure drop ratio but it has the advantage that it may be easily estimated without performing any experiment, nor any computer simulation. Figure 3.9b shows that when the dimensionless groups are rearranged in the CORFU criterion, the curves reported in Figures 3.5, 3.7 and 3.8 converge towards one V-shaped curve only with minimal radial flux maldistribution (i.e. 1-η) at CORFU=0. This suggests that the CORFU criterion accounts well for the effect of all dimensionless groups on the uniformity of radial flux distribution. The α_H and α_E values used are also in agreement with the correction factors of the kinetic factors in Equation 3.11 obtained for the actual model-predicted axial velocity profiles and with those suggested in literature for laminar flow (Perry et al., 1999; White, 2011). Figure 3.9 indicates that an ideally uniform radial flux distribution is achieved for CORFU$\rightarrow$0. Increasing absolute values of CORFU correlate well with increasing degrees of radial flux maldistribution (i.e. decreasing values of η). For practical purposes, Figure

3.9 shows that a total axial pressure drop in the void spaces up to ±10% of that across the construct thickness yields a radial flux maldistribution (i.e. 1-η) that does not exceed 10%. Support to this level of tolerance comes from the uniform cell distribution along the scaffold length experimentally obtained by Xie et al. (Xie et al., 2006) and Olivier et al. (Olivier et al., 2007) when cells were seeded and cultured under conditions yielding CORFU=0.117 and 0.095, respectively, hence in the presence of uniform enough perfusion radial fluxes. This is also in good agreement with the tolerance level recommended for industrial radial flow reactors treating turbulent gaseous streams (Celik and Ackley, 2012).

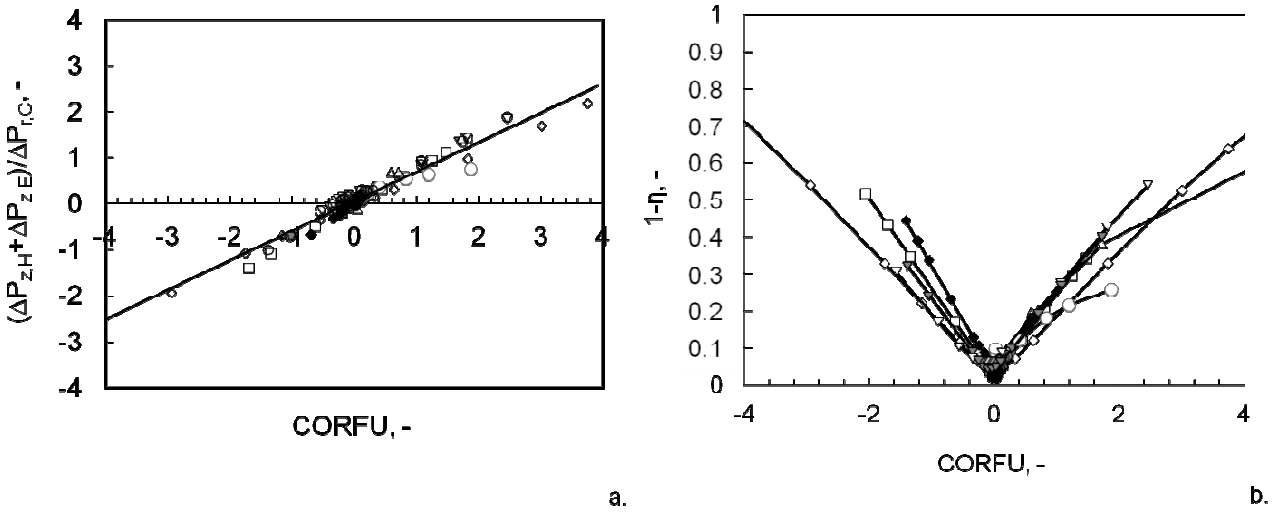

Figure 3.8 Model-predicted effect of the criterion CORFU on radial flux maldistribution, (1-η), under the following conditions: (□) same as in Figure 3.5a; (◊) same as in Figure 3.5b; (∇) same as in Figure 3.5c; (○) same as in Figure 3.6; (Δ) same as in Figure 3.8. The shade of grey of empty symbols identifies model predictions at varying parameter values, as follows: (black) minimal; (grey) intermediate; (white) maximal.

Taken altogether, these results suggest that the actual construct permeability and the design of bioreactor void spaces strongly influence the distribution of medium radial flux along the bioreactor length, hence the medium flow rate perfusing cells at different distances from the bioreactor entrance. The CORFU criterion provides a useful tool in the first design phases for selecting rPBBs in which cells are perfused at a uniform medium flux independent of their position in the construct, and for adjusting rPBB operation so as to maintain a uniform radial flux distribution as tissue matures. As for any theoretical model, the application of the criterion is limited by the assumptions

inherent in the model and in the use of the equation of mechanical energy to a liquid flowing under laminar regime, by the possible stagnation of medium in the void spaces of the bioreactor, and by unreliable parameter estimates. It should also be considered that the effect on bioreactor performance of the non-uniform radial perfusion of cells in an annular construct depends on the uniformity of cell seeding and on their sensitivity to the actual concentration of dissolved oxygen, nutrients and biochemical cues.

3.4 Conclusions

This is the first study reporting on the complete set of dimensionless groups determining the distribution of medium radial flux along the length of radial packed-bed bioreactors, on their effect on the actual radial flux distribution, and on a criterion to design and operate bioreactors in which radial fluxes are uniformly distributed under conditions typical of tissue engineering applications. The design criterion of radial flux uniformity introduced in this paper accounts well for the effect of all dimensionless groups determining medium radial flux distribution along the bioreactor length, and indicates that the total axial pressure drop along the void spaces should be within ±10% of that across the construct thickness to ensure a uniform radial flux distribution. Bioreactor designs and operation meeting the proposed criterion will contribute to avoid unwanted consequences on tissue formation caused by the non-uniform distribution of medium radial flow to cells in the construct, such as non-uniform cell proliferation or non-uniform tissue structure and functional properties, an often underestimated effect. However, the criterion should be applied with caution because of the possible mismatch between the model assumptions and the actual medium and scaffold properties.

In the next chapter, it will be presented a more comprehensive mathematical model in which mass transport is coupled to momentum transport to evaluate the effect of the actual distribution of medium radial flux on bioreactor performance and tissue reconstruction.

ppendix A – Evaluation of the pressure P_{out} at the outlet of the culture chamber of the rPBB

As shown in Figure 3.1, the pressure at which the medium leaves the culture chamber, P_{out}, differs from the atmospheric pressure by an amount given by the sum of the local pressure drops in the bioreactor zones 1-3, as follows

$$P_{out} = \Delta P_1 + \Delta P_2 + \Delta P_3 . \quad (A.1)$$

The local pressure drop of the i-th zone, ΔP_i, was expressed according to Perry et al. (Perry et al., 1999), as follows:

$$\Delta P_i = \frac{k_i}{2} \rho v_i^2 \quad (A.2)$$

where k_i is the loss coefficient associated to the change of the cross-sectional area, v_i is the average velocity in the downstream cross-sectional area of the i-th zone. k_i in zones 1-3 was estimated from the correlations reported in Perry et al. (Perry et al., 1999), Idelchick (Idelchick, 1960), and Munson et al. (Munson et al., 2013). In particular:

zone 1: k_1 was estimated as the loss coefficient for the sudden expansion from the annular cross-sectional area comprised between the circle of radius ($R + \delta_C + \delta_E$) and that of radius ($R + \delta_C$), to the annular cross-sectional area comprised between the circle of radius ($R + \delta_C + \delta_E$) and that of radius R. Under laminar flow conditions, k_1 may be expressed as follows (Perry et al., 1999):

$$k_1 = 2\left(1 - \frac{\pi((R+\delta_C+\delta_E)^2 - (R+\delta_C)^2)}{\pi((R+\delta_C+\delta_E)^2 - R^2)}\right)^2 = 2\left(1 - \frac{\delta_E{}^2 + 2(R+\delta_C)\delta_E}{(\delta_C+\delta_E)(\delta_C+\delta_E+2R)}\right)^2 . \quad (A.3)$$

v_1 was estimated from medium flow rate across the same section, as follows:

$$v_1 = \frac{Q}{\pi((R+\delta_C+\delta_E)^2 - (R+\delta_C)^2)} = \frac{u_{in}\pi R^2}{\pi((R+\delta_C+\delta_E)^2 - (R+\delta_C)^2)} . \quad (A.4)$$

Combining Equations A.2 and A.4 yields the pressure drop across zone 1:

$$\Delta P_1 = \frac{k_1}{2}\rho v_1^{\,2} = \frac{k_1}{2}\rho\left(\frac{u_{in}R^2}{(R+\delta_C+\delta_E)^2-(R+\delta_C)^2}\right)^2 = \frac{k_1}{2}\rho\left(\frac{u_{in}R^2}{\delta_E(\delta_E+2(R+\delta_C))}\right)^2 =$$

$$= \frac{k_1}{2}\rho\frac{u_{in}^{\,2}}{\frac{\delta_E^{\,2}}{R^2}\frac{(\delta_E+2(R+\delta_C))^2}{R^2}} = \frac{k_1}{2}\rho\frac{u_{in}^{\,2}}{\frac{\delta_E^{\,2}}{R^2}\left(\frac{\delta_E}{R}+2+2\frac{\delta_C}{R}\right)^2} \quad . \qquad \text{(A.5)}$$

Combining Equations 3.1 and A.5 yields ΔP_1 in terms of the dimensionless groups of Table 2, as follows:

$$\Delta P_1^* = \Delta P_1\frac{R^2}{\mu\, L\, u_{in}} = \frac{k_1}{2}\rho\frac{u_{in}^{\,2}}{\frac{\delta_E^{\,2}}{R^2}\left(\frac{\delta_E}{R}+2+2\frac{\delta_C}{R}\right)^2}\frac{R^2}{\mu\, L\, u_{in}} = \frac{k_1}{2}\frac{\rho\, u_{in}\, R}{\mu}\frac{R}{L}\frac{1}{\frac{\delta_E^{\,2}}{R^2}\left(\frac{\delta_E}{R}+2+2\frac{\delta_C}{R}\right)^2} = \qquad \text{(A.6a)}$$

$$= \frac{k_1}{2}\mathrm{Re}_{in}\, g_1$$

where

$$g_1 = \frac{1}{\frac{\delta_E^{\,2}}{R^2}\left(\frac{\delta_E}{R}+2+2\frac{\delta_C}{R}\right)^2} \quad . \qquad \text{(A.6b)}$$

zone 2: k_2 was estimated as the loss coefficient for the gradual contraction from the annular cross-sectional area comprised between the circle of radius ($R+\delta_C+\delta_E$) and that of radius R, to the annular cross-sectional area comprised between the circle of radius ($R_2 = R+c_2\,\delta_E$) and that of radius R. c_2 was used to define the geometry of zone 2 as the geometry of the culture chamber was varied in the simulations to give a 60% contraction of the cross-sectional area from zone 1 to zone 2, and a contraction angle θ=75 degrees. For each bioreactor geometry considered, and shown in Table 3.1, the value of k_2 was estimated from the chart reported in Munson et al. (Munson et al., 2013) under laminar flow conditions. v_2 was estimated from the liquid flow rate, as follows:

$$v_2 = \frac{Q}{\pi(R_2^{\,2}-R^2)} = \frac{Q}{\pi((R+c_2\delta_E)^2-R^2)} = \frac{u_{in}\pi R^2}{\pi((R+c_2\delta_E)^2-R^2)}. \qquad \text{(A.7)}$$

Combining Equations A.2 and A.7 yields the local pressure drop across zone 2, as follows:

$$\Delta P_2 = \frac{k_2}{2}\rho v_2{}^2 = \frac{k_2}{2}\rho\left(\frac{u_{in}R^2}{(R+c_2\delta_E)^2 - R^2}\right)^2 = \frac{k_2}{2}\rho\frac{u_{in}{}^2R^4}{((R+c_2\delta_E)^2 - R^2)^2} =$$

$$\frac{k_2}{2}\rho\frac{u_{in}{}^2R^4}{(c_2{}^2\delta_E{}^2 + 2Rc_2\delta_E)^2} = \frac{k_2}{2}\rho\frac{u_{in}{}^2}{\left(c_2{}^2\frac{\delta_E{}^2}{R^2} + 2c_2\frac{\delta_E}{R}\right)^2} \quad . \qquad \text{(A.8)}$$

Combining Equations 3.1 and A.8 yields ΔP_2 in terms of the dimensionless groups of Table 3.2, as follows:

$$\Delta P_2^* = \Delta P_2\frac{R^2}{\mu L u_{in}} = \frac{k_2}{2}\rho\frac{u_{in}{}^2}{\left(c_2{}^2\frac{\delta_E{}^2}{R^2} + 2c_2\frac{\delta_E}{R}\right)^2}\frac{R^2}{\mu L u_{in}} = \frac{k_2}{2}\frac{\rho u_{in}R}{\mu}\frac{R}{L}\frac{1}{\left(c_2{}^2\frac{\delta_E{}^2}{R^2} + 2c_2\frac{\delta_E}{R}\right)^2} = \qquad \text{(A.9a)}$$

$$= \frac{k_2}{2}\mathrm{Re}_{in}\, g_2$$

where

$$g_2 = \frac{1}{\left(c_2{}^2\frac{\delta_E{}^2}{R^2} + 2c_2\frac{\delta_E}{R}\right)^2} \quad . \qquad \text{(A.9b)}$$

zone 3: k_3 was estimated as the loss coefficient for the sudden contraction from the annular cross-sectional area comprised between the circle of radius (R_2=R+c_2 δ_E) and that of radius *R*, to the annular cross-sectional area comprised between the circle of radius (R_3 =R+c_3 δ_E) and that of radius *R*. c_3 was used to define the geometry of zone 3 as the geometry of the culture chamber was varied in the simulations so as to give a 35% contraction of the cross-sectional area from zone 2 to zone 3. For each geometry and operating condition reported in Table 3.1, the value of k_3 was estimated from the chart reported in Idelchik (Idelchick, 1960). v_3 was estimated from the liquid flow rate, as follows:

$$v_3 = \frac{Q}{\pi(R_3{}^2 - R^2)} = \frac{Q}{\pi((R+c_3\delta_E)^2 - R^2)} = \frac{u_{in}\pi R^2}{\pi((R+c_3\delta_E)^2 - R^2)}. \qquad \text{(A.10)}$$

Combining Equations A.2 and A.10 yields the pressure drop across zone 3, as follows:

$$\Delta P_3 = \frac{k_3}{2}\rho v_3^{\,2} = \frac{k_3}{2}\rho \frac{u_{in}^{\,2}}{\left(c_3^{\,2}\frac{\delta_E^{\,2}}{R^2} + 2c_3\frac{\delta_E}{R}\right)^2} \quad . \tag{A.11}$$

Combining Equations 3.1 and A.11 yields ΔP_3 in terms of the dimensionless groups of Table 3.2, as follows:

$$\Delta P_3^{*} = \frac{k_3}{2}\frac{\rho u_{in} R}{\mu}\frac{R}{L}\frac{1}{\left(c_3^{\,2}\frac{\delta_E^{\,2}}{R^2} + 2c_3\frac{\delta_E}{R}\right)^2} = \frac{k_3}{2}\mathrm{Re}_{in}\, g_3 \tag{A.12a}$$

where

$$g_3 = \frac{1}{\left(c_3^{\,2}\frac{\delta_E^{\,2}}{R^2} + 2c_3\frac{\delta_E}{R}\right)^2} \quad . \tag{A.12b}$$

Appendix B – Expression of the CORFU criterion in terms of the dimensionless groups determining momentum transport in the rPBB

B1. Evaluation of axial pressure drops in the void spaces of the rPBB

The axial pressure drops in the void spaces of the rPBB as medium is distributed across or collected from the porous construct were estimated under the following assumptions: i) medium flows axially in laminar flow; ii) the radial flux is uniformly distributed along the construct length; iii) the inner and outer construct lateral surface areas are greater than the cross-sectional surface area of the zones through which medium enters or leaves the culture chamber, respectively; iv) negligible local pressure drops associated with the change of medium direction and of the cross-sectional surface area. The deviation of the axial velocity profiles from the uniform flat profile were accounted for along that suggested in Bird et al. (Bird et al., 2002) by introducing a kinetic correction factor α_i, with i=H or E, defined as follows:

$$\frac{1}{\alpha_i} = \frac{1}{A_i}\int_{A_i}\left(\frac{u_i(r)}{u_{i,ave}}\right)^3 dA_i \tag{B.1}$$

where: A_i is the cross-sectional area through which medium axially enters or leaves the culture chamber; $u_i(r)$ is the axial velocity profile at the same section; $u_{i,ave}$, is the average axial velocity at the same sections. The assumption of radial flux uniformity at the construct lateral surfaces yields $\alpha_i=1$, for both i=H and E. Hence, hereinafter α_i is considered only for the inlet and outlet cross-sectional areas.

B1.1 Axial pressure drop in the inner hollow cavity, $\Delta P_{z,H}$

Under the assumptions reported above, the macroscopic continuity equation and balance of mechanical energy about the whole inner hollow cavity yield what follows, respectively (Bird et al., 2002):

$$\frac{u_{in}}{v_R} = 2\frac{L}{R} = \frac{1}{\beta_H} \tag{B.2}$$

$$\frac{{v_R}^2}{2} - \frac{{u_{in}}^2}{2\alpha_H} + \frac{P_{H,out} - P_{H,in}}{\rho} + \hat{E}_{,v,H} = 0 \tag{B.3}$$

where: v_R is the radial velocity at the inner construct lateral surface; $P_{H,out}$ and $P_{H,in}$ are the pressures at the inner construct lateral surface and inlet section, respectively; $\hat{E}_{v,H}$ is the viscous dissipation term; β_H is the cross-sectional area ratio. As medium flows in the inner hollow cavity and it is distributed across the porous construct, $\hat{E}_{v,H}$ may be written as follows (Bird et al., 2002):

$$\hat{E}_{v,H} = \frac{1}{2}\int_0^L u_H(z)^2 \frac{4 f_H(z)}{2R} dz \tag{B.4}$$

where $f_H(z)$ is the Fanning friction factor in the hollow cavity. For a uniform radial flux along the construct length, the continuity equation yields the axial velocity at any distance from medium entrance as follows:

$$u_H(z) = u_{in}\left(1 - \frac{z}{L}\right) . \tag{B.5}$$

In laminar regime, the friction factor in the hollow cavity was estimated as follows (Bird et al., 2002):

$$f_H(z) = 16\frac{\mu}{u_H(z)\ 2R\ \rho}. \qquad \text{(B.6)}$$

Combining Equations B.4-B.6 yields:

$$\hat{E}_{v,H} = 8\frac{\mu}{\rho\ R^2}u_{in}\int_0^L\left(1-\frac{z}{L}\right)dz = 8\frac{\mu}{\rho R^2}u_{in}\frac{L}{2} = \frac{1}{2}u_{in}{}^2\ \frac{8}{\mathrm{Re}_{in}}. \qquad \text{(B.7)}$$

Combining equations B.2, B.3 and B.7 yields:

$$P_{H,in} - P_{H,out} = \Delta P_{z,H} = \rho\left\{\frac{v_R{}^2}{2} + \frac{1}{2}u_{in}{}^2\left[-\frac{1}{\alpha_H} + \frac{8}{\mathrm{Re}_{in}}\right]\right\} = \rho\frac{1}{2}u_{in}{}^2\left[\beta_H{}^2 - \frac{1}{\alpha_H} + \frac{8}{\mathrm{Re}_{in}}\right]. \qquad \text{(B.8)}$$

Under the conditions at which the simulations were obtained $\beta_H{}^2 << 1$, hence $\Delta P_{z,H}$ becomes:

$$\Delta P_{z,H} = \frac{1}{2}\rho u_{in}{}^2\left(\frac{8}{\mathrm{Re}_{in}} - \frac{1}{\alpha_H}\right). \qquad \text{(B.9)}$$

B1.2 Axial pressure drop in the outer peripheral annulus, $\Delta P_{z,E}$

The macroscopic continuity equation about the whole outer peripheral annulus yields:

$$\frac{u_{E,out}}{v_{R_C}} = \frac{2R_C\ L}{\left(R_E^2 - R_c^2\right)} = \frac{1}{\beta_E} \qquad \text{(B.10)}$$

where: R_C is the construct outer radius, $R_C = R + \delta_C$; R_E is the inner radius of the culture chamber, $R_E = R_C + \delta_E$; $u_{E,out}$ is the average axial velocity at the outlet section; v_{RC}, is the radial velocity at the outer construct surface; β_E is the cross-sectional area ratio. The continuity of mass between the sections through which medium enters and leaves the culture chamber gives a relationship between $u_{E,out}$ and u_{in} which may be combined with Equation B.10 to yield:

$$\frac{u_{in}}{v_{R_C}} = \frac{2R_C\ L}{R^2}. \qquad \text{(B.11)}$$

Under the assumptions reported above, the macroscopic balance of mechanical energy about the whole outer peripheral annulus yields what follows:

$$\frac{u_{E,out}{}^2}{2\alpha_E} - \frac{v_{R_C}{}^2}{2} + \frac{P_{E,out} - P_{E,in}}{\rho} + \hat{E}_{v,E} = 0 \qquad \text{(B.11)}$$

where $P_{E,out}$ and $P_{E,in}$ are the pressures at the outlet section and outer construct lateral section, respectively; $\hat{E}_{v,E}$ is the viscous dissipation term in the peripheral annulus. As medium flows in the peripheral annulus and is collected from the porous construct, $\hat{E}_{v,E}$ may be written as follows (Bird et al., 2002):

$$\hat{E}_{v,E} = \frac{1}{2}\int_0^L u_E(z)^2 \frac{f_E(z)}{R_{HE}} dz \tag{B.12}$$

where $f_E(z)$ is the Fanning friction factor in the peripheral annulus, and R_{HE} is the hydraulic radius of the peripheral annulus defined as follows:

$$R_{HE} = \frac{1}{2}\frac{R_E^2 - R_C^2}{R_E + R_C}. \tag{B.13}$$

For uniform radial flux along the construct length, the continuity equation yields the axial velocity at any distance from medium outlet as follows:

$$u_E(z) = \frac{z}{L} u_{E,out} . \tag{B.14}$$

In laminar regime, the friction factor in the peripheral annulus may be estimated as follows (Bird et al., 2002):

$$f_E(z) = 4\frac{\mu}{u_E(z)\ R_{HE}\ \rho}. \tag{B.15}$$

Combining Equations B.12-B.15 yields:

$$\hat{E}_{v,E} = 2\frac{\mu}{\rho R_{HE}^2}\frac{L}{2}u_{E,out} . \tag{B.16}$$

Combining Equations B.10-B.16 yields $\Delta P_{z,E}$, as follows:

$$\Delta P_{z,E} = \frac{1}{2}\rho u_{in}^2 \left(\frac{R^2}{R_E^2 - R_C^2}\right)^2 \left\{\frac{1}{\alpha_E} - \beta_E^2 + 8\frac{1}{\mathrm{Re}_{in}}\frac{(R_E + R_C)^2}{R_E^2 - R_C^2}\right\}. \tag{B.17a}$$

Under the conditions at which the simulations were obtained $\beta_E^2 << 1$, hence $\Delta P_{z,H}$ may be written in terms of the dimensionless groups in Table 3.2 as follows:

$$\Delta P_{z,E} = \frac{1}{2}\,\rho\, u_{in}^{\,2}\;\frac{1}{\left\{\frac{\delta_E}{R}\left[2\left(1+\frac{\delta_C}{R}\right)+\frac{\delta_E}{R}\right]\right\}^2}\;\left\{\frac{1}{\alpha_E}+\frac{8}{\mathrm{Re}_{in}}\left[2\,\frac{R}{\delta_E}\left(1+\frac{\delta_C}{R}\right)+1\right]\right\}. \qquad \text{(B.17b)}$$

B2. Evaluation of radial pressure drop across the porous construct

The radial pressure drop across the porous construct, $\Delta P_{r,C}$, was estimated by assuming that medium flow may be described according to the Darcy's equation, as follows (Bird et al., 2002):

$$v_R = \frac{k}{\mu\, R}\,\frac{1}{\ln\left(1+\frac{\delta_C}{R}\right)}\,\Delta P_{r,C}. \qquad \text{(B.18)}$$

Combining Equations B.2 and B.18, $\Delta P_{r,C}$ may be expressed in dimensionless form as follows:

$$\Delta P_{r,C} = \frac{v_R}{\frac{k}{\mu\, R}\,\frac{1}{\ln\left(1+\frac{\delta_C}{R}\right)}} = \frac{1}{2}\rho\, u_{in}^{\,2}\;\frac{R^2}{k}\left(\frac{R}{L}\right)^2\;\frac{1}{\mathrm{Re}_{in}}\;\ln\left(1+\frac{\delta_C}{R}\right). \qquad \text{(B.19)}$$

B3. Expression of the CORFU criterion as total axial-to-radial pressure drop ratio

The CORFU criterion was defined as the ratio between the total axial pressure drop in the void spaces and the radial pressure drop across the construct. Combining Equations B.9, B.17b, and B.19, the CORFU criterion may be expressed as a function of the dimensionless groups in Table 3.2 as follows:

$$CORFU = \frac{\Delta P_{z,H}+\Delta P_{z,E}}{\Delta P_{r,C}} = \frac{\left\{\left(8\,\frac{1}{\mathrm{Re}_{in}}-\frac{1}{\alpha_H}\right)\right\}+\left\{\frac{1}{\left\{\frac{\delta_E}{R}\left[2\left(1+\frac{\delta_C}{R}\right)+\frac{\delta_E}{R}\right]\right\}}\left[\frac{1}{\alpha_E}+8\,\frac{1}{\mathrm{Re}_{in}}\left(2\left(\frac{1+\frac{\delta_C}{R}}{\frac{\delta_E}{R}}\right)+1\right)\right]\right\}}{\left(\frac{R^2}{k}\,\left(\frac{R}{L}\right)^2\,\ln\left(1+\frac{\delta_C}{R}\right)\frac{1}{\mathrm{Re}_{in}}\right)} \qquad \text{.(B.20)}$$

Appendix C – Expression of Chang's criterion, ξ, in dimensionless form

Genkin et al. (Genkin et al., 1973) define the parameter ξ as the inner hollow cavity-to-peripheral annulus cross sectional area ratio, as follows:

$$\xi = \frac{A_H}{A_E} = \frac{\pi R^2}{\pi((R+\delta_C+\delta_E)^2-(R+\delta_C)^2)} \quad . \tag{C.1}$$

Re-arranging the denominator according to Equation 3.1 permits to express ξ as a function of the dimensionless groups determining momentum transport in the rPBB, as follows:

$$\xi = \frac{A_H}{A_E} = \frac{R^2}{\delta_E{}^2 + 2\delta_E(R+\delta_C)} = \frac{R^2}{\delta_E{}^2\left(1+2\frac{R+\delta_C}{\delta_E}\right)} = \frac{\left(\frac{R}{\delta_E}\right)^2}{1+2\frac{R}{\delta_E}\left(1+\frac{\delta_C}{R}\right)} = f_2\left(\frac{R}{\delta_C},\frac{R}{\delta_E}\right) \quad . \tag{C.2}$$

Chapter 4

Study of the effect of radial flux distribution on pericellular oxygen concentration in radial flow packed-bed bioreactors with a 2D stationary transport model

4.1 Introduction

In the previous chapter, a complete description of momentum transport in all the rPBB compartments with the aim of proposing a criterion to optimize the geometry of the void spaces and the operational conditions of rPBBs for given construct properties to ensure uniform radial flux distribution along the construct length was provided. However, the momentum transport model discussed in chapter 3 does not provide any description of mass transport phenomena occurring in the bioreactor compartments nor suggests how radial flux distribution actually influences mass transport towards cells at different cell concentrations.

In this chapter, a two-dimensional steady-state model is proposed describing mass and momentum transport in the three compartments of an rPBB for tissue engineering to determine the actual effect of medium radial flux distribution on oxygen supply to cells during tissue reconstruction and to design rPBBs providing physiological supply of biochemical cues to cells depending on their metabolic requirements, for a given therapeutic objective. Dissolved oxygen was considered the limiting solute according to the experimental results reported in literature (Rotem et al., 1994; Griffith and George, 2009), and it is consequently assumed that other solutes, such as glucose and glutamine, are present at concentrations that do not limit tissue development. Momentum transport in the void spaces of the rPBB is described with Navier-Stokes equation, whereas Darcy-Brinkman equation is used to describe momentum transport in the construct, according to the model proposed in the previous chapter. Transport of dissolved oxygen is described with convection-diffusion and convection-diffusion-reaction equations in the void spaces of the rPBB and in the construct, respectively. Oxygen consumption is described according to

Michaelis-Menten kinetics. The oxygen mass transfer coefficients at the interface between medium bulk in the construct pores and cell surface are estimated for a bed of Raschig rings transport-equivalent to 3D scaffolds typically used in tissue engineering applications. The dimensionless groups determining bioreactor behavior are obtained from dimensional analysis and account for construct transport properties and rPBB geometry and operating conditions. Their influence on oxygen supply to cells is investigated with the integration of the model equations under working conditions typical of tissue engineering in order to determine the dependence of the pericellular environment on the distribution and the extent of the medium radial fluxes.

4.2 Materials and methods

4.2.1 Model development

A scheme of an rPBB is shown in Figure 4.1. The bioreactor consists of a vessel in which it is coaxially located a 3D annular porous scaffold. Cells are seeded and cultured in the pores of the construct, which is continuously perfused with medium supplying dissolved oxygen and nutrients and removing metabolic wastes along its radius. Medium perfusion is assumed to occur in a flow configuration referred to as CF-π flow. According to such configuration, medium flows from the inner hollow cavity towards the outer peripheral annulus (centrifugal configuration, CF), to enhance mass transport across the construct in case of uniform radial flux distribution along the construct length as compared to the opposite configuration (chapter 2), and that medium flow directions in the inner hollow cavity and the peripheral annulus are opposite (π), as suggested by the results reported by Kareeri et al. to reduce the degree of radial flux maldistribution in industrial reactors treating gaseous streams (Kareeri et al., 2006). Dissolved oxygen is transported into the construct by convection and diffusion and is consumed by the cells. The conservation equations governing rPBB behavior were obtained under the following assumptions: axial symmetry; steady-state isothermal conditions; incompressible Newtonian fluid; transport in the porous construct, assumed isotropic, described according to a pseudo-homogeneous approach; momentum transport in the construct

described according to the Darcy-Brinkman equation (Brinkman, 1947); momentum transport in the inner channel and the peripheral annulus described according to the Navier-Stokes equations (Bird et al., 2003); dissolved oxygen cellular consumption described according to Michaelis-Menten kinetics. Upon introducing the following dimensionless coordinates and variables

$$r^*=\frac{r}{R};\ z^*=\frac{z}{L};\quad u_i^*=\frac{u_i}{u_{in}};\quad v_i^*=\frac{v_i}{u_{in}}\frac{L}{R};\quad P_i^*=\frac{P_i}{u_{in}\mu L/R^2};\ C_i^*=\frac{C_i}{C_o};\ \beta=\frac{K_M}{C_o} \tag{4.1}$$

pressure and velocity profiles are calculated by solving the dimensionless momentum conservation equations, with the correspondent boundary conditions, proposed in the previous chapter on the account that mass and momentum conservation equations are uncoupled for constant construct properties. In addition, the governing mass conservation equations may be re-arranged in non-dimensional form to give:

Hollow cavity (convection-diffusion equation)

$$Pe_{rad,\max}\ \frac{R}{\delta_C}\frac{D_C}{D_H}\left(v_H^*\frac{\partial C_H^*}{\partial r^*}+u_H^*\frac{\partial C_H^*}{\partial z^*}\right)=\frac{1}{r^*}\frac{\partial}{\partial r^*}\left(r^*\frac{\partial C_H^*}{\partial r^*}\right)+\left(\frac{R}{L}\right)^2\frac{\partial^2 C_H^*}{\partial z^{*2}} \tag{4.2}$$

Construct (convection-diffusion-reaction equation)

$$Pe_{rad,\max}\ \frac{R}{\delta_C}\left(v_C^*\frac{\partial C_C^*}{\partial r^*}+u_C^*\frac{\partial C_C^*}{\partial z^*}\right)=\frac{1}{r^*}\frac{\partial}{\partial r^*}\left(r^*\frac{\partial C_C^*}{\partial r^*}\right)+\frac{R^2}{L^2}\frac{\partial^2 C_C^*}{\partial z^{*2}}-\phi_C^{*2}\frac{R^2}{\delta_C{}^2}\frac{C_{Ci}^*}{\beta+C_{Ci}^*} \tag{4.3}$$

Outer annulus (convection-diffusion equation)

$$Pe_{rad,\max}\ \frac{R}{\delta_C}\frac{D_C}{D_E}\left(v_E^*\frac{\partial C_E^*}{\partial r^*}+u_E^*\frac{\partial C_E^*}{\partial z^*}\right)=\frac{1}{r^*}\frac{\partial}{\partial r^*}\left(r^*\frac{\partial C_E^*}{\partial r^*}\right)+\left(\frac{R}{L}\right)^2\frac{\partial^2 C_E^*}{\partial z^{*2}} \tag{4.4}$$

Equations #4.1-4.4 are subject to the following boundary conditions: uniform oxygen concentration profile in the stream entering the bioreactor; bioreactor axis impervious to mass (*i.e.* $\forall\, z^*$, for $r^*=0$, $\partial C_H{}^*/\partial r^*=0$); continuity of oxygen concentration at the interface between inner hollow cavity and construct, and between construct and outer peripheral annulus; walls of the housing impervious to mass; no further oxygen concentration changes at the bioreactor exit. At the cell surface, the reaction rate is equal to the overall transport rate, as follows:

$$\frac{\phi_S{}^2}{Sh_p}\frac{C_{Ci}^*}{\beta + C_{Ci}^*} = C_C{}^* - C_{Ci}{}^* \tag{4.5}$$

which may be rearranged to give

$$C_{Ci}^* = \frac{1}{2}\left(C_C^* - \beta - \phi_S^2 / Sh_p + \sqrt{(C_C^* - \beta - \phi_S^2 / Sh_p)^2 + 4\beta\ C_C^*}\right) \tag{4.6}$$

In order to predict the value of the mass transfer coefficient, *kc*, a criterion was developed to derive a transport equivalence between a hollow cylindrical porous scaffold for tissue engineering and a porous bed of solid particles. In particular, it was assumed that the complex morphology of a 3D porous scaffold might be resembled by that of a bed of Raschig rings randomly packed, because of their similarity in terms of the patterns for momentum and mass transport. In particular, it was assumed that the transport equivalence between a 3D porous scaffold and a bed of Raschig rings may be found in terms of porosity and specific surface. According to this assumption, the given porous scaffold and the equivalent packed bed are supposed to have the same porosity and specific surface (*i.e.* $\varepsilon_{bed} = \varepsilon_{scaffold}$ and $a_{c,bed} = a_{c,scaffold}$). The specific surface of the single Raschig ring, a_{Vp}, is then calculated as (Bird et al., 2003):

$$a_{Vp} = \frac{a_{c,bed}}{1 - \varepsilon_{bed}} \tag{4.7}$$

With the value of a_{Vp} calculated from Equation 4.7, the equivalent diameter of the Raschig ring, $d_{p,e}$, is calculated from the correlation found by interpolating the experimental data reported in Perry et al. (Perry et al., 1999) (Figure A.1 in Appendix A), as follows:

$$1/a_{Vp} = 0.2167\, d_{p,e} \tag{4.8}$$

The oxygen mass transfer coefficient at the interface between the medium bulk in the construct pores and the cell surface was finally estimated for a bed of Raschig rings transport-equivalent to 3D porous scaffolds typically used in tissue engineering applications. In particular:

$$kc = Sh_p \frac{D_H}{d_{p,e}} \tag{4.9}$$

where the particle Sherwood number, Sh_p, is obtained from a general correlation valid for Raschig rings in liquid phase under laminar flow for the value of the maximal radial superficial velocity v_o and for a void fraction of the packed bed ranging from 0.63 to 0.76 (Shulman et al., 1955):

$$Sh_p = 25.1\left(1.3\frac{v_o d_{p,e}\rho}{\mu}\right)^{0.45}\left(\frac{\mu}{\rho D_H}\right)^{0.5} \tag{4.10}$$

The consistency of the transport equivalence between a bed of Raschig rings and a porous scaffold was assessed in terms of Darcy permeability. Reference was made to scaffold properties reported for bone tissue engineering. In particular, the bed Darcy permeability was calculated from the values of ε_{bed} and $d_{p,e}$ according to the Carman-Kozeny equation:

$$k_{bed} = \frac{\varepsilon_{bed}^{\ 3}}{(1-\varepsilon_{bed})^2}\frac{d_{p,e}^{\ 2}\varphi^2}{180} = \frac{\varepsilon_{scaffold}^{\ 3}}{(1-\varepsilon_{scaffold})^2}\frac{d_{p,e}^{\ 2}\varphi^2}{180} \tag{4.11}$$

where φ is the particle shape factor and was reported to be equal to 0.3 for Raschig rings (Geankoplis, 1993, Perry et al., 1999). For values of scaffold porosities ranging from 0.5 to 0.9, and scaffold specific surfaces ranging from 1410 m^2/m^3 to 5420 m^2/m^3 , typical of scaffolds used for bone tissue engineering (Karageorgiou and Kaplan, 2005; Van Cleynenbreugel et al., 2006), the values of the bed Darcy permeability, k_{bed}, found from Equation 4.11 result to be of the same order of magnitude of the scaffold Darcy permeabilities reported in literature, *i.e.* from 10^{-10} m^2 to 10^{-8} m^2 (Dias, 2012; Ochoa, 2009; Mitsak, 2012; Lee, 2006). This justifies the consistency of the assumption of transport equivalence between a 3D porous scaffold and a bed of Raschig rings.

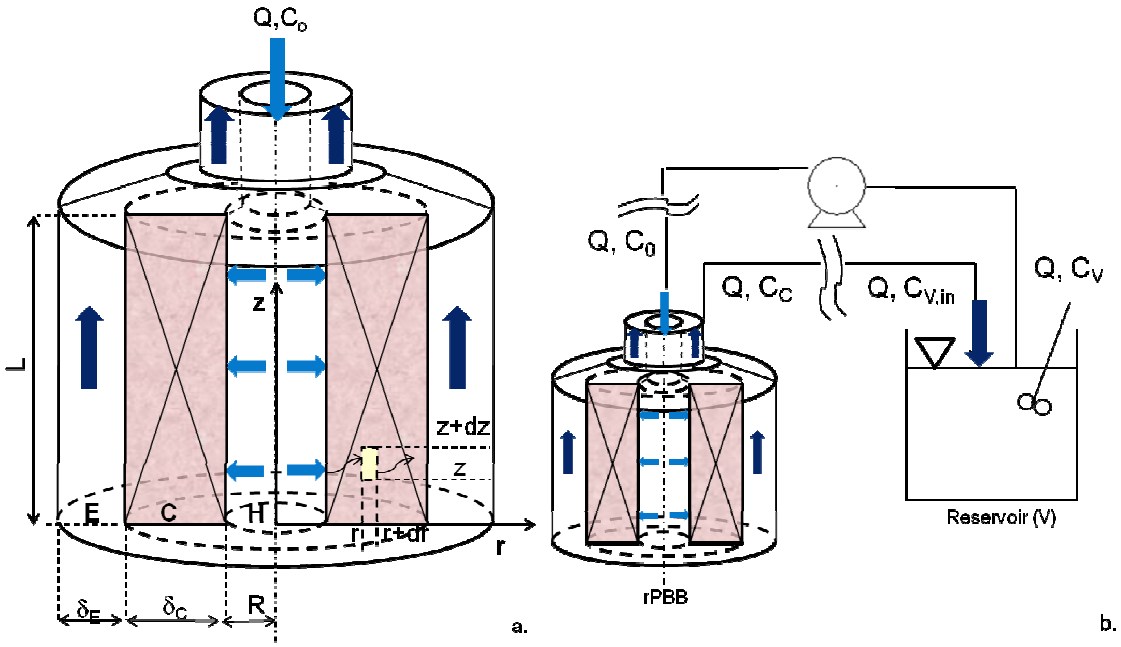

Figure 4.1 (a) Scheme of an rPBB showing the three compartments (i.e. inner hollow cavity, H; construct, C; outer peripheral annulus, E) and an exemplary differential control volume; (b) Scheme of the complete rPBB culture system, with the rPBB coupled in a closed loop to a completely-mixed reservoir where solutes concentrations are measured.

4.2.2 Dimensionless groups

The analysis of the dimensionless conservation equations 4.1-4.6 and of the related boundary conditions suggests that the bioreactor behavior depends on the dimensionless groups reported in Table 4.1. The physical meaning of most of them may be found in literature (Fogler et al., 2006; Bird et al., 2003).

The reduced Reynolds number, Re_{in}, accounts for the extent of the flow rate at the bioreactor inlet, and increases for higher inlet flow rates. Together with Re_{in}, in this work the effect of all the dimensionless groups determining momentum transport on bioreactor behavior is assessed in terms of the criterion of radial flux uniformity (CORFU) defined previously as:

$$CORFU = \frac{\left\{\left(8\,\frac{1}{\mathrm{Re}_{in}} - \frac{1}{\alpha_H}\right)\right\} + \left\{\xi^2\left[\frac{1}{\alpha_E} + 8\,\frac{1}{\mathrm{Re}_{in}}\left(2\left(\frac{1+\frac{\delta_C}{R}}{\frac{\delta_E}{R}}\right)+1\right)\right]\right\}}{\left(\frac{R^2}{k}\left(\frac{R}{L}\right)^2 \ln\left(1+\frac{\delta_C}{R}\right)\frac{1}{\mathrm{Re}_{in}}\right)} = f_1\left(\mathrm{Re}_{in}, \frac{L}{R}, \frac{\delta_C}{R}, \frac{\delta_E}{R}, \frac{k}{R^2}\right) \quad (4.12)$$

where α_H and α_E are the kinetic energy correction factors in the hollow cavity and in the peripheral annulus, respectively, and ξ is the hollow cavity-to-peripheral annulus cross-sectional area ratio:

$$\xi = \frac{A_H}{A_E} = \frac{\left(\frac{R}{\delta_E}\right)^2}{1 + 2\frac{R}{\delta_E}\left(1 + \frac{\delta_C}{R}\right)} = f_2\left(\frac{R}{\delta_C}, \frac{R}{\delta_E}\right) \tag{4.13}$$

Values of the dimensionless groups giving CORFU → 0 have been shown to ensure uniform radial flux distribution of the culture medium along the construct length (chapter 3).

The effect of cells metabolic requirements on oxygen concentration profiles may be assessed in terms of the oxygen Thiele modulus, which is defined as the ratio between the maximal zero-th order oxygen consumption rate, $V_{max} = C_{cell} \cdot G$, and the maximal rate of diffusive oxygen transport, $C_o D_C / \delta_C^2$. Higher Thiele moduli are generally related to higher cell metabolic requirements.

In the following, reference will be made on the influence of the reduced Reynolds number, Re_{in}, and the oxygen Thiele modulus, ϕ_C on oxygen supply to the cells since they are the two operational parameters determining bioreactor behavior, for a given bioreactor geometry.

Dimensionless group	**description**
1. $\rho u_{in} R/\mu$ R/L	reduced Reynolds number, Re_{in}
2. R/L	aspect ratio
3. R/δ_C	inner radius-to-construct thickness ratio
4. R/δ_E	inner radius-to-outer channel thickness ratio
5. k/R^2	construct-to-hollow cavity permeability ratio
6. $u_{in}\delta_C R/(D_C L)$	maximal radial Peclet number $Pe_{rad,\max}$
7. D_C/D_H	construct diffusivity-to-hollow cavity diffusivity ratio
8. D_C/D_E	construct diffusivity-to-peripheral annulus diffusivity ratio
9. K_M/C_o	saturation parameter β
10. $\sqrt{(V_{max}\delta_C^2/(C_o D_C))}$	Thiele modulus ϕ_C
11. $(V_{max} d_{p,e}^2/(4.61 C_o D_C(1-\varepsilon)))/(d_{p,e} kc/D_C)$	squared surface Thiele modulus-to-Sherwood number ratio, ϕ_S^2/Sh_p

Table 4.1 Dimensionless groups determining rPBB performance

4.2.3 Computational methods

Model equations with the related boundary conditions were solved numerically with the commercial finite element method code Comsol Multiphysics (Comsol Inc., Burlington, MA, USA) in order to predict the spatial profiles of axial and radial velocity, pressure and dissolved oxygen concentrations for values of model parameters and dimensionless groups typical of tissue engineering, as reported in Tables 4.2 and 4.3, unless otherwise specified. Bioreactor compartments were discretized with rectangular elements, which number and distribution was chosen in order to keep the relative error on the predicted mixing cup concentration at bioreactor exit below 0.05% for each set of dimensionless groups. Bioreactor geometrical parameters and construct properties (i.e. porosity, Darcy permeability and specific surface) were chosen in the ranges of those reported for bone tissue engineering (Gardel et al., 2013; Olivier et al., 2007; Ochoa et al., 2009; Dias et al., 2002; Jeong et al., 2011; Lee et al., 2006; Mitsak et al., 2012; Van Cleynenbreugel et al., 2006; Karageorgiou and Kaplan, 2005), unless otherwise stated. The oxygen diffusion coefficient in the hollow cavity and the peripheral annulus was assumed to be equal to that in the water, whereas the oxygen effective diffusivity in the construct was calculated by multiplying the oxygen diffusivity in water and the construct porosity (Fogler et al., 2006).

The dependence of the oxygen concentration profiles in the construct on the ability of the bioreactor to enhance oxygen transport towards the cells was assessed in terms of the overall effectiveness factor, defined as the ratio between the actual total average oxygen consumption rate in the construct to the oxygen consumption rate calculated as if all the cells in the construct were exposed to the bulk conditions. However, for tissue engineering applications it was considered to be more useful to express the effectiveness of dissolved oxygen supply to the cells in terms of the non-hypoxic fractional construct volume (NHy-FCV), which measures the fractional volume of the construct in which cells are exposed to values of oxygen concentration higher than a hypoxic threshold, that was established to be equal to $2 \cdot 10^{-2}$ mol/m^3 (Loiacono and Shapiro, 2010). The

uniformity of oxygen concentration distribution along the bioreactor length was characterized in terms of a dimensionless parameter, η_c, defined as:

$$\eta_c = \int_1^{1+\frac{\delta_C}{R}} C_{ci}^{*}|_{z^*=1}(r^*)dr^* - \int_1^{1+\frac{\delta_C}{R}} C_{ci}^{*}|_{z^*=0}(r^*)dr \quad (4.14)$$

Values of $\eta_c = 0$ characterize an ideally uniform oxygen concentration distribution along the bioreactor length.

Parameter	**value**	**unit**	**description**	**reference**
L	0.042	m	bioreactor length	Gardel, 2013
R	$4 \cdot 10^{-3}$	m	construct inner radius	Melchels et al., 2011
δ_C	$5 \cdot 10^{-3}$	m	construct thickness	Gardel, 2013; Olivier et al., 2007
δ_E	$6 \cdot 10^{-3}$	m	external channel thickness	
ρ	993.37	kg/m^3	fluid density	Ma , 2009
μ	$6.94 \cdot 10^{-4}$	kg/(m·s)	fluid viscosity	Abdullah 2006
ε	0.75	-	construct porosity	Bancroft, 2002; Karageorgiou and Kaplan, 2005
k	1.5×10^{-9}	m^2	construct permeability	Dias, 2012; Ochoa, 2009; Mitsak, 2012; Grimm et al., 1997
$a_{c,scaffold}$	1410	m^2/m^3	construct specific surface	Van Cleynenbreugel, 2006, Martin, 1984
D_H, D_E	$2.64 \cdot 10^{-9}$	m^2/s	oxygen diffusivity in H and E	Han & Bartels, 1996
C_o	0.216	mol/m^3	inlet oxygen concentration	Han & Bartels, 1996
G	$2.64 \cdot 10^{-17}$	mol/(s·cell)	oxygen consumption rate	Lavrentieva et al., 2010
K_M	$1.1 \cdot 10^{-2}$	mol/m^3	oxygen Michaelis constant	Zhao et al., 2007

Table 4.2 Model parameter values used for model predictions, unless otherwise stated

Dimensionless group	value	Application
1. $\rho u_{in} R\mu$ R/L	0.01 – 10	BTE, LTE, CTE (Hongo et al., 2005; Melchels et al., 2011; Shao et al., 2009)
2. L/R	10.5	BTE, LTE (Hongo et al., 2005; Shao et al., 2009)
3. R/δ_C	0.8	HP (Noble et al., 1988)
4. R/δ_E	0.62 – 4	BTE, LTE (Park et al., 2008, Olivier et al., 2007; Arano et al., 2010)
5. k/R^2	9.4 x 10^{-5}	BTE, HP (Li et al., 2003; Dias et al., 2012; Grimm et al., 1997)
6. $u_{in}\delta_C R/(D_C L)$	42-2314	BTE, LTE, CTE (Hongo et al., 2005; Melchels et al., 2011; Shao et al., 2009)
7. D_C/D_H , D_C/D_E	0.75	BTE, LTE (Xie et al, 2006; Hongo et al., 2005)
8. ϕ_S^2/Sh_p	5 x 10^{-8} – 0.4	LTE (Hongo et al., 2005)
9. $\sqrt{(V_{max}\delta_C^2/(C_o D_C))}$	0.1-11.6	BTE, LTE, HTE, CTE (Sullivan et al., 2007; Lavrentieva et al., 2000; Komarova et al., 2000; Stockwell, 1971; Zhao et al., 2005)
10. K_M/C_o	0.05	BTE (Zhao et al., 2007)

Table 4.3 Dimensionless groups values used for model predictions, unless otherwise stated. Applications: BTE – bone tissue engineering; CTE – cartilage tissue engineering; HP – human physiology; LTE – liver tissue enginering; HTE – cardiac tissue engineering.

4.2.4 Model validation

In order to assess model reliability, due to the lack of appropriate experimental results reported for oxygen consumption during cell culture in rPBBs for tissue engineering, the model was validated by comparing model predictions to the experimental results reported by Hongo et al. for glucose consumption by HepG2 cells cultured in an rPBB packed with spherical hydroxyapatite beads and perfused inwards (Hongo et al., 2005 and 2006), and to those reported by Olivier et al. for glucose consumption by osteosarcoma cells in an rPBB packed with a β-TCP porous scaffold

perfused outwards (Olivier et al., 2007), for liver and bone tissue engineering applications, respectively, under the geometrical and working conditions reported by the authors. In both cases, the bioreactor was coupled in a closed loop to a reservoir where glucose concentration was measured daily (Figure 4.1b), the volume of which was reported to be equal to 200 ml and 100 ml, respectively. Accordingly, glucose consumption rate was estimated from the model-predicted glucose concentration decrease in the reservoir after 24 hours by coupling model equations 4.1-4.6 to that resulting from an unsteady-state balance of glucose in the reservoir, that was obtained under the following assumptions: the volume of the pipes were negligible as compared to that of the reservoir; completely-mixed reservoir; bioreactor dynamics negligible with respect to that of the reservoir because of the higher reservoir volume (*i.e.* higher hold-up time) as compared to that of the bioreactor; constant glucose consumption rate within 24 h. In particular, under these assumptions, the unsteady-state balance of glucose in the reservoir gives, in dimensional form:

$$V_V \frac{dC_V}{dt} = Q(C_{V,in} - C_V) \tag{4.15a}$$

where V_V represents the volume of the reservoir and

$$C_{V,in} = C_C \tag{4.15b}$$

Equation 4.15a may be solved with the initial condition:

$$I.C. \qquad t = 0 \qquad C_V = C_o \tag{4.15c}$$

The HepG2 cell-specific glucose consumption rate was estimated as the value of glucose consumption rate averaged between those reported by Hongo et al. at days 1 and 8 (Hongo et al., 2005), and it was found to be equal to 1.57 x 10^{-17} mol/(s cell), consistent with the values reported in literature (Iyer et al., 2010). In addition, the Michaelis constants for glucose consumption by HepG2 was assumed to be equal to 6.75 x 10^{-4} mol/m^3 (Sugiura et al., 2011). Furthermore, in this case the glucose mass transfer coefficient was calculated from the correlation reported by Karabelas et al. for spherical particles under laminar flow (Karabelas et al., 1971), as follows:

$$Sh_p = 4.58\left(\frac{v_o d_p \rho}{\mu}\right)^{1/3}\left(\frac{\mu}{\rho D_H}\right)^{1/3} \quad (4.16)$$

where d_p represents the diameter of a spherical bead. The cell-specific glucose consumption rate for osteosarcoma cells was estimated as the averaged value between those reported by Olivier et al. at days 7 and 28 (Olivier et al., 2007), and was found to be equal to 1.39 x 10^{-16} mol/(s cell), consistent with the value reported by White et al. (White et al., 1983). Furthermore, the Michaelis constant for glucose consumption by osteosarcoma cells was assumed to be equal to 0.52 mol/m^3 (White et al., 1983). In both cases, cell concentration after 24 h was calculated by dividing the correspondent value of the glucose consumption rate reported by the authors for the value of the cell-specific glucose consumption rate previously estimated.

4.3. Results and discussion

The model proposed in this work is used to investigate how radial flux distribution actually influences dissolved oxygen transport inside the construct at different cell metabolic requirements in order to design rPBBs enhancing physiological oxygen supply to the cells for a given therapeutic objective. This is the first model providing a systematic analysis of the dimensionless groups determining rPBB behavior in which the effect of the fluid dynamics of rPBB void spaces and construct transport properties are accounted for that permits to adjust bioreactor design to ensure adequate pericellular environment for cells at a given cell concentration. The possible establishment of external resistance to mass transport from the bulk fluid in the pores towards the cell surface on oxygen supply to cells was also taken into account in model development. However, such effect was found to be negligible for all the conditions considered in this work, so it will not be discussed in the following. The assumption of steady-state does not represent a limitation, since the characteristic time of bioreactor dynamics and that of cell growth kinetics differ for several orders of magnitudes (minutes vs. days, respectively). This permits to adjust the values of the dimensionless groups as cell concentration increases.

4.3.1 Model validation

Figure 4.3a shows the good agreement between model predictions and experimental glucose consumption by HepG2 cells reported by Hongo et al. (Hongo et al., 2005). In addition, Figure 4.3b shows the good agreement between model-predicted consumption of glucose and that reported for the experimental results obtained by Olivier et al. for the culture of osteosarcoma cells (Olivier et al., 2007). The agreement between model-predicted and experimental results reported by the authors is also more accurate than that predicted in our previous work, at 7 and 28 days of culture, in which it had been assumed that radial flux distribution of the culture medium was uniform along the construct length (chapter 2). This shows that accounting for the effect of the fluid dynamics of the bioreactor void spaces gives results closer to the actual cases.

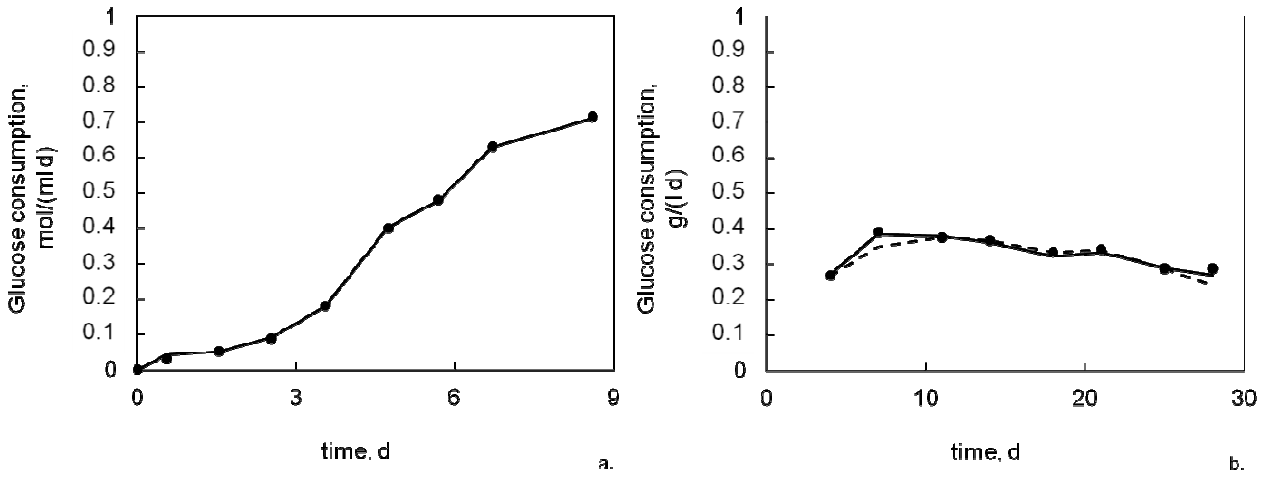

Figure 4.2 (a) Comparison of the model-predicted glucose consumption (−) with the experimental results (●) of Hongo et al., (Hongo et al., 2005). Re_{in} = 0.088, L/R=10, R/δ_C = 0.18, k/R^2 = 1.1 x 10^{-2}, β_g = 1.2 x 10^{-4}, $Pe_{rad,max,g}$ = 468, $D_g/D_{H,g}$ = 0.8; (b) Comparison of the model-predicted glucose consumption according to the model presented in this work (−) or in Donato et al. (Donato et al., 2014) (x) with experimental results (●) of Olivier et al. (Olivier et al., 2007). Re_{in} = 1, L/R = 11, R/δ_C = 0.4, R/δ_E = 0.33, k/R^2 = 7.5 x 10^{-5}, $Pe_{rad,max,g}$ = 456, $D_{C,g}/D_{H,g}$ = 0.65, β_g = 0.02.

4.3.2 Effect of medium radial flux distribution on oxygen pericellular concentration at given Re_{in}

Non-uniform radial flux distribution – Figure 4.3 shows how non-uniform medium radial flux distribution along bioreactor length influences dissolved oxygen concentration profiles at Re_{in} = 0.1, corresponding to a value of the radial superficial velocity equal to 1.1 x 10^{-5} m/s, typical of bone tissue engineering applications (Gardel et al., 2013) for three different values of ϕ_C. Figure 4.3a

shows the non-uniform radial flux distribution at the interface between the inner hollow cavity and the construct (*i.e.* $r^* = 1$), which was obtained by adjusting the values of the dimensionless groups so that CORFU becomes equal to about 1.47. Figure 4.3b shows that at $\phi_C = 1.24$, corresponding to the culture of human mesenchymal stem cells (hMSC) consuming oxygen at 2.64 x 10^{-17} mol/(s cell) (Lavrentieva et al., 2010) at a cell concentration equal to 10^{12} cell/m^3, dissolved oxygen concentration at bioreactor entrance decreases from $z^* = 0.9$ (*i.e.* close to the bioreactor top) towards $z^* = 0.1$ (*i.e.* close to the bioreactor bottom) and causes η_c to be equal to 0.097. Figure 4.3c shows that an increase of ϕ_C up to 3.93, corresponding to hMSC proliferating up to 10^{13} cell/m^3, causes a higher decrease of dissolved oxygen concentration from the top towards the bottom of the bioreactor than at $\phi_C = 1.24$, due to the increasing cell metabolic requirements, which result in η_c = 0.53. Furthermore, oxygen concentration decrease causes NHy-FCV = 0.71. Figure 4.3d shows that increasing ϕ_C up to 11.6, typical of hMSC proliferating up to 4.22 x 10^{13} cell/m^3 (Zhao et al., 2005) and subsequently differentiating into osteoblasts, i.e. cell-specific oxygen consumption rate increasing up to 5.5 x 10^{-17} mol/(s cell) (Komarova et al., 2000), the NHy-FCV decreases down to 0.1, whereas η_c decreases down to 0.13 due to the anoxic conditions establishing inside the 77% of the construct volume.

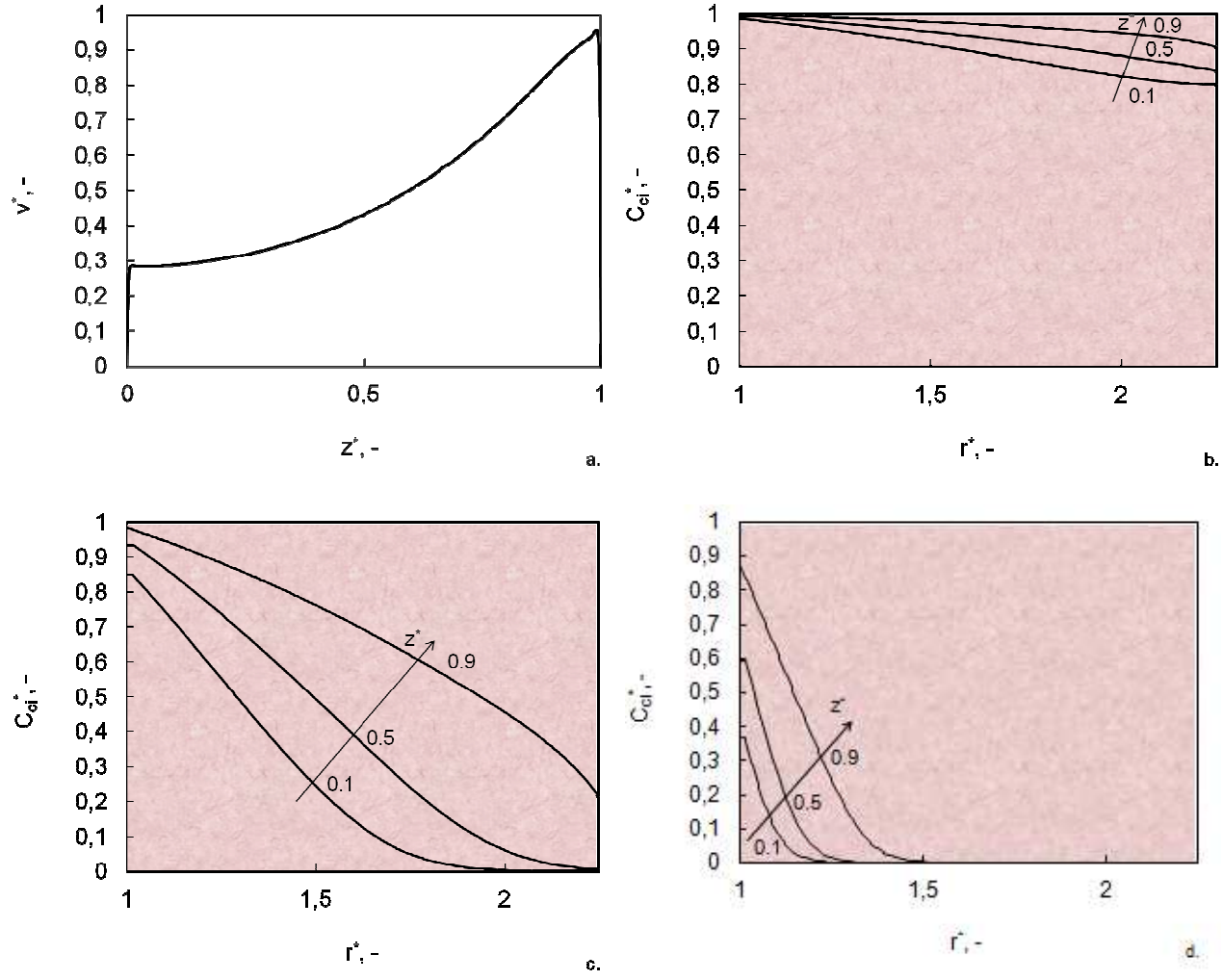

Figure 4.3 Radial velocity at construct entrance (a) and dissolved oxygen concentration profile (b-d) at Re_{in} = 0.1 for non-uniform radial flux distribution. Parameter values: (b) ϕ_C = 1.24; (c) ϕ_C = 3.93; (d) ϕ_C = 11.6. R/δ_E = 4, CORFU = 1.47. Other parameters as in Tables 4.2 and 4.3.

Uniform radial flux distribution – Figure 4.4 shows how oxygen distribution inside the construct is influenced by uniform distribution of radial flux at Re_{in} = 0.1 for the same values of ϕ_C as in Figure 4.3. Figure 4.4a shows the uniform radial flux distribution at r^* = 1, which was obtained by reducing the value of R/δ_E from 4 to 0.67 so that CORFU decreases down to about 0.1. Figure 4.4b shows that, for ϕ_C = 1.24 oxygen concentration remains ca. uniform along the axial coordinate and remains higher than about 80% that at the inlet throughout the construct. In particular, η_c results to be equal to 0.007. As the Thiele modulus increases up to 3.93, dissolved oxygen concentration decreases in the radial direction due to the increasing unbalance between oxygen depletion and oxygen supply (Figure 4.4c), while remaining uniform along the axial coordinate. In particular, η_c is equal to 0.05,

whereas the NHy-FCV decreases down to 0.8. Figure 4.4d shows that a further increase of ϕ_C up to 11.6 causes η_c to decrease down to 0.015 due to the high oxygen depletion that causes the NHy-FCV to decrease down to 0.1, with the 77% of the cells cultured under anoxic conditions.

The increasing η_c at given Re_{in} and ϕ_C for CORFU increasing from 0.1 to 1.47 may be explained by the fact that, under non-uniform medium radial flux distribution (e.g. CORFU = 1.47), the increasing cell metabolic requirements cause oxygen to decrease to a greater extent in the zones of the constructs perfused at lower medium velocity, whereas for uniform medium radial flux distribution (e.g. CORFU = 0.1) the balance between oxygen supply to, and oxygen consumption by, the cells does not depend on the axial position. Furthermore, Figures 4.3 and 4.4 suggest that, at a given Re_{in}, medium radial flux distribution influences the uniformity of oxygen distribution along the axial coordinate as ϕ_C increases without causing anoxic conditions, and may cause cells to proliferate and differentiate non-uniformly inside the construct if non-uniform oxygen supply is provided to the cells, even if the NHy-FCV is not affected by medium radial flux distribution.

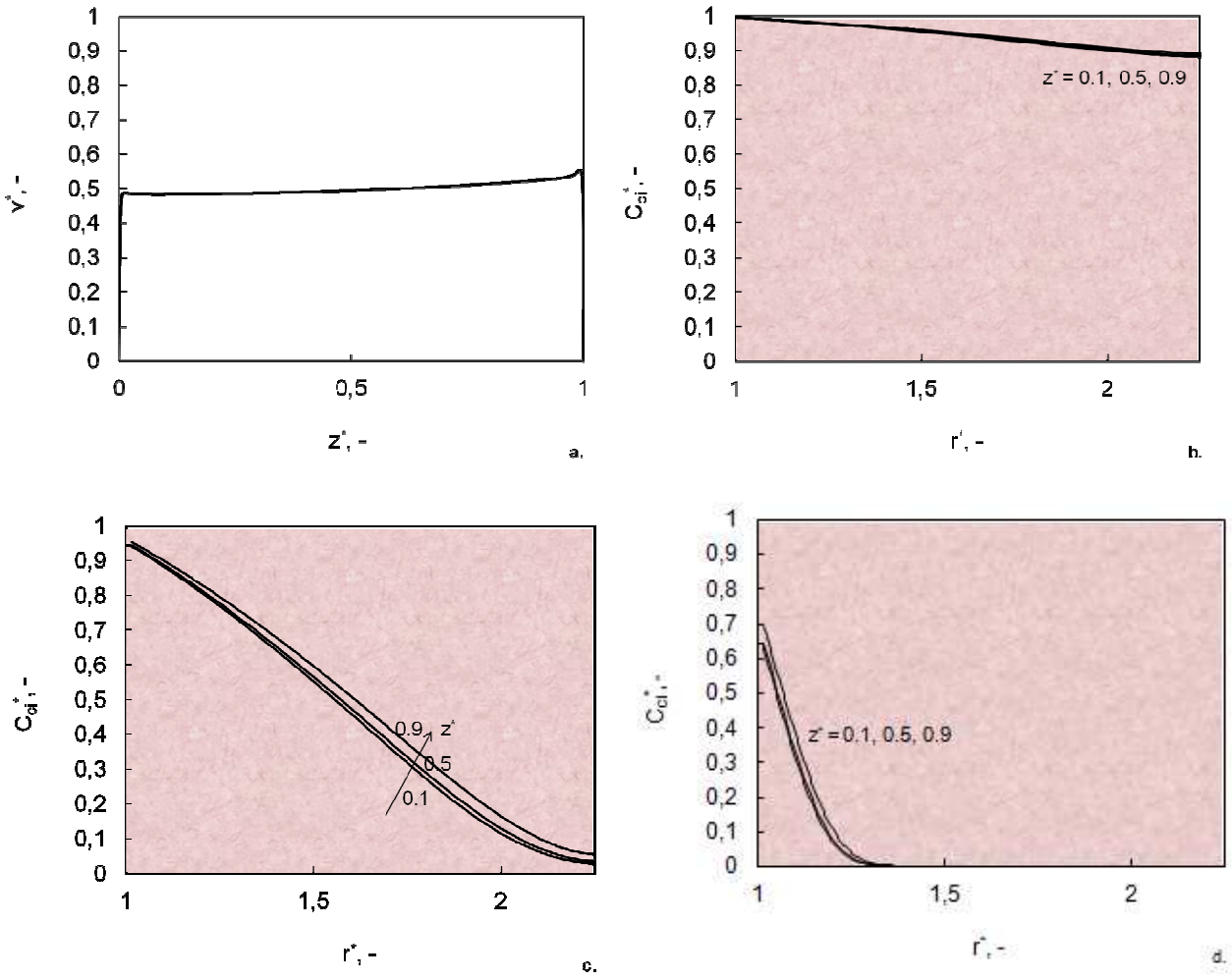

Figure 4.4 Radial velocity at construct entrance (a) and dissolved oxygen concentration profile (b-d) at Re_{in} = 0.1 for uniform radial flux distribution. Parameter values: (b) ϕ_C = 1.24; (c) ϕ_C = 3.93; (d) ϕ_C = 11.6. R/δ_E = 0.67, CORFU = 0.1. Other parameters as in Tables 4.2 and 4.3.

4.3.3 Effect of Re_{in} on oxygen distribution

Figure 4.5 shows the effect of Re_{in} on oxygen supply to the cells for ϕ_C = 3.93 for non-uniform medium radial flux distribution. In particular, Re_{in} is increases of one order of magnitude from 1 to 10, both typical of bone tissue engineering applications (Oliveir et al., 2007; Xie et al., 2006; Shao et al., 2009). For the same bioreactor geometry this does not significantly influence medium radial flux distribution, causing CORFU to decrease from 1.47 to 1.3. Figure 4.5 shows that for ϕ_C = 3.93 increasing Re_{in} from 1 (Figure 4.5a) to 10 (Figure 4.5b) causes oxygen concentration to become more uniform in the axial coordinate, with η_c decreasing from 0.073 to 0.02, while the NHy-FCV is equal to 1 in both cases.

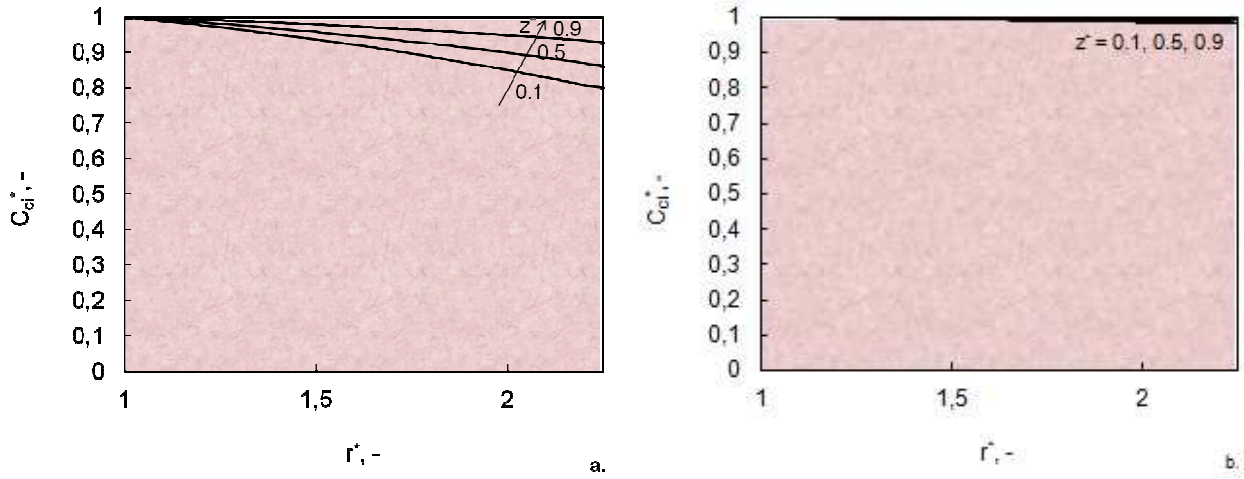

Figure 4.5 Dissolved oxygen concentration profile at ϕ_C = 1.24 for increasing Re_{in}. Parameter values: (a) Re_{in} = 1, CORFU = 1.46; (b) Re_{in} = 10, CORFU = 1.3. Other parameters as in Tables 4.2 and 4.3.

Figure 4.6 shows that the effect of Re_{in} on oxygen distribution increases as ϕ_C increases up to 11.6. In particular, Figure 4.6 shows that for increasing Re_{in} from 1 to 10 makes η_c decrease from 0.43 (Figure 4.6a) to 0.05 (Figure 4.6b), while making NHy-FCV increase from 0.8 to 1.

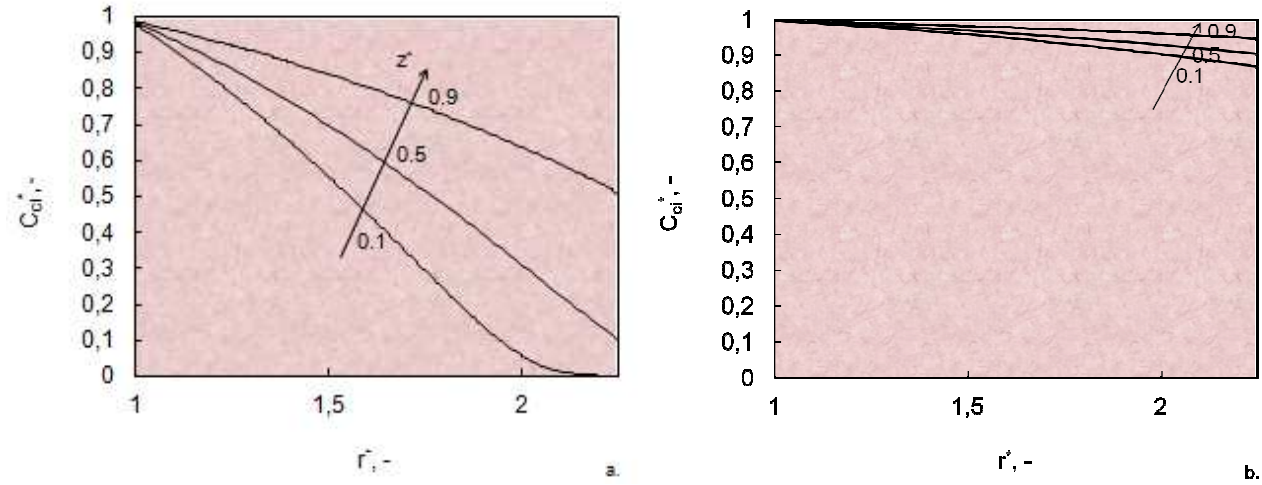

Figure 4.6 Dissolved oxygen concentration profiles at: (a) Re_{in} = 1, ϕ_C = 3.93; (b) Re_{in} = 10, ϕ_C = 3.93; (c) Re_{in} = 1, ϕ_C = 11.6; (d) Re_{in} = 10, ϕ_C = 11.6. Parameter values as in Tables 4.2 and 4.3.

4.3.4 Towards a unifying approach to optimal design of rPBBs

The analysis of oxygen concentration profiles for varying perfusion conditions is important to understand the phenomena to account for when designing rPBBs during tissue development. Nevertheless, the prediction of the interplay of all the dimensional parameters is difficult and gives

poor insight into bioreactor scale-up. Dimensional analysis of the transport equations offers the designer a valid tool to predict the complex interplay between the dimensional parameters controlling bioreactor behavior and to scale the bioreactor up for a given application.

In this work, the behavior of the rPBB was expressed in terms of the overall effectiveness factor and the NHy-FCV. Figure 4.7a and 4.7b show how the overall oxygen effectiveness factor, η_{ov}, and the NHy-FCV vary with increasing ϕ_C, at values of the reduced Reynolds number, Re_{in}, varying of three orders of magnitude, under uniform medium radial flux distribution. Independent of Re_{in}, at low enough ϕ_C, the dissolved oxygen concentration profile is uniform throughout the construct and both the overall effectiveness factor and the NHy-FCV approach 1 (*i.e.* the bioreactor is operated under kinetic control). As ϕ_C increases, oxygen is rapidly depleted by the cells due to an increase of the cell metabolic requirements and of the overall transport resistance, and both η_{ov} and NHy-FCV become lower than 1 (*i.e.* the bioreactor is operated under transport control). The transition between kinetic and transport control increases as Re_{in} increases, since, at the same ϕ_C, higher perfusion flow rates result in smoother oxygen concentration profiles. As a result, Figure 4.7 suggests that, as cell concentration increases and cells require higher oxygen supply than at seeding, the pericellular oxygen supply may be controlled by gradually increasing the inlet flow rate to increase the value of Re_{in}. In particular, at the beginning of the culture (*i.e.* low cell concentrations as those typicial of cell seeding) low values of Re_{in} permit to balance out the cells metabolic requirements, whereas, in order to ensure cell survival throughout the construct as cells metabolic requirements increase as a result of cell proliferation or differentiation (i.e. for increasing ϕ_C), the perfusion flow rate should be gradually increased. For instance, the literature data reported in Table 4.4 suggest that low Re_{in} (e.g. Re_{in} = 0.01) would enable culture of cells with low oxygen metabolic requirements (e.g. chondrocytes), but would allow the culture of cells consuming oxygen at higher cell-specific oxygen consumption rates (e.g. hepatocytes) only at cell concentrations typical of seeding. If Re_{in} is increased from 0.01 to 10, the rPBB may enable about a 30 fold higher activity

(i.e. Thiele modulus) while maintaining adequate oxygenation of the same fractional construct volume. This result finds also experimental evidence in literature for the culture of hMSC onto 3D construct in a perfusion bioreactor. In fact, it has been shown that, low flow rates have to be preferred for cell culture when they are not reorganized in tissues (*i.e.* at low C_{cell}) in order to prevent cell washout, whereas medium flow rate has to be increased to exploit mechanical stimulation promoting cell differentiation towards the osteoblast phenotype in the culture of human mesenchymal stem cells when cells start to secrete extracellular matrix, while ensuring cell survival (Zhao et al., 2005 and 2007).

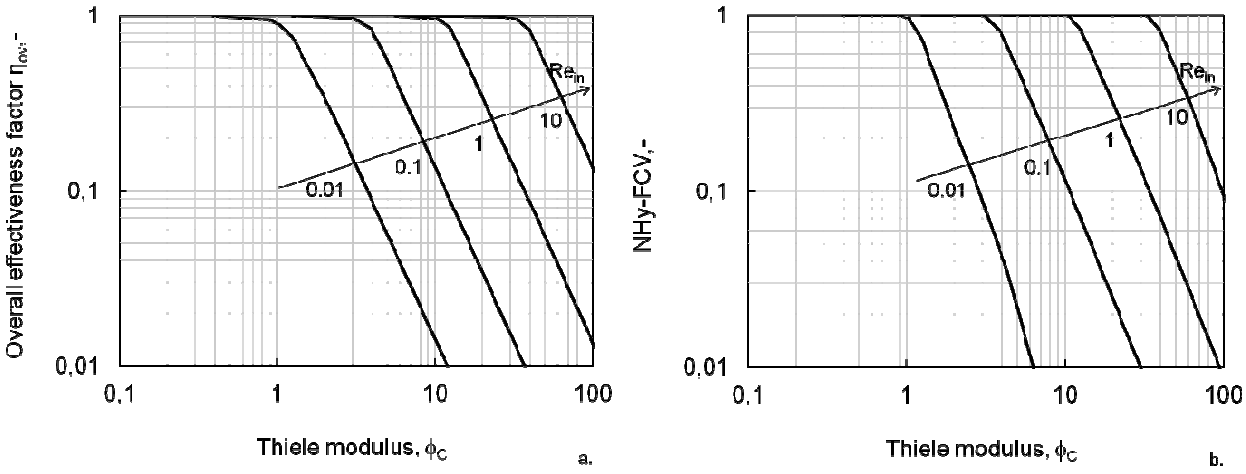

Figure 4.7 (a) Oxygen overall effectiveness factor and (b) NHy-FCV at varying ϕ_C for increasing Re_{in}. Parameters as in Tables 4.2 and 4.3.

Cell type	cell-specific OCR (mol/(s·cell))	reference	C_{cell}/seed (cell/m^3)	ϕ_C/seed	C_{cell}/vitro (cell/m^3)	ϕ_C/vitro	reference
bovine chondrocytes	3.43 x 10^{-19}	Stockwell et al., 1971	10^{12}	0.14	2 x 10^{13}	0.63	Stockwell, 1971
rat hepatocytes	1.4 x 10^{-16}	Sullivan et al., 2007	10^{12}	2.86	10^{15}	10.1	Sullivan et al., 2007
osteoblasts	5.5 x 10^{-17}	Komarova et al., 2000	10^{12}	1.79	4.2 x 10^{13}	11.6	Zhao et al., 2005
hMSC	2.64 x 10^{-17}	Lavrentieva et al., 2011	10^{12}	1.24	4.2 x 10^{13}	8.1	Zhao et al., 2005

Table 4.4 Thiele modulus for oxygen consumption, ϕ_C, for various cell types and concentrations of therapeutic interest, for the values of geometric and operating variables reported in Table 4.2.

Figures 4.8a and 4.8b show that the curves shown in Figures 4.7a and 4.7b, respectively, converge in one curve only when the η_{ov} and NHy-FCV are reported as a function of the minimal radial Damköhler number, $Da_{rad,min}$, where

$$Da_{rad,\min} = \frac{\phi_C^{\,2}}{Pe_{rad,\max}} = \frac{V_{\max}\delta_C}{C_O u_{in}\frac{R}{L}} \tag{4.17}$$

for any given value of $Pe_{rad,max}$ reported in this work (*i.e.* $Pe_{rad,max} > 4$). This suggests that, for such values of the maximal radial Peclet number, oxygen transport is dominated by convection. Figure 4.8 shows that cells may be cultured in the construct at a uniform dissolved oxygen concentration under conditions that result in small $Da_{rad,min}$ (i.e. for low cell concentration or metabolic activity, or high perfusion rates). In particular, bioreactor design according to which $Da_{rad,min}$ is kept close to the values corresponding to the transition from the kinetic- to the transport-limited region ensures cell survival throughout the construct with the lowest possible radial superficial velocity and consequent shear stress at any given cell concentration for a given application.

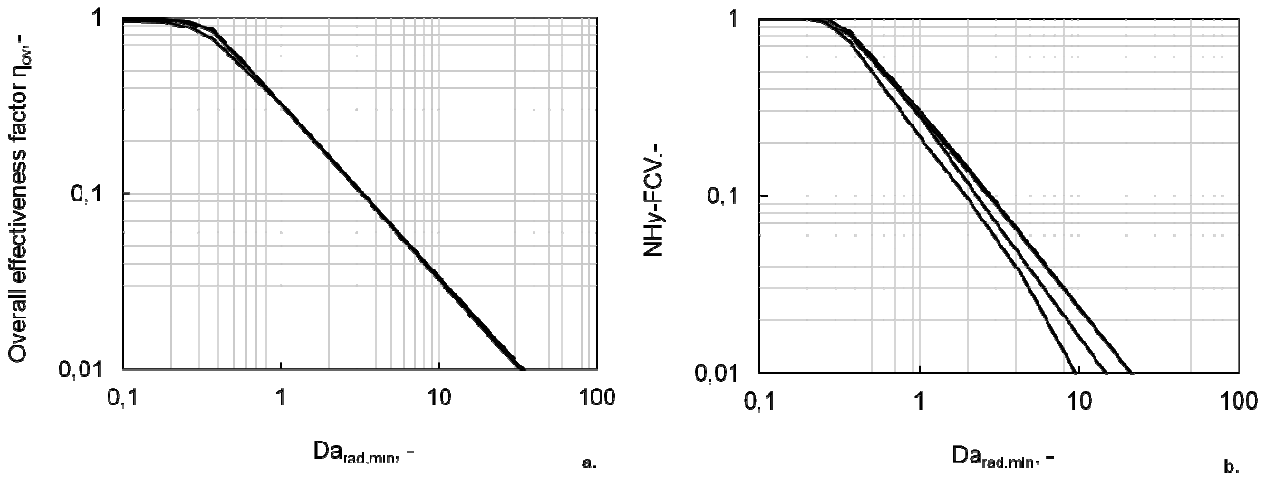

Figure 4.8 (a) Oxygen overall effectiveness factor and (b) NHy-FCV at varying $Da_{rad,min}$. All parameters as in Figures 4.7a-b. Other parameters as in Tables 4.2 and 4.3.

4.3.5 Use of the model for analysis of experimental data

In the realization of a clinical-scale constructs for tissue replacement, the environmental conditions for cell survival and activity have to be similar to those of the native tissue for any given therapeutic objective. In particular, the metabolic activity of cells may vary in space depending on their native tissue. For instance, in the human liver, the metabolic activities of the hepatocytes change in space along the length of the sinusoids inside the liver lobules (i.e. liver zonation) (Gebhardt, 1992), whereas in long bones blood is uniformly supplied along their length to cells by means of the radial Volkmann canals, that branches out of the axial Haversian canals (Gray et al., 1995). In the following, the effect of radial flux distribution on glucose supply to cells is assessed for the experimental results reported by Hongo et al. (Hongo et al., 2005) and Olivier et al. (Olivier et al., 2007) for the culture of HepG2 cells and osteosarcoma cells in rPBBs for a bioartificial liver (BAL) and for the bioengineering of a large-scale bone graft, respectively.

Bioartificial liver – Figure 4.9 shows how non-uniform medium radial flux distribution along the construct length influences glucose concentration profiles in the case of a bioreactor for BAL in which an annular porous construct 15 mm long and 10 mm in outer diameter with an inner hollow cavity of radius R = 1.5 mm, is cultured at Thiele modulus equal to 5.3 and Re_{in} equal to 0.088, corresponding to an average value of radial superficial velocity of 3 x 10^{-6} m/s at construct external

surface, assuming inward construct perfusion (Hongo et al., 2005). In this case, the construct Darcy permeability was calculated with the Carman-Kozeny equation assuming construct porosity equal to 0.8 and d_p = 0.6 mm, as reported by the authors (Hongo et al., 2005). Figure 4.9a shows that the parameters reported by the authors result in non-uniform radial flux distribution at $r^* = 1+\delta_C/R$, that gives CORFU equal to 4.65. Figure 4.9b shows that at $\phi_{C,g}$ = 5.3, corresponding to the culture of HepG2 consuming glucose at 1.57 x 10^{-17} mol/(s cell) (Iyer et al., 2010) at a cell concentration equal to 10^{14} cell/m^3, glucose concentration is distributed non-uniformly along the construct length. In particular, $\eta_{c,g}$ results to be equal to 1.05. This result suggests that bioreactor design resulting in non-uniform medium radial flux distribution may help reproduce the physiological pericellular environment for liver cells activity.

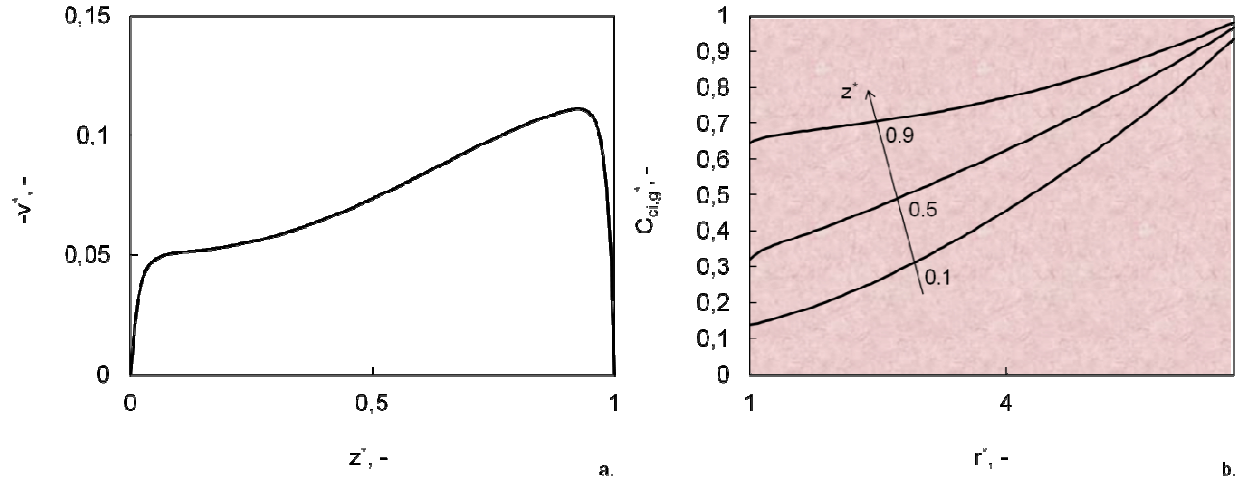

Figure 4.9 Radial velocity at construct entrance (a) and glucose concentration profile (b) $\phi_{C,g}$ = 5.27 in the bioreactor for BAL as reported by Hongo et al. (Hongo et al., 2005). Parameter values: $Pe_{rad,max}$ = 468, $D_{C,g}/D_{H,g}$ = 0.8, R/δ_E = 0.18, CORFU = 4.65, Re_{in} = 0.088, k/R^2 = 1.1 x 10^{-2}, L/R = 10, R/δ_C = 0.18, β_g = 1.2 x 10^{-4}.

Bioreactor for bone tissue engineering – Figure 4.10 shows how glucose distribution inside the construct is influenced by uniform distribution of radial flux for the case of a bioengineered annular porous construct 33 mm in length with *R* = 2 mm and δ_C = 5 mm, at Re_{in} = 1 (Olivier et al., 2007). In this case, construct Darcy permeability was assumed to be equal to 0.3 x 10^{-9} m^2, as reported by Li et al. for calcium phosphate scaffolds for bone tissue engineering (Li et al., 2003). Figure 4.10a shows the uniform radial flux distribution at $r^* = 1$, resulting from the parameters reported by the

authors that give CORFU = 0.1. Figure 4.10b shows that, for $\phi_{C,g}$ = 0.08, corresponding to osteosarcoma cells consuming glucose at 1.39 x 10^{-16} mol/(s cell) at C_{cell} = 1.21 x10^{13} cell/m^3, glucose concentration remains uniform along the axial coordinate and remains higher than about 95% that at the inlet throughout the construct.

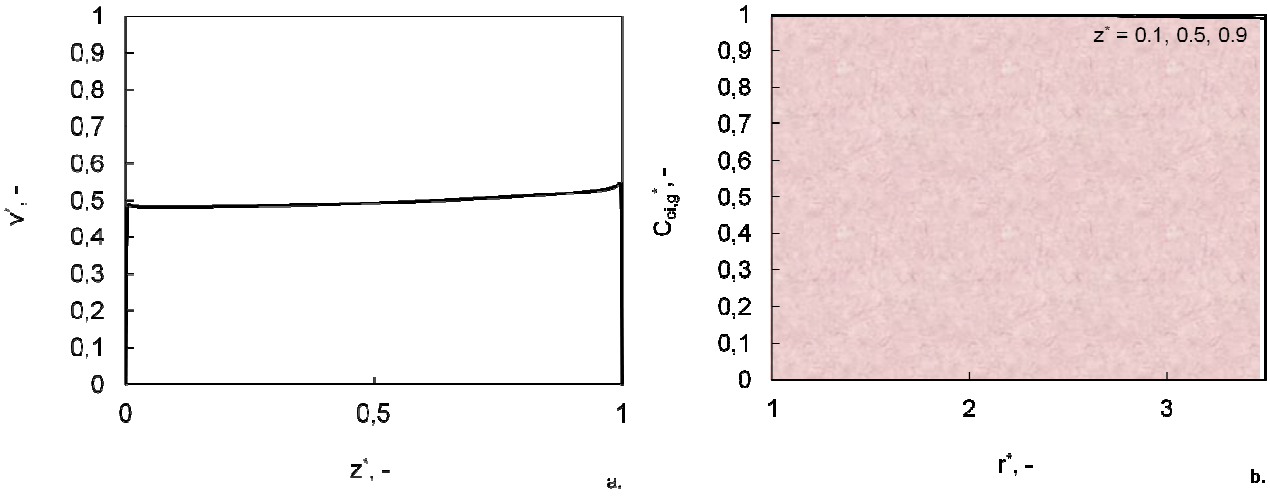

Figure 4.10 Radial velocity at construct entrance (a) and glucose concentration profile (b) at the conditions reported by Olivier et al. for the culture of osteosarcoma cells in rPBB (Olivier et al., 2007). Parameter values: $Pe_{rad,max}$ = 456, D_C/D_H = 0.65, R/δ_E = 0.33, CORFU = 0.1, Re_{in} = 1, k/R^2 = 7.5 x 10^{-5}, L/R = 11, R/δ_C = 0.4, β = 0.02.

The results shown in Figures 4.9 and 4.10 confirm the goodness of the radial perfusion configuration proposed for the culture of large-scale constructs at cell concentrations close to those found *in vitro*, under acceptable perfusion flow rates, and suggest that the transport model reported in this work may be very helpful to predict the pericellular environment under which cells develop and to scale the bioreactor up for a given therapeutic objective.

4.4. Conclusions

In this work, a two-dimensional stationary transport model is proposed to design radial flow bioreactors packed with 3D annular porous scaffolds ensuring the physiological supply of dissolved oxygen to the cells at different cell concentrations under optimal medium radial flux distribution, for a given therapeutic objective. Dimensional analysis was used to identify the most relevant dimensionless groups affecting rPBB behavior, expressed in terms of the non-hypoxic fractional construct volume and in a dimensionless parameter accounting for the uniformity of oxygen

distribution along bioreactor length. Medium radial flux distribution along the bioreactor length was shown to significantly influence oxygen supply to the cells during tissue reconstruction at higher cell metabolic requirements for a given Re_{in}. Model predictions also suggest that Re_{in} influences oxygen spatial distribution from the top towards the bottom of the bioreactor for non-uniform medium radial flux distribution, giving higher uniformity of oxygen distribution along bioreactor length. Furthermore, the value of Re_{in} has to be chosen independent of spatial distribution of medium radial fluxes to enable adequate supply of dissolved oxygen to the cells while preventing cell wash out, at any given stage of tissue development. In particular, model predictions suggest that at the beginning of the culture Re_{in} (*i.e.* medium flow rate) may be kept low to avoid cell damage or wash out, whereas, as cells proliferate and differentiate (*i.e.* for increasing Thiele modulus, ϕ_C), Re_{in} should be gradually increased to balance out the increasing metabolic requirements of cells. Finally, for the culture conditions considered in this work, choosing perfusion rates that cause minimal radial Damköhler number, $Da_{rad,min}$, to be small were shown to ensure adequate pericellular oxygenation (i.e. NHy-FCV around 1) for tissue development, for values of the maximal radial Peclet number, $Pe_{rad,max}$, higher than 4. Model predictions suggest that the transport model reported in this work may be very helpful for bioreactor scale-up for the development of clinical-size bioengineered constructs for tissue engineering applications.

Appendix A – Calculation of $d_{p,e}$ from $a_{V,p}$ by interpolating data from Perry et al. (Perry et al., 1999)

Figure A.1 reports the value of $1/a_{Vp}$ as a function of $d_{p,e}$ obtained from Perry et al. (Perry et al., 1999) for beds packed with Raschig rings.

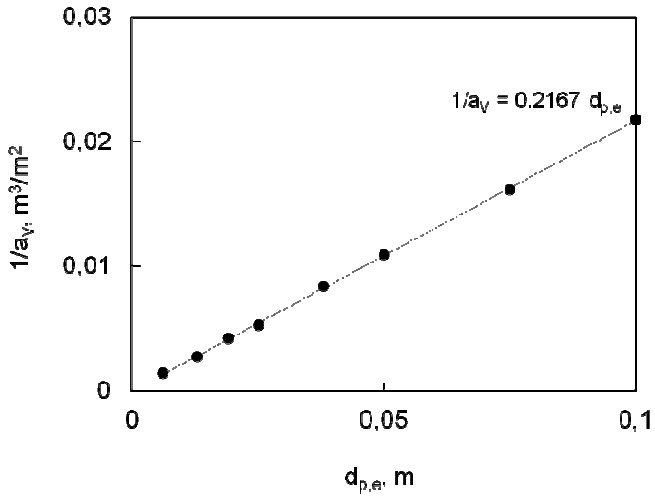

Figure A.1 Interpolation of data to determine the equivalent diameter of a Raschig ring from its specific surface reported by Perry et al. (Perry et al., 1999).

Conclusions

A promising alternative to synthetic grafts for tissue replacement is the use of engineered biological substitutes of tissues or organs. To this purpose, isolated human adult or stem cells are seeded in three-dimensional porous scaffolds, and the cell constructs are cultured in bioreactors in which cells are guided to re-organize and differentiate as in natural tissues and organs by means of the application of physiological biochemical and mechanical cues. Optimization of bioreactor design and operation for tissue engineering is important to control the pericellular environment and ensure cell survival, proliferation, organization and differentiation to the given phenotype.

One of the major limitations for the development of bioengineered substitutes for tissue replacement is the difficult supply of dissolved oxygen and nutrients towards, and metabolic wastes removal from, the cell compartment. In fact, to reach cells anywhere in the construct, dissolved oxygen, nutrients and biochemical cues supplied in the culture medium have to be transported external to the construct (i.e. from the fresh medium bulk to the construct upstream surface), inside the construct across the cell mass (i.e. from the upstream to the downstream surface), and again external to the construct from its downstream surface into the bulk spent medium leaving the bioreactor. Transport and metabolic reaction phenomena in the bioreactor may cause the concentration of soluble metabolic species in the stream entering and leaving the bioreactor to be significantly different from its pericellular value. This may lead to biased evaluation of the conditions under which cells are cultured and of their functions, and may even cause cell death. In particular, oxygen concentration gradients that establish across 3D constructs in static bioreactors (e.g. Petri dishes or flasks) have been acknowledged to cause poor cell oxygenation and limit the development of engineered substitutes mimicking natural human tissues and organs. To minimize the diffusive limitations to external solute transport, bioreactors have been proposed in which medium flow around the cell construct enhances transport by superimposing external convection over pure diffusion (e.g. spinner flasks and rotating wall vessel bioreactors). Axial perfusion of 3D

porous constructs with medium in axial flow packed bed bioreactors (aPBBs) uses convection to enhance transport of soluble metabolic species to cells internal to the construct. At low axial superficial velocity, steep concentration gradients of soluble metabolic species may establish in the construct which decrease the amount supplied to cells, and may cause cell death towards the end of the construct. On the other hand, perfusion at high axial superficial velocity enhances transport (and minimizes the axial concentration gradients), but may detach and wash cells out of the construct. The large pressure drop that establishes at the ends of long 3D constructs may also compress and change the morphology of soft scaffolds during culture.

In recent years, radial perfusion of cell-seeded 3D annular porous scaffolds in radial flow packed-bed bioreactors (rPBBs) has been proposed to overcome the transport limitations typical of static and axial flow packed-bed bioreactors, in particular for the development of engineered liver tissue and bone. In rPBBs, fresh medium is distributed along the construct length, flows radially across the cell construct, and spent medium is collected along the construct length before leaving the bioreactor. Medium may flow from the inner hollow cavity towards the outer peripheral annulus (outwards or centrifugal configuration, CF), or from the outer peripheral annulus towards the inner hollow cavity (inwards or centripetal configuration, CP). Fresh medium entering and spent medium leaving the bioreactor may flow in the same direction (co-current or z-configuration), or in opposite directions (counter-current or π-configuration). Similar to aPBBs, species transport to (and away from) cells occurs mainly by convection and is more efficient than pure diffusion. Hollow constructs radially perfused with medium also feature larger cross-sectional areas for solute transport and shorter solute transport path-lengths than axially perfused cylindrical constructs. This enables cell culture in rPBBs at lower pressure drop, lower superficial velocity (hence lower shear stresses), and smoother and more controllable concentration gradients of dissolved oxygen and metabolites in the direction of perfusion than aPBBs.

Despite these significant advantageous features, the design of rPBBs is more difficult as compared to that of axial flow bioreactors. First of all, the annular bed geometry and the perfusion

flow configuration and conditions (e.g the direction and the extent of the radial superficial velocity) may significantly influence mass distribution across the cell compartment. Furthermore, the extent and the distribution along the construct length of the medium radial fluxes, which depends on the fluid dynamics of the rPBB void spaces, should be optimized in order to enhance adequate mass transport towards the cells for a given therapeutic objective.

In the optimization of bioreactor design, mathematical models may be useful to investigate how the different parameters influence bioreactor performance and to optimize bioreactor geometry and operations for a given application, provided that they are validated with experimental results. However, a systematic analysis of the dimensionless groups accounting for the influence of all the geometrical, transport and operational parameters to optimize the design of radial flow packed-bed bioreactors for tissue engineering has not been reported yet.

Accordingly, a model-based framework, which accounts for the effect of all the geometrical, transport and operational parameters on solute transport towards, or from, the cells, aimed to optimize the design of radial flow packed-bed bioreactors for the development of bioengineered substitutes for tissue replacement was developed and it was described in the present thesis. In particular, bioreactor design according to such framework should enable the supply of physiological amounts of dissolved oxygen, low molecular weight nutrients and biochemical cues to the cells in order to prevent their starvation and to guide their differentiation towards a given phenotype. In order to develop this framework, the present work was divided in three different steps, that were discussed in the previous chapters and that are summarized as follows:

1. A steady-state one-dimensional model was developed to optimize the geometry of hollow cylindrical constructs, and direction and magnitude of perfusion flow, to ensure cell oxygenation and culture at controlled oxygen concentration profiles, under the assumption of uniform radial flux distribution along the construct length. Momentum transport was described according to the Darcy equation, whereas dissolved oxygen transport was described according to the convection-dispersion-reaction equation. The kinetics of dissolved oxygen consumption was assumed to be

Michaelian. Dimensional analysis was used to combine more effectively geometric and operational variables in the dimensionless groups determining bioreactor performance. The effectiveness of cell oxygenation was expressed in terms of the non-hypoxic fractional construct volume. First, model predictions suggest that outward radial perfusion of 3D annular porous constructs may lead to better oxygenation than inward perfusion. For a given cell concentration and radial superficial velocity (*i.e*. for a given Damköhler number), this results from the fact that, for outward perfusion, culture medium carrying dissolved oxygen enters the construct through its inner surface at the maximal superficial radial velocity, so that cells located close to such surface are not given time enough to consume high amounts of oxygen, which remains available for the cells located close to the outer construct surface. On the other hand, for inward perfusion, medium carrying dissolved oxygen enters the construct from its outer surface at the minimal radial superficial velocity, so that cells located there are given time enough to consume high oxygen amounts, which does not remain available for the cells located close to the construct inner surface, and steeper dissolved oxygen concentration gradients establish across the construct path-length. At a given Damköhler number, the dependence of the direction of medium perfusion on oxygen distribution inside the construct decreases as the construct inner hollow cavity radius-to-construct thickness ratio increases. High construct curvatures were also shown to enable more effective oxygenation. Furthermore, model predictions suggest that high perfusion flow rates (i.e. high maximal radial Peclet numbers) permit to culture constructs at higher cell concentration. rPBBs operated according to these predictions were shown to be more convenient than static or axial perfusion bioreactors for the culture of large-scale 3D construct and to provide adequate oxygenation to the cells under tolerable pressure drops.

2. In order to optimize radial flux distribution along the construct length, a two-dimensional axisymmetric model was developed for steady-state momentum transport in all the three compartments of rPBBs. Transport in the hollow cavity and the peripheral annulus was described according to the Navier-Stokes equations, while the Darcy-Brinkman equation was used to describe momentum transport across the annular construct. Model predictions were qualitatively validated

against literature data. The effect on radial flux distribution along bioreactor length of the performance-determining dimensionless groups found by dimensional analysis was investigated under operation typical of tissue engineering. First, model predictions showed that an optimal value of the reduced Reynolds number, Re_{in}, exists for high construct-to-hollow cavity permeability ratios and given bioreactor geometry. This results from the opposite effects of friction at the wall surface and momentum recovery, due to the variation of the axial flow rate induced by suction, on pressure variation in the direction of decreasing flow, the balance of which depends on the value of the perfusion flow rate. In particular, while friction in the hollow cavity prevails over that in the outer peripheral annulus for low Re_{in}, thus causing poor perfusion of the bottom part of the construct, momentum recovery in the hollow cavity prevails over friction in the peripheral annulus at high Re_{in}, thus causing poor perfusion of the upper part of the construct. For very permeable constructs, the extent of radial flux maldistribution significantly increases with increasing L/R at any given Re_{in}, but close to the optimal value of Re_{in} (i.e. $Re_{in,opt}$), whereas $Re_{in,opt}$ increases for increasing hollow cavity-to-peripheral annulus cross-sectional areas, ξ, at given L/R. When very permeable and slender constructs are operated at low inlet flow rates medium stagnation at bioreactor bottom contributes to further worsening the radial flux maldistribution. Furthermore, model predictions show that, for very permeable constructs and at given Re_{in} and ξ, higher L/R yield progressively more uniform radial fluxes up to an optimal value, whereas further increases of L/R make radial flux maldistribution increase as a result of the decrease of the intercompartmental radial pressure drop towards the bioreactor bottom caused by friction in the outer peripheral annulus. In addition, for high construct permeability and given Re_{in} and L/R, increasing the value of ξ progressively increase radial flux maldistribution as a result of the high friction in the outer peripheral annulus which makes radial pressure drop decrease towards bioreactor bottom, thus causing poor perfusion therein. The effect of all the dimensionless groups on radial flux distribution along the construct length becomes less important for decreasing construct-to-hollow cavity permeability ratios, k/R^2.

Finally, a criterion was proposed to design and operate bioreactors so that radial fluxes may be uniformly distributed along bioreactor length under operation typical of tissue engineering (i.e. the CORFU criterion). The developed design criterion was shown to depend on the value of all the dimensionless groups determining radial flux distribution of the culture medium along the bioreactor length, which account for the fluid dynamics of the bioreactor void spaces and the time-changing construct transport properties, and indicates that uniform radial flux distribution may be achieved by keeping the total axial pressure drop along the void spaces within ±10% of the radial pressure drop across the construct thickness. Bioreactor designs and operation meeting this criterion permit to avoid non-uniform development of tissue structure and functional properties.

3. In order to evaluate the actual effect of medium radial flux distribution along the construct length and of the extent of the perfusion rates on bioreactor performance and tissue reconstruction, and to design rPBBs enhancing oxygen supply towards clinical-scale porous constructs cultured in rPBBs during tissue development for a given therapeutic objective, a more comprehensive two-dimensional stationary transport model was developed in which mass transport was coupled to momentum transport. Momentum transport in the void spaces of the bioreactor and in the construct was described according to the aforementioned 2D momentum transport model (i.e. with the Navier-Stokes and Darcy-Brinkman equations, respectively). Transport of dissolved oxygen in the cell construct was described with the convection-diffusion-reaction equation and oxygen consumption was described according to Michaelis-Menten kinetics. Oxygen mass transfer coefficients accounting for external mass transport at the medium/cell interface were estimated for a bed of Raschig rings transport-equivalent to porous scaffolds adopted in tissue engineering. The effect of the dimensionless groups determining bioreactor behavior, expressed in terms of the non-hypoxic fractional construct volume, on oxygen supply to cells was investigated under working conditions typical of tissue engineering. Model predictions suggest that medium radial flux distribution along the construct length significantly influences oxygen supply to the cells at higher values of the oxygen Thiele modulus, ϕ_C, for a given Re_{in}. The effect of medium radial flux

distribution on oxygen supply becomes less important if oxygen consumption is compensated by oxygen supply. Model predictions also suggest that higher Re_{in} influences oxygen spatial distribution from the top towards the bottom of the bioreactor for non-uniform medium radial flux distribution, giving higher uniformity of oxygen distribution along bioreactor length. In addition, the extent of the radial perfusion rates have to be optimized to enable adequate dissolved oxygen supply to the cells while preventing cell wash out, at any given stage of tissue development. Model predictions suggested that at the beginning of the culture (i.e. cell seeding), perfusion rates may be kept low enough to ensure adequate cell oxygenation while preventing cell damage or wash out, due to the low metabolic requirements of the cells. As cells proliferate and differentiate, the perfusion rates should be gradually increased to balance out the increased metabolic requirements of the cells. Adequate oxygen supply may generally be ensured by increasing Re_{in} for a given Thiele modulus, ϕ_C. However, when transport occurs mainly by convection, the balance between transport and metabolic consumption rates is better evaluated in terms of the minimal radial Damköhler number rather than the Thiele modulus. In particular, for the culture conditions considered in this work, *i.e.* for values of the maximal radial Peclet number, $Pe_{rad,max}$, higher than 4, choosing perfusion rates that cause minimal radial Damköhler number, $Da_{rad,min}$, to be small enable adequate pericellular oxygenation for tissue development,

rPBB design matching the model-based framework described in this thesis may permit adequate control of the pericellular environment in order to ensure cell survival and guidance of cell proliferation and differentiation, in the development of clinical-scale engineered biological substitutes for tissue replacement.

Nomenclature

$a_{c,bed}$	construct specific surface [m^2/m^3]
$c_i = \frac{R_i - R_i}{\delta_E}$	geometric coefficient [-]
C_i	dissolved oxygen concentration in i-th rPBB compartment [mol/m^3]
C_{Ci}	dissolved oxygen concentration at cell surface [mol/m^3]
C_{cell}	cell concentration in the construct [$cells/m^3$]
C_o	dissolved oxygen concentration in the feed [mol/m^3]
CORFU	criterion of radial flux uniformity, defined in Equation 3.11 [-]
D_I	oxygen diffusion coefficient in the i-th compartment [m^2/s]
$Da_{rad,min}$	minimal radial Damköhler number in the construct [-]
D_C	oxygen diffusion coefficient in the construct [m^2/s]
$D_{eff} = D_H \cdot \varepsilon$	effective oxygen diffusion coefficient in the construct [m^2/s]
$d_{p,e}$	equivalent diameter of a Raschig ring [m]
$\hat{E}_{v,H}$	viscous dissipation term in the i-th compartment [m^2/s^2]
f_i	Fanning friction factor in the i-th compartment [-]
G	maximal cell-specific oxygen metabolic consumption rate [mol/(s cell)]
g_i	characteristic geometry-dependent function of the i-th bioreactor outlet zone, defined in Equation A.6b, A.9b and A.12b [-]

K_M	Michaelis constant for oxygen consumption [mol/m^3]
k	Darcy permeability of construct [m^2]
kc	oxygen mass transfer coefficient [m/s]
k_i	loss coefficient for the i-th bioreactor outlet zone [-]
L	construct length [m]
NHy-FCV	non-hypoxic fractional construct volume [-]
P_i	pressure in the i-th rPBB compartment [Pa]
$Pe_{ax} = u_o L/D_C$	axial Peclet number [-]
$Pe_{rad,max}$	maximal radial Peclet number [-]
Q	medium feed flow rate [m^3/s]
R	construct inner radius [m]
R_i	radius of the i-th bioreactor outlet zone [m]
$Re_{in} = u_{in}R\rho/\mu$ R/L	reduced inlet Reynolds number [-]
R_C	construct outer radius [m]
$R_E = R_C + \delta_E$	inner radius of the culture chamber [m]
R_{HE}	hydraulic radius of the peripheral annulus, Equation B.13 [m]
r	radial coordinate [m]
Sh_p	Particle Sherwood number [-]
u_i	axial velocity in the i-th compartment [m/s]

u_{in}	axial velocity entering the construct [m/s]
$V_{max} = C_{cell}G$	maximal metabolic consumption rate of oxygen [mol/(m^3s)]
v_i	radial velocity in the i-th compartment [m/s]
v_o	maximal radial velocity in construct at r = R [m/s]
V_V	volume of the reservoir [m^3]
z	axial coordinate [m]

Greek Symbols

α_i	kinetic energy correction factor in the i-th bioreactor compartment [-]
$\beta = K_M/C_o$	saturation parameter [-]
β_i	cross-sectional area ratio between relative to the i-th compartment [-]
γ	perfusion flow direction parameter [-]
$\delta_C = R_C\text{-}R$	thickness of construct annular wall [m]
δ_E	thickness of peripheral annulus [m]
ΔP_i	pressure drop in the i-th zone at bioreactor outlet[Pa]
ε	construct porosity [-]
Φ	particle shape factor [-]
$\varphi_C = \sqrt{(V_{max}\,\delta_C/(D_C\,C_o))}$	Thiele modulus in construct perfused with medium [-]
$\varphi_D = \sqrt{(V_{max}\,\delta_C/(D_{eff}\,C_o))}$	Thiele modulus in construct under static operation [-]
$\phi_S = \sqrt{(V_{max}\,d_{p,e}^2/(4.61 D_C\,C_o\,(1\text{-}\varepsilon))}$	oxygen Thiele modulus at cell surface [-]

η	degree of radial flux uniformity, as defined in Equation 3.10 [-]
η_c	degree of concentration uniformity, as defined in Equation 4.14 [-]
η_{ov}	overall effectiveness factor [-]
μ	medium viscosity [Pa·s]
ρ	fluid density [kg/m^3]
τ	average shear stress in construct [Pa]
ξ	hollow cavity-to-peripheral annulus cross-sectional area ratio [-]

Superscripts and Subscripts

avg	average
ax	axial
bed	of the bed
C	construct
E	peripheral annulus
g	glucose
H	hollow cavity
in	inlet
max	maximal
min	minimal
opt	optimal

out	outlet
p	particle
rad	radial
Res	reservoir
*	dimensionless

References

Abdullah, N.S.; Das, D.B.; Ye, H.; Cui, Z.F. 3-D bone tissue growth in hollow fibre membrane bioreactor: Implications of various process parameters on tissue nutrition. *Int. J. Artif. Organs* **2006**, *29*, 841–851.

Allen, J.W.; Khetani, S.R.; Bhatia, S.N. *In vitro* zonation and toxicity in a hepatocyte bioreactor. *Toxicol. Sci*. **2005**, *84*, 110–119.

Altman, G.H.; Horan, R.L.; Lu, H.H.; Moreau, J.; Martin, I.; Richmond, J.C., Kaplan, D. L. Silk matrix for tissue engineered anterior cruciate ligaments. *Biomater* **2002**, 23, 4131–4141.

Alvarez-Barreto, J.F.; Linehan, S.M.; Shambaugh, R.L.; Sikavitsas, V.I. Flow perfusion improves seeding of tissue engineering scaffolds with different architectures, *Ann. Biomed. Eng.* **2007**, 35, 429–442.

Amit, M.; Carpenter, M.K.; Inokuma, M.S.; Chiu, C.P.; Harris, C.P.; Waknitz, M.A.; Itskovitz-Eldor, J.; Thomson, J.A. Clonally derived human embryonic stem cell lines maintain pluripotency and proliferative potential for prolonged periods of culture. *Dev Biol* **2000**, 227, 271–278.

Arano, T.; Sato, T.; Matsuzaka, K.; Ikada, Y.; Yoshinari, M. Osteoblastic cell proliferation with uniform distribution in a large scaffold using radial-flow bioreactor. *Tissue Eng Part C* **2010**, 16(6), 1387-1398.

Arinzeh, T.L.; Tran, T.; McAlary, J.; Daculsi, G. A comparative study of biphasic calcium phosphate ceramics for human mesenchymal stem-cell-induced bone formation. *Biomater* **2005**, 26, 3631–3638.

Atala, A.; Vacanti, J.P.; Peters, C.A.; Mandell, J.; Retik, A.B.; Freeman, M.R. Formation of urothelial structure in vivo from disassociated cells attached to biodegradable polymers scaffolds in vitro. *J Urol* **1992**, 148, 658.

Awad, H.A.; Wickham, M.Q.; Leddy, H.A.; Gimble, J.M.; Guilak, F. Chondrogenic differentiation of adipose-derived adult stem cells in agarose, alginate, and gelatin scaffolds. *Biomater* **2004**, 25, 3211–3222.

Balin, A.K.; Fisher, A.J.; Carter, D.M. Oxygen modulates growth of human cells at physiologic partial pressures. *J Exp Met* **1984**, 160, 152-166.

Balis, U.J.; Behnia, K.; Dwarakanath, B.; Bhatia, S.N.; Sullivan, S.J.; Yarmush, M.L.; Toner, M. Oxygen consumption characteristics of porcine hepatocytes. *Metab. Eng*. **1999**, *1*, 49–62.

Bancroft, G.N.; Sikavitsas, V.I.; van der Dolder, J.; Sheffield, T.L.; Ambrose, C.G.; Jansen, J.A.; Mikos, A.G. Fluid flow increases mineralized matrix deposition in 3D perfusion culture of marrow stromal osteoblasts in a dose-dependent manner. *Proc. Natl. Acad. Sci. USA* **2002**, 99, 12600–12605.

Barry, F.P.; Murphy, J.M. Mesenchymal stem cells: clinical applications and biological characterization. *Int J Biochem Cell Biol* **2004**, 36, 568–584.

Bassett, C.; Herrmann, I. Influence of oxygen concentration and mechanical factors on differentiation of connective tissuesin vitro. *Nature* **1961**, 190, 460.

Benoit, D.S., Anseth, K.S. Heparin functionalized PEG gels that modulate protein adsorption for hMSC adhesion and differentiation. *Acta Biomaterialia* **2005**, 1, 461–470.

Bhang, S.H.; Lim, J.S.; Choi, C.Y.; Kwon, Y.K.; Kim, B.S. The behavior of neural stem cells on biodegradable synthetic polymers. *J Biomater Sci* **2007**, 18, 223–239.

Bird, R.B.; Stewart, W.E.; Lightfoot, E.N. *Transport Phenomena*, 2nd ed.; John Wiley & Sons, Inc.: New York, NY, USA, 2007; pp. 545–568.

Bjornson C.R.; Rietze, R.L.; Reynolds, B.A.; Magli, M.C.; Vescovi, A.L. Turning brain into blood: a hematopoietic fate adopted by adult neural stem cells in vivo. *Science* **1999**, 283, 534-537.

Blau, H.M.; Brazelton, T.R.; Weimann, J.M. The evolving concept of a stem cell: entity or function? *Cell* **2001**, 105, 829-841.

Böhmann, A.; Pörtner, R.; Schmieding, J.; Kasche, V.; Markl, H. The membrane dialysis bioreactor with integrated radial-flow fixed bed—A new approach for continuous cultivation of animal cells. *Cytotechnology* **1992**, *9*, 51–57.

Brinkman, N.C. A calculation of the viscous force exerted by a flowing fluid on a dense swarm of particles. *Appl. Sci. Res.* **1947**, A(1), 27-34.

Bruder, S.P.; Kurth, A.A.; Shea, M.; Hayes, W.C.; Jaiswal, N.; Kadiyala, S. Bone regeneration by implantation of purified, culture-expanded human mesenchymal stem cells. *J Orthop Res* **1998**, 16, 155–162.

Bueno, E.M.; Laevsky, G.; Barabino, G.A. Enhancing cell seeding of scaffolds in tissue engineering through manipulation of hydrodynamic parameters. *J Biotechnol* **2007**, 129, 516–531.

Buxton, A.N.; Zhu, J.; Marchant, R.; West, J.L.; Yoo, J.U.; Johnstone, B. Design and characterization of poly(ethylene glycol) photopolymerizable semi-interpenetrating networks for chondrogenesis of human mesenchymal stem cells. *Tissue Eng* **2007**, 13, 2549–2560.

Campbell, N.A.; Reece, J.B.; Mitchell, L.G. *Biology. Vol. 5*. Benjamin/Cummings, California, 1999.

Cao,Y.; Vacanti, J.P.; Ma, X.; Paige, K.T.; Upton, J.; Chowanski, Z.; Schloo, B.; Langer, R.; Vacanti, C.A. The generation of neo-tendon using synthetic polymers seeded with tenocytes. *Transplant Proc* **1994**, 26, 3390.

Carrier, R.L.; Papadaki, M.; Rupnick, M.; Schoen, F.J.; Bursac, N.; Langer, R.; Freed, L.E.; Vunjak-Novakovic, G. Cardiac tissue engineering: cell seeding, cultivation parameters, and tissue construct characterization. *Biotechnol Bioeng* **1999**, 64, 580–589.

Carrier, R.L.; Rupnick, M.; Langer, R.; Schoen, F.J.; Freed, L.E.; Vunjak-Novakovic, G. Perfusion improves tissue architecture of engineered cardiac muscle. *Tissue Eng* **2002**, 8, 175–188.

Catapano, G.; de Bartolo, L.; Lombardi, C.P.; Drioli, E. The effect of oxygen transport resistances on the viability and functions ofisolated rat hepatocytes. *Int J Artif Organs* **1996**, 19, 31–41.

Catapano, G. Mass transfer limitations to the performance of membrane bioartificial liver support devices. *Int. J. Artif. Organs* **1996**, *19*, 51–68.

Catapano, G.; Gerlach, J.C. Bioreactors for liver tissue engineering. On-line encyclopedia of tissue engineering. In *Topics in Tissue Engineering;* Ashammakhi, N., Reis, R., Chiellini, E., Eds.; Biomaterials and Tissue Engineering Group: Oulu, Finland, Volume 3, Chapter 8, pp. 1–42, 2007. Available online: http://www.oulu.fi/spareparts/ebook_topics_in_t_e_vol3/

Celik, C.E.; Ackley, M.W. Radial bed vessels having uniform flow distribution, US Patent US2012/0079938 A1 **2012**.

Chan, B.P.; Hui, T.Y.; Yeung, C.W.; Li, J.; Mo, I.; Chan, G.C. Self-assembled collagen-human mesenchymal stem cell microspheres for regenerative medicine. *Biomaterials* **2007**, 28, 4652–4666.

Chang, H.C.; Saucier, M.; Calo, J.M. Design criterion for radial flow fixed-bed reactors. *AIChE J.* **1983**, *29*, 1039–1041.

Chastain, S.R.; Kundu, A.K.; Dhar, S.; Calvert, J.W.; Putnam, A.J. Adhesion of mesenchymal stem cells to polymer scaffolds occurs via distinct ECM ligands and controls their osteogenic differentiation. *J Biomed Mater Res* **2006**, 78, 73–85.

Chen, H.C.; Hu, Y.C. Bioreactors for tissue engineering. *Biotechnol Lett* **2006**, 28, 1415-1423.

Chen, G.; Palmer, A.F. Hemoglobin-based oxygen carrier and convection enhanced oxygen transport in a hollow fiber bioreactor. *Biotechnol. Bioeng.* **2009**, *102*, 1603–1612.

Choi, Y.S.; Park, S.N.; Suh, H. Adipose tissue engineering using mesenchymal stem cells attached to injectable PLGA spheres. *Biomater* **2005**, 26, 5855–5863.

Christi, Y. Hydrodynamic damage to animal cells. *Crit. Rev. Biotechnol.* **2001**, *21*, 67–110.

Cima, L.G.; Blanch, H.W.; Wilke, C.R. A theoretical and experimental evaluation of a novel radial-flow hollow fiber reactor for mammalian cell culture. *Bioprocess Eng.* **1990**, *5*, 19–30.

Clarke, B. Normal bone anatomy. *Clin. J. Am. Soc. Nephrol*. **2008**, *3*, S131–S139.

Cross, M.; Dexter, T.M. Growth factors in development, transformation, and tumorigenesis. *Cell* **1991**, 64(2), 271-80.

Davisson, T.; Sah, R.L.; Ratcliffe, A. Perfusion increases cell content and matrix synthesis in chondrocyte three-dimensional cultures. *Tissue Eng* **2002**, 8, 807–816.

Delgado, J. A critical review of dispersion in packed beds. *Heat Mass Transfer* **2006**, *42*, 279–310.

De Napoli, I.E. ; Scaglione, S.; Giannoni, P.; Quarto, R. ; Catapano, G. Mesenchymal stem cell culture in convection-enhanced hollowfibre membrane bioreactors for bone tissue engineering. *J. Membr. Sci.* **2011**, 379, 341–352.

Dennis, J.E.; Caplan, A.I. Porous ceramic vehicles for rat-marrow-derived (Rattus norvegicus) osteogenic cell delivery: effects of pre-treatment with fibronectin or laminin. *J Oral Implantol* **1993**, 19, 106–115; discussion 136–107.

Dias, M.R.; Fernandes, P.R.; Guedes, J.M.; Hollister, S.J. Permeability analysis of scaffolds for bone tissue engineering. *J. Biomech.* **2012**, 45, 938–944.

Doran, P.M. *Bioprocess engineering principles*, Elsevier, 1995.

Duval, D.; Demangel, C.; Munier-Jolain, K.; Geahel, I. Factors controlling cell proliferation and antibody production in mouse hybridoma cells: I. Influence of aminoacid supply. *Biotechnol Bioeng* **1991**, 38: 561–570.

Fassnacht, D.; Pörtner, R. Experimental and theoretical considerations on oxygen supply for animal cell growth in fixed-bed reactors. *J Biotechnol* **1999**, 72, 169–184.

Ferrari, G.; Cusella-De Ngelis, G.; Coletta M.; Paolucci, E.; Stornauolo, A.; Cossu, G.; Mavilio, F. Muscle regeneration by bone marrow-derived myogenic progenitors. *Science* **1998**, 279, 1528-1530.

Flynn, L.E.; Prestwich, G.D.; Semple, J.L.; Woodhouse, K.A. Proliferation and differentiation of adipose-derived stem cells on naturally derived scaffolds. *Biomater* **2008**, 29(12), 1862-1871.

Fogler, H.S. Elements of Chemical Reaction Engineering, 4th ed.; Prentice Hall: Westford, MA, USA, 2006.

Fournier, R.L. *Basic Transport Phenomena in Biomedical Engineering*, 3rd ed., CRC Press, Boca Raton, 2012.

Freed, L.E., Marquis, J.C.; Nohria, A; Mikos, A.G.; Emmanual, J.; Langer, R. Neocartilage formation in vitro and in vivo using cells cultured on synthetic biodegradable polymers. *J Biomed Mater Res* **1993**, 27, 11.

Freed, L.E.; Grande, D.A.; Lingbin, Z.; Marquis, J.C.; Emmanual, J.; Langer, R. Joint resurfacing using allograft chondrocytes and synthetic biodegradable polymer scaffolds. *J Biomed Mater Res*, **1994**, 28, 891.

Freed, L.E.; Vunjak-Novakovic, G. Cultivation of cellpolymer tissue constructs in simulated microgravity. *Biotechnol Bioeng* **1995**, 46, 306–313.

Freed, L.E.; Guilak, F. Engineering functional tissues. In *Principles of Tissue engineering, 3rd ed.*; Lanza, R; Langer, R., Vacanti, J., Eds.; Elsevier Inc., 2007, pp. 137-153.

Freed, L.E.; Langer, R.; Martin, I.; Pellis, N.R.; Vunjak-Novakovic, G. Tissue engineering of cartilage in space. *Proc Natl Acad Sci USA* **1997**, 94, 13885-13890.

Freed, L.E.; Vunjak-Novakovic, G. Microgravity tissue engineering. *In Vitro Cell Dev Biol Anim* **1997**, 33, 381–385.

Freed, L.E.; Hollander, A.P.; Martin, I.; Barry, J.R.; Langer, R.; Vunjak-Novakovic, G. Chondrogenesis in a cell-polymer bioreactor system. *Exp Cell Res* **1998**, 240, 58–65.

Friedenstein, A.J.; Petrakova, K.V. Osteogenesis in transplants of bone marrow cells. *J Embryol Exp Morphol* **1966**, 16, 381-390.

Fröhlich, M.; Grayson, W.L.; Marolt, D.; Gimble, J.M.; Kregar-Velikonja, N.; Vunjak-Novakovic, G. Bone grafts engineered from human adipose-derived stem cells in perfusion bioreactor culture. *Tissue Eng.* **2010**, *16*, 179–189.

Furth, M.E.; Atala, A. Future perspectives. In *Principles of Tissue engineering, 3rd ed.*; Lanza, R; Langer, R., Vacanti, J., Eds.; Elsevier Inc., 2007, pp. 33-50.

Gao, J.; Caplan, A.I. Mesenchymal stem cells and tissue engineering for orthopaedic surgery. *Chir Organi Mov* **2003**, 88, 305–316.

Gardel, L.S.; Correia-Gomes, C.; Serra, L.A.; Gomes, M.E.; Reis, R.L. A novel bidirectional continuous perfusion bioreactor for the culture of large-sized bone tissue-engineered constructs. *J Biomed Mater Res Part B* **2013**, 101B, 1377–1386.

Gaspar, D.A.; Gomide, V.; Monteiro, F.J. The role of perfusion bioreactors in bone tissue engineering. *Biomatter* **2012**, 2, 1–9.

Geankoplis, C.J. *Transport Processes and Unit Operations*, 3th Edition, Prentice-Hall International, 1993.

Gebhardt, R. Metabolic zonation of the liver: regulation and implications for liver function. *Pharmacol Ther* **1992**, 53, 275-354.

Genkin, V.S.; Dil'man, V.V.; Sergeev, S.P. The distribution of a gas stream over a radial contact apparatus. *Int. Chem. Eng.* **1973**, 13, 24.

Gerecht-Nir, S.; Ziskind, A.; Cohen, S.; Itskovitz-Eldor, J. Human embryonic stem cells as an in vitro model for human vascular development and the induction of vascular differentiation. *Laboratory investigation; a journal of technical methods and pathology* **2003**, 83, 1811–1820.

Glicklis, R.; Shapiro, L.; Agbaria, R.; Merchuk, J.C.; Cohen, S. Hepatocyte behavior within three-dimensional porous alginate scaffolds. *Biotechnol. Bioeng.* **2000**, *67*, 344–353.

Gódia, F.; Cairó, J. Cell metabolism. In: *Cell Culture Technology for Pharmaceutical and Cell-Based Therapies*; Ozturk, S.S., Hu, W.-S. Eds. New York: Taylor & Francis, 2006.

Goldstein, A.S.; Juarez, T.M.; Helmke, C.D.; Gustin, M.C.; Mikos, A.G. Effect of convection on osteoblastic cell growth and function in biodegradable polymer foam scaffolds. *Biomaterials* **2001**, 22, 1279–1288.

Gooch, K.J.; Kwon, J.H.; Blunk, T.; Langer, R.; Freed, L.E.; Vunjak-Novakovic, G. Effects of mixing intensity on tissue-engineered cartilage. *Biotechnol Bioeng* **2001**, 72, 402–407.

Granet, C.; Laroche, N.; Vico, L.; Alexandre, C.; Lafage-Proust, M.H. Rotating-wall vessels, promising bioreactors for osteoblastic cell culture: comparison with other 3D conditions. *Med Biol Eng Comput* **1998**, 36, 513-519

Gray, H.; Williams, P.L.; Bannister, L.H. *Gray's Anatomy – The anatomical basis of medicine and surgey*, 38th ed., Churcill Livingstone, 1995.

Griffith, C.K.; George, S.C. Diffusion limits of an in vitrothick prevascularized tissue. *Tissue Eng* **2005**, 11, 257–266.

Griffith, C.K.; George, S.C. The effect of hypoxia on in vitro prevascularization of a thick soft tissue. *Tissue Eng Part A* **2009**, 15(9), 2423-2434.

Grimm, M.J.; Williams, J.L. Measurements of permeability in human calcaneal trabecular bone. *J. Biomech.* **1997**, 30(1), 743-745.

Guillouzo, A.; Guguen-Guillouzo, C. Evolving conceptsin liver tissue modeling and implications for in vitrotoxicology. *Expert Opin Drug Metab Toxicol* **2008**, 4, 1279–1294.

Han, P.; Bartels, D.M. Temperature dependence of oxygen diffusion in H_2O and D_2O. *J. Phys. Chem*. **1996**, *100*, 5597–5602.

Hassel, T.; Gleave, S.; Butler, M. Growth inhibition in animal cell culture. The effect of lactate and ammonia. *Appl Biochem Biotechnol* **1991**, 30, 29.

Heggs, P.J.; Ellis, D.I.; Ismail, M.S. Evaluation of pressure drop profiles and overall pressure drop for flow through annular packed bed configuration. *Gas Sep. Purif.* **1995**, 9, 171-180.

Hofmann, S.; Knecht, S.; Langer, R.; Kaplan, D.L.; Vunjak-Novakovic, G.; Merkle, H.P.; Meinel, L. Cartilage-like tissue engineering using silk scaffolds and mesenchymal stem cells. *Tissue Eng* **2006**, 12, 2729–2738.

Hofmann, S.; Hagenmuller, H.; Koch, A.M.; Muller, R.; Vunjak-Novakovic, G.; Kaplan, D.L.; Merkle, H.P.; Meinel, L. Control of in vitro tissue-engineered bone-like structures using human mesenchymal stem cells and porous silk scaffolds. *Biomater* **2007**, 28, 1152–1162.

Holy, C.E.; Shoichet, M.S.; Davies, J.E. Engineering three-dimensional bone tissue in vitro using biodegradable scaffolds: investigating initial cell-seeding density and culture period. *J Biomed Mater Res* **2000**, 51, 376–382.

Hongo, T.; Kajikawa, M.; Ishida, S.; Ozawa, S.; Ohno, Y.; Sawada, J.; Umezawa, A.; Ishikawa, Y.; Kobayashi, T.; Honda, H. Three-dimensional high-density culture of HepG2 cells in a 5-mL radial flow bioreactor for construction of artificial liver. *J Biosci Bioeng* **2005**, 99, 237–244.

Hongo, T.; Kajikawa, M.; Ishida, S.; Ozawa, S.; Ohno, Y.; Sawada, J.; Ishikawa, Y.; Honda, H. Gene expression property of high-density three-dimensional tissue of HepG2 cells formed in radial-flow bioreactor. *J Biosci Bioeng* **2006**, 101(3), 243-250.

Idelchik, I.E. *Handbook of Hydraulic Resistance*, NTIS, Washington, DC, 1960.

Ishii, Y.; Saito, R.; Marushima, H.; Ito, R.; Sakamoto, T.; Yanaga, K. Hepatic reconstruction from fetal porcine liver cells using a radial flow bioreactor. *World J Gastroenterol* **2008**, 14, 2740–2747.

Iwahori, T.; Matsuura, T.; Maehashi, H.; Sugo, K.; Saito, M.; Hosokawa, M.; Chiba, K.; Masaki, T.; Aizaki, H.; Ohkawa, K.; Suzuki, T. CYP3A4 Inducible model for in vitro analysis of human drug metabolism using a bioartificial liver. *Hepathol* **2003**, 37(3), 665-673.

Iyer, V.V.; Jang, H.; Ierapetritou, M.G.; Roth, C.M. Effects of glucose and insulin on HepG2-C3A cell metabolism. *Biotechnol. Bioeng.* **2010**, 107(2), 347-356.

Jackson, K.A.; Tiejuan, M; Goodell, M. Hematopoietic potential of stem cells isolated from murine skeletal muscle. *PNAS* **1999**, 96(25), 14482-14486.

Jaesung, P.; Yawen, L.; Berthiaume, F.; Toner, M.; Yarmush, M.L.; Tilles, A.W. Radial flow hepatocyte bioreactor using stacked microfabricated grooved substrates. *Biotechnol. Bioeng*. **2008**, *99*, 455–467.

Jeong, C.; Zhang, H.; Hollister, S. Three-dimensional poly(1,8-octanediol–co-citrate) scaffold pore shape and permeability effects on sub-cutaneous in vivo chondrogenesis using primary chondrocytes, *Acta Biomater*. **2011**, 7, 505–514.

Karabelas, A.J.; Wegner, T.H., Hanratty, T.J. Use of asymptotic relations to correlatemass transfer data in packed beds. *Chem. Eng. Sci.* **1971,** 26, 1581-1589.

Karageorgiou, V.; Kaplan D. Porosity of 3D biomaterial scaffolds and osteogenesis. *Biomater.* **2005**, 26, 5474–5491.

Kareeri, A.A.; Zughbi, H.D.; Al-Ali, H.H. Simulation of flow distribution in radial flow reactors, *Ind. Eng. Chem. Res.* **2006**, 45, 2862-2874.

Katayama, A.; Arano, T. Sato, T.; Ikada, Y.; Yoshinari, M. Radial-flow bioreactor enables uniform proliferation of human mesenchymal stem cells throughout a three-dimensional scaffold. *Tissue Eng Part C* **2013**, 19(2), 109-116.

Kawada, M.; Nagamori, S.; Aizaki, H.; Fukaya, K.; Niiya, M.; Matsuura, T.; Sujino, H.; Hasumura, S.; Yashida, H.; Mizutani, S. Massive culture of human liver cancer cells in a newly developed radial flow bioreactor system: Ultrafine structure of functionally enhanced hepatocarcinoma cell lines. *In Vitro Cell Dev Biol Anim* **1998**, 34, 109–115.

Khdemhosseini, A.; Karp, J.M.; Gerecht, S.; Ferreira, L.; Vunjak-Novakovic, G.; Langer, R. Embryonic Stem Cells as a Cell Source for Tissue Engineering. In *Principles of Tissue engineering, 3rd ed.*; Lanza, R; Langer, R., Vacanti, J., Eds.; Elsevier Inc., 2007, pp. 445-458.

Kim, H.J.; Kim, U.J.; Vunjak-Novakovic, G.; Min, B.H.; Kaplan, D.L. Influence of macroporous protein scaffolds on bone tissue engineering from bone marrow stem cells. *Biomater* **2005**, 26, 4442–4452.

Kim, H.; Kim, H.W.; Suh, H. Sustained release of ascorbate-2-phosphate and dexamethasone from porous PLGA scaffolds for bone tissue engineering using mesenchymal stem cells. *Biomater* **2003**, 24, 4671–4679.

Kim, B.S. Putnam, A.J.; Kulik, T.J.; Mooney D.J. Optimizing seeding and culture methods to engineer smooth muscle tissue on biodegradable polymer matrices. *Biotechnol Bioeng* **1998**, 57, 46–54.

Kim, S.S.; Sundback, C.A.; Kaihara, S.; Benvenuto,M.S.; Kim, B.-S.; Mooney, D.J.; Vacanti, J.P. Dynamic seeding and in vitroculture of hepatocytes in a flow perfusion system. *Tissue Eng* **2000**, 6, 39–44.

Kino-Oka, M.; Taya, M. Design and operation of a radial flow bioreactor for reconstruction of cultured tissues. In *Bioreactors for Tissue Engineering*, 1st ed.; Chauduri, J., Al-Rubeai, M., Eds.; Springer Verlag: Dordrecht, The Netherlands, 2005; pp. 115–133.

Kitagawa, T.; Yamaoka, T.; Iwase, R.; Murakami, A. Three-dimensional cell seeding and growth in radial-flow perfusion bioreactorfor in vitro tissue reconstruction. *Biotechnol Bioeng* **2006**, 93, 947–954.

Komarova, S.V.; Ataullakhanov, F.I.; Globus, R.K. Bioenergetics and mitochondrial transmembrane potential during differentiation of cultured osteoblasts. *Am. J. Physiol. Cell Physiol.* **2000**, *279*, C1220–C1229.

Kotobuki, N.; Ioku, K.; Kawagoe, D.; Fujimori, H.; Goto, S.; Ohgushi, H. Observation of osteogenic differentiation cascade of living mesenchymal stem cells on transparent hydroxyapatite ceramics. *Biomater* **2005**, 26, 779–785.

Kurosawa, H.; Markl, H.; Niebhur-Redder, C.; Matsamura, M. Dialysis bioreactor with radial flow fixed bed for animal cell culture. *J Ferment Bioeng* **1991**, 72, 41–45.

Lamalice, L.; Le Boeuf, F; Huot, J. Endothelial cell migration during angiogenesis. *Circ Res* **2007**, 100, 782 –794.

Langer, R.; Vacanti, J.P. Tissue Engineering. *Science* **1993**, 260, 920-926.

Langer, R.; Vacanti, J.P.; Vacanti, C.A.; Atala, A.; Freed, L.E.; Vunjak-Novakovic, G. Tissue engineering: Biomedical applications. *Tissue Eng* **1995**, 1, 151-161.

Lavrentieva, A.; Majore, I., Kasper, C.; Hass, R. Effects of hypoxic culture conditions on umbilicar cord-derived human mesenchymal stem cells. *Cell Comm. Sign.* **2010**, 8, 18.

Lee, K.W.; Wang, S.; Lu, L., Jabbari, R.; Currier, B.; Yaszemski, M. Fabrication and characterization of poly(propylenefumarate) scaffolds with controlled pore structures using 3-dimensional printing and injection molding. *Tissue Eng*. **2006**, 12, 10.

Lee, K.; Silva, E.A.; Mooney, D.J. Growth factor delivery-based tissue engineering: general approaches and a review of recent developments. *J R Soc Interface* **2011**, 8, 153–170.

Li, S.; Wijn, J.; Li, J.; Layrolle, P.; Groot, K. Macroporous Biphasic Calcium Phosphate Scaffold with High Permeability/Porosity Ratio. *Tissue Eng.* **2003**, 9, 535–548.

Liang, L.; Bickenbach J.R. Somatic epidermal stem cells can produce multiple cell lineages during development. *Stem Cells* **2002**, 20, 21-31.

Loiacono, L.A.; Shapiro, D.S. Detection of hypoxia at the cellular level. *Crit. Care Clin.* **2010**, *26*, 409–421.

Lysaght, M.J.; Loughlin, J.A. Demographic scope and economic magnitude of contemporary organ replacement therapies. *ASAIO J* **2000**, 46, 515-521.

Ma, W.; Fitzgerald, W.; Liu, Q.Y.; O'Shaughnessy, T.J.; Maric, D.; Lin, H.J.; Alkon, D.L.; Barker, J.L. CNS stem and progenitor cell differentiation into functional neuronal circuits in three-dimensional collagen gels. *Experimental neurology* **2004**, 190, 276–288.

Ma, T.; Grayson, W.L.; Fröhlich, M.; Vunjak-Novakovic G. Hypoxia and set-cell-based engineering of mesenchymal tissues. *Biotechnol. Prog.* **2009**, 25, 32-42.

MacArthur, B.D; Oreffo, R.O.C. Bridging the gap. *Nature* **2005**, 433, 19.

Maguire, T.; Novik, E.; Schloss, R.; Yarmush, M. Alginate-PLL microencapsulation: effect on the differentiation of embryonic stem cells into hepatocytes. *Biotechnol Bioeng* **2006**, 93, 581–591.

Mahoney, M.J.; Anseth, K.S. Three-dimensional growth and function of neural tissue in degradable polyethylene glycol hydrogels. *Biomater* **2006**, 27, 2265–2274.

Malda, J.; Martens, D.E.; Tramper, J.; van Blitterswijk, C.A.; Riesle, J. Cartilage tissue engineering: controversy in the effect of oxygen. *Crit Rev Biotechnol* **2003**, 23, 175.

Malda, J.; Rouwkema, J.; Martens, D.E.; Le Comte, E.P.; Kooy, F.K.; Tramper, J.; van Blitterswijk, C.A.; Riesle, J. Oxygen gradients in tissue-engineered PEGT/PBT cartilaginous constructs: measurement and modeling. *Biotechnol Bioeng* **2004**, 86, 9.

Malda, J.; Klein, T.J.; Upton, Z. The roles of hypoxia in the in vitro engineering of tissues. *Tissue Eng* **2007**, 13, 2153-2162.

Marcacci, M.; Kon, E.; Moukhachev, V.; Lavroukov, A.; Kutepov, S.; Quarto, R.; Mastrogiacomo, M.; Cancedda, R. Stem cells associated with macroporous bioceramics for long bone repair: 6- to 7-year outcome of a pilot clinical study. *Tissue Eng* **2007**, 13, 947–955.

Martin, R.B. Porosity and specific surface of bone. *CRC Crit Rev Biomed Eng* **1984**, 10, 179–222

Martin, G.R. Isolation of a pluripotent cell line from early mouse embryos cultured in medium conditioned by teratocarcinoma stem cells. *Proc. Natl. Acad. Sci. U.S.A.* **1981**, 78, 7634–7638.

Martin, I.; Wendt, D; Heberer, M. The role of bioreactors in tissue engineering. *TRENDS Biotechnol* **2004**, 22(2), 80-86.

McClelland, R.E.; Coger, R.N. Use of micropathways to improve oxygen transport in a hepatic system. *Trans. ASME* **2000**, *122,* 268–273.

McClelland, R.E.; Coger, R.N. Effects of enhanced O_2 transport on hepatocytes packed within a bioartificial liver device. *Tissue Eng*. **2004**, *10*, 253–266.

Mehta, K.; Mehta, G.; Takayama, S.; Linderman, J. Quantitative inference of cellular parameters from microfluidic cell culture systems. *Biotechnol. Bioeng.* **2009**, *103*, 966–974.

Meinel, L.; Fajardo, R.; Hofmann, S.; Langer, R.; Chen, J.; Snyder, B.; Vunjak-Novakovic, G.; Kaplan, D. Silk implants for the healing of critical size bone defects. *Bone* **2005**, 37, 688–698.

Melchels, F.P.W.; Tonnarelli, B.; Olivares, A.L.; Martin, I.; Lacroix, D.; Feijen, J.; Wendt, D.J.; Grijpma, D.W. The influence of the scaffold design on the distribution of adhering cells after perfusion cell seeding. *Biomaterials* **2011**, 32, 2878-2884.

Meyer, U.; Joos, U.; Wiesmann, H.P. Biological and biophysical principles in extracorporeal bone tissue engineering, Part I. *Oral Maxillofacial Surgery* **2004**, 33, 325-332.

Miskon, A.; Sasaki, N.; Yamaoka, T.; Uyama, H.; Kodama, M. Radial flow type bioreactor for bioartificial liver assist using PTFE non-woven fabric coated with poly-amino acid urethane copolymer. *Macromol Symp* **2007**, 249–250, 151–158.

Mitsak, A.G., Kemppainen, J.M.; Harris, M.T.; Hollister, S.J. Effect of Polycaprolactone Scaffold Permeability on Bone Regeneration In Vivo. *Tissue Eng. Part A* **2011**, 17, 1831-9.

Morsiani, E.; Galavotti, D.; Puviani, A.C.; Valieri, L.; Brogli, M.; Tosatti, S.; Pazzi, P.; Azzena, G. Radial flow bioreactor outperforms hollow-fiber modulus as a perfusing culture system for primary porcine hepatocytes. *Transplant Proc* **2000**, 32, 2715–2718.

Morsiani, E.; Brogli, M.; Galavotti, D.; Bellini, T.; Ricci, D.; Pazzi, P.; Puviani, A.C. Long-term expression of highly differentiated functions by isolated porcine hepatocytes perfused ina radial-flow bioreactor. *Artif Organs* **2001**, 25, 740–748.

Moustafa, T.; Badr, S.; Hassan, M.; Abba, I.A. Effect of flow direction on the behavior of radial flow catalytic reactors. *Asia-Pac. J. Chem. Eng.* **2012**, *7*, 307–316.

Mu, Z.; Wang, J.; Tiefeng, W.; Jin, Y. Optimum design of radial moving-bed reactors based on mathematical hydrodynamic model. *Chem. Eng. Proc.* **2003**, 42, 409-417.

Munson, B.R.; Young, D.F.; Okiishi, T.H.; Huebsch, W.W.; Rothmayer A.P. *Fundamentals of Fluid Mechanics*, 7th ed., Wiley & Sons Inc., Hoboken NJ, 2013.

Murray-Thomas, T.; Cowie, M. R. Epidemiology and clinical aspects of congestive heart failure. *J. Renin Angiotensin Aldosterone Syst.* **2003**, 4, 131–136.

Muschler, G.F.; Nakamoto, C; Griffith, L.G. Engineering principles of clinical cell-based tissue engineering. *J Bone Joint Surg* **2004**, 86, 1541-1557.

Myers, S.R.; Partha, V.N.; Soranzo, C.; Price, R.D.; Navsaria, H.A. Hyalomatrix: a temporary epidermal barrier, hyaluronan delivery, and neodermis induction system for keratinocyte stem cell therapy. *Tissue Eng* **2007**, 13, 2733–2741.

Nauman, E.A.; Fong, K.E.; Keaveny, T.M. Dependence of intertrabecular permeability on flow direction and anatomic site. *Ann. Biomed. Eng*. **1999**, 27, 517–524.

Navarro, F.A.; Mizuno, S.; Huertas, J.C.; Glowacki, J.; Orgill, D.P. Perfusion of medium improves growth of human oral neomucosal tissue constructs. *Wound Repair Regen* **2001**, 9, 507–512

Navdeep, S.; Chandel, G.R.; Budinger, S. The cellular basis for diverse responses to oxygen. *Free Radic. Biol. Med*. **2007**, *42*, 165–174.

Nerem, R.M. The challenge of imitating nature. In *Principles of Tissue engineering, 3rd ed.*; Lanza, R; Langer, R., Vacanti, J., Eds.; Elsevier Inc., 2007, pp. 7-14.

Neubauer, M.; Hacker, M.; Bauer-Kreisel, P.; Weiser, B.; Fischbach, C.; Schulz, M.B.; Goepferich, A.; Blunk, T. Adipose tissue engineering based on mesenchymal stem cells and basic fibroblast growth factor in vitro. *Tissue Eng* **2005**, 11, 1840–1851.

Niu, M.; Hammond, P.; Coger, R.N. The effectiveness of a novel cartridge-based bioreactor design in supporting liver cells. *Tissue Eng. Part A* **2009**, *15*, 2903–2916.

Noble, P.C.; Alexander, J.W.; Lindahl, L.J.; Yew, D.T.; Granberry, W.M.; Tullos, H.S. The anatomic basis of femoral component design. *Clin. Orthop. Relat. Res.***1988**, 235, 148-165.

Noth, U.; Schupp, K.; Heymer, A.; Kall, S.; Jakob, F.; Schutze, N.; Baumann, B.; Barthel, T.; Eulert, J.; Hendrich, C. Anterior cruciate ligament constructs fabricated from human mesenchymal stem cells in a collagen type I hydrogel. *Cytotherapy* **2005**, 7, 447–455.

O'Brien, F.J. Biomaterials and scaffolds for tissue engineering. *Materials today* **2011**, 14, 88-95.

O'Connor, S.M.; Stenger, D.A.; Shaffer, K.M.; Maric, D.; Barker, J.L.; Ma, W. Primary neural precursor cell expansion, differentiation and cytosolic Ca(2+) response in three-dimensional collagen gel. *J Neurosci Methods* **2000**, 102, 187–195.

Ochoa, I.; Sanz-Herrera, J.; Aznar, J.; Doblare, M.; Yunos, D.; Boccaccini, A. Permeability evaluation of 45S5 Bioglass-based scaffolds for bone tissue engineering. *J. Biomech*. **2009**, 42, 257–260.

Olivier, V.; Hivart, P.; Descamps, M.; Hardouin, P. In vitroculture of large bone substitutes in a new bioreactor: Importance of the flow direction. *Biomed Mater* **2007**, 2, 174–180.

Ontiveros, C.; McCabe, L.R. Simulated microgravity suppresses osteoblast phenotype, Run2 levels and AP-1 transactivation. *J Cell Biochem* **2003**, 88, 427-437.

Organ, G.M.; Mooney, D.J.; Hansen, L.K.; Schloo, B.; Vacanti, J.P. Design and transplantation of enterocyte polymer constructs: A small animal model for neointestinal replacement i n short bowel syndrome. *Am Coll Surg Surgical Forum* **1993**, 44, 432.

Otzurk, S.S.; Riley, M.R.; Palsson, B.O. Effects of ammonia and lactate on hybridoma growth, metabolism and antibody production. *Biotechnol Bioeng* **1992**, 39, 418-431.

Park, J.; Li, Y.; Berthiaume, F.; Toner, M.; Yarmush, M.L.; Tilles, A.W. Radial flow hepatocyte bioreactor using stacked microfabricated grooved substrates. *Biotechnol. Bioeng*. **2008**, 99(2), 455-467.

Perry, R.H.; Green, D.W.; Maloney J.O. *Perry's Chemical Engineers' Handbook.* 7th ed., McGraw-Hill, New York, 1999.

Piret, J.M.; Devens, D.A.; Cooney, C.L. Nutrient and metabolite gradients in mammalian-cell hollow fiber bioreactors. *Can J Chem Eng* **1991**, 69, 421–428.

Plunkett, N.; O'Brien, F.J. Bioreactors in tissue engineering. *Technol Health Care* **2011**, 19, 55–69.

Ponzi, P.R.; Kaye, L.A. Effect of flow maldistribution on conversion and selectivity in radial flow fixed-bed reactors. *AIChE J*. **1979**, *25*, 100–108.

Portner, R.; Nagel-Heyer, S.; Goepfert, C.; Adamietz, P.; Meenen, N.M. Bioreactor design for tissue engineering. *J Biosci Bioeng* **2005**, 100(3), 235-245.

Pörtner, R.; Platas, O.B.; Fassnacht, D.; Nehring, D.; Czermak, P.; Markl, H. Fixed bed reactors for the cultivation of mammalian cells: Design, performance and scale-up. *Open Biotechnol. J*. **2007**, *1*, 41–46.

PP, B.M.; Pedro, A.J.; Peterbauer, A.; Gabriel, C.; Redl, H.; Reis, R.L. Chitosan particles agglomerated scaffolds for cartilage and osteochondral tissue engineering approaches with adipose tissue derived stem cells. *J Mater Sci* **2005**, 16, 1077–1085.

Radisic, M.; Euloth, M.; Yang, L.; Langer, R.; Freed, L.E.; Vunjak-Novakovic, G. High density seeding of myocytes cells for cardiac tissue engineering, *Biotechnol. Bioeng.* **2003**, 82(4), 403–414.

Radisic, M.; Deen, W.; Langer, R.; Vunjak-Novakovic, G. Mathematical model of oxygen distribution in engineered cardic tissue with parallel channel array perfused with culture medium containing oxygen carriers. *Am. J. Physiol. Heart Circ. Physiol*. **2005**, *288*, H1278–H1289.

Radisic, M.; Malda, J.; Epping, E.; Geng, W.; Langer, R.; Vunjak-Novakovic, G. Oxygen gradients correlate with cell density and cell viability in engineered cardiac tissue. *Biotechnol Bioeng* **2006**, 93, 332.

Riha, G.M.; Lin, P.H.; Lumsden, A.B.; Yao, Q.; Chen, C. Review: application of stem cells for vascular tissue engineering. *Tissue Eng* **2005**, 11, 1535–1552.

Robins, J.C.; Akeno, N.; Mukherjee, A.; Dalal, R.R.; Aronow, B.J.; Koopman, P.; Clemens, T.L. Hypoxia induces chondrocyte-specific gene expression in mesenchymal cells in association with transcriptional activation of Sox9. *Bone* **2005**, 37, 313.

Rotem, A.; Toner, M.; Bhatia, S.N.; Foy, B.D.; Tomkins, R.G.; Yarmush, M.L. Oxygen is a factor determining *in vitro* tissue assembly: Effects on attachment and spreading of hepatocytes. *Biotechnol. Bioeng.* **1994**, *43*, 654–660.

Rowley, J.A.; Timmins, M.; Galbraith, W.; Garvin, J.; Kosovsky, M.; Heidaran, M. Oxygen consumption as a predictor of growth and differentiation of MC3T3-E1 osteoblasts on 3D biodegradable scaffolds. *Mol. Biol. Cell* **2002**, *13*, 345a.

Saito, M.; Matsuura, T.; Masaki, T.; Maehashi, H.; Shimizu, K.; Hataba, Y.; Iwahori, T.; Suzuki, T.; Braet, F. Reconstruction of liver organoid using bioreactor. *World J Gastroenterol* **2006**, 12, 1881–1888.

Salim, A.; Nacamuli, R.P.; Morgan, E.F.; Giaccia, A.J.; Longaker, M.T. Transient changes in oxygen tension inhibit osteogenic differentiation and Runx2 expression in osteoblasts. *J Biol Chem* **2004**, 279, 40007–40016

Schop, D.; Janssen, F.W.; van Rijn, L.D.S.; Fernandes, H.; Bloem, R.M.; de Bruijn, J.D.; van Dijkhuizen-Radersma, R. Growth, metabolism and growth inhibitors of mesenchymal stem cells. *Tissue Eng A* **2009**, 15(8), 1877-1886.

Schneider, M.; Marison, I.W.; von Stockar, U. The importance of ammonia in mammalian cell culture. *J Biotechnol* **1996**, 46, 161-185.

Schugens C.; Maquet, V.; Grandfils, C.; Jerome, R.; Teyssie, P. Polylactide macroporous biodegradable implants for cell transplantation. II. Preparation of polylactide foams by liquid-liquid phase separation. *J Biomed Mater Res* **1996**, 30(4), 449-461.

Seaberg, R.M.; van der Kooy, D. Stem and progenitor cells: the premature desertion of rigorous definitions. *Trends in Neurosci* **2003**, 26, 125-131.

Shao, W. The effect of radial convection on cell proliferation in bone tissue engineering, University of Minnesota Ph.D. dissertation, 2009. Retrieved from the University of Minnesota Digital Conservancy, http://purl.umn.edu/52395.

Shibata, S.I.; Marushima, H.; Asakura, T.; Matsuura, T.; Eda, H.; Aoki, K.; Matsudaira, H.; Ueda, K.; Ohkawa, K. Three-dimensional culture using a radial flow bioreactor induces matrix metalloprotease 7-mediated EMT-like process in tumor cells via TGFß1/Smad pathway. *Int J Oncol* **2009**, 34, 1433-1448.

Shimaoka, H.; Dohi, Y.; Ohgushi, H.; Ikeuchi, M.; Okamoto, M.; Kudo, A.; Kirita, T.; Yonemasu, K. Recombinant growth/differentiation factor-5 (GDF-5) stimulates osteogenic differentiation of marrow mesenchymal stem cells in porous hydroxyapatite ceramic. *J Biomed Mater Res* **2004**, 68, 168–176.

Shipley, R.J.; Waters, S.L. Fluid and mass transport modeling to drive the design of cell-packed hollow fibre bioreactors for tissue engineering applications. *Math. Med. Biol.* **2011**, 29 (4), 329–359.

Shulman, H.L., Ullrich, C.F.; Proulx, A.Z.; Zimmerman, J.O. Performance of packed columns. 2. Wetted and effective interfacial areas, gas- and liquid-phase mass transfer rates. *AIChE J.* **1955**, 1, 253, 1955.

Sidoli, F.R.; Mantalaris, A.; Asprey S.P. Modelling of mammalian cells and cell culture processes. *Cytotechnology* **2004**, 44, 27–46.

Sikavitsas, V.I.; Bancroft, G.N.; Mikos, A.G. Formation of three-dimensional cell/polymer constructs for bone tissue engineering in a spinner flask and a rotating wall vessel bioreactor. *J. Biomed. Mater. Res.* **2002**, *62*, 36–48.

Singh, H.; Ang, E.S.; Lim, T.T.; Hutmacher, D.W. Flow modeling in a novel non-perfusion conical bioreactor. *Biotechnol Bioeng* **2007**, 97, 1291–1299.

Smyth, S.; Heron, A. Diabetes and obesity: the twin epidemics. *Nat. Med.* **2006**, 12, 75–80

Stockwell, R.A. The interrelationship of cell density and cartilage thickness in mammalian articular cartilage. *J. Anat.* **1971**, 109 (3), 411–421.

Sugiura, S.; Sakai, Y.; Nakazawa, K.; Kanamori, T. Superior oxygen and glucose supply in perfusion cell cultures compared to static cell cultures demonstrated by simulations using the finite element method. *Biomicrofluidics* **2011**, 5(022202),_1-11.

Sullivan, J.P.; Palmer, A.F. Targeted oxygen delivery within hepatic hollow fiber bioreactors via supplementation of hemoglobin-based oxygen carriers. *Biotechnol. Prog*. **2006**, *22*, 1374–1387.

Sumanasinghe, R.D.; Bernacki, S.H.; Loboa, E.G. Osteogenic differentiation of human mesenchymal stem cells in collagen matrices: effect of uniaxial cyclic tensile strain on bone morphogenetic protein (BMP-2) mRNA expression. *Tissue Eng* **2006**, 12, 3459–3465.

Tharakan, J.P.; Chau, P.C. Modeling and analysis of radial flow mammalian cell culture. *Biotechnol. Bioeng*. **1987**, *29*, 657–671.

Thomson, J. A.; Kalishman, J.; Golos, T.G.; Durning, M.; Harris, C.P.; Becker, R.A.; Hearn, J.P. Isolation of a primate embryonic stem cells line. *Proc Natl Acad Sci USA* **1995**, 92, 7844–7848.

Thomson, J.A.; Itskovitz-Eldor, J.; Shapiro, S.S.; Waknitz, M.A.; Swiergiel, J.J.; Marshall, V.S.; Jones, J.M. Embryonic stem cell lines derived from human blastocysts. *Science* **1998**, 282, 1145–1147.

Tortora, G.J.; Derrickson, B. *Principles of Anatomy and Physiology*, 11th ed.; John Wiley & Sons, Inc.: New York, NY, USA, 2006.

Tuan, R.S.; Boland, G.; Tuli, R. Adult mesenchymal stem cells and cell-based tissue engineering. *Arthritis Res Ther* **2003**, 5, 32–45.

Tuncay, O.C.; Ho, D.; Barker, M.K. Oxygen tension regulates osteoblast function, *Am J Orthod Dentofacial Orthop* **1994**, 105, 457–463

Uematsu, K.; Hattori, K.; Ishimoto, Y.; Yamauchi, J.; Habata, T.; Takakura, Y.; Ohgushi, H.; Fukuchi, T.; Sato, M. Cartilage regeneration using mesenchymal stem cells and a three-dimensional poly-lactic-glycolic acid (PLGA) scaffold. *Biomater*, **2005**, 26, 4273–4279.

Underhill, G.H.; Chen, A.A.; Albrecht, D.R.; Bhatia, S.N. Assessment of hepatocellular function within PEG hydrogels. *Biomater* **2007**, 28, 256–270.

Utting, J.C.; Robins, S.P.; Brandao-Burch, A.; Orriss, I.R.; Behar, J.; Arnett, T.R. Hypoxia inhibits the growth, differentiation and bone-forming capacity of rat osteoblasts. *Exp Cell Res* **2006**, 312, 1693.

Uyama, S.; Kaufmann, P-M.; Takeda, T.; Vacanti, J.P. Delivery of whole liver-equivalent hepatocyte mass using polymer devices and hepatotrophic stimulation. *Transplantation* **1993**, 55, 932.

Vacanti, C.A.; Langer, R.; Schloo, B; Vacanti, J.P. Synthetic polymers seeded with chondrocytes provide a template for new cartilage formation. *Plastic Reconstr Surg* **1991**, 88, 753.

Vacanti, C.A.; Kim, W.; Upton, J.; Vacanti, M.P.; Mooney, D.; Schloo, B.; Vacanti, J.P. Tissue engineering growth of bone and cartilage. *Transplant Proc* **1993**, 25, 1019.

Van Blitterswijk, C.A.; Thomsen, P.; Lindahl, A.; Hubbell, J.; Wiliams, D.; Cancedda, R.; de Bruijn, J.D.; Sohier, J. *Tissue Engineering*. Vol. 1. Elsevier, 2008.

Van Cleynenbreugel, T.; Schrooten, J.; Van Oosterwyck, H.; Vander Sloten, J. Micro-CT-based screening of biomechanical and structural properties of bone tissue engineering scaffolds. *Med. Bio. Eng. Comput.* **2006**, 44, 517–525.

VandeVord, P.J.; Nasser, S.; Wooley, P.H. Immunological responses to bone soluble proteins in recipients of bone allografts. *J. Orthop. Res.* **2005**, *23*, 1059–1064.

Volkmer, E.; Drosse, I.; Otto, S.; Stangellmayer, A.; Stengele, M.; Kallukalam, B.C.; Mutschler, W.; Schieker, M. Hypoxia in static and dynamic 3D culture systems for tissue engineering of bone. *Tissue Eng Part A* **2008**, 14, 1331–1340.

Vunjak-Novakovic, G.; Obradovic, B.; Martin, I.; Bursac, P.M.; Langer, R.; Freed, L.E. Dynamic cell seeding of polymer scaffolds for cartilage tissue engineering. *Biotechnol Prog* **1998**, 14, 193–202.

Vunjak-Novakovic, G.; Martin, I.; Obradovic, B.; Treppo, S.; Grodzinsky, A.J.; Langer, R.; Freed, L.E. Bioreactor cultivation conditions modulate the composition and mechanical properties of tissue-engineered cartilage. *J Orthop Res* **1999**, 17, 130–138.

Wagers, A.J.; Weissman, I.L. Plasticity of adult stem cells. *Cell* **2004**, 116, 639-648.

Wang, S.; Tarbell, J.M. Effect of fluid flow on smooth muscle in a 3-dimensional collagen gel model. *Arterioscler. Thromb. Vasc. Biol*. **2000**, *20*, 2220–2225.

Wang, Y.; Kim, U.J.; Blasioli, D.J.; Kim, H.J.; Kaplan, D.L. In vitro cartilage tissue engineering with 3D porous aqueous-derived silk scaffolds and mesenchymal stem cells. *Biomater* **2005**, 26, 7082–7094.

Warnock, J.N.; Bratch, K.; Al-Rubeai, M. Packed-bed bioreactors. In *Bioreactors for Tissue Engineering*, 1st ed.; Chauduri, J., Al-Rubeai, M., Eds.; Springer Verlag: Dordrecht, The Netherlands, 2005; pp. 87–114.

Watanabe, K.; Nakamura, M.; Okano, H.; Toyama, Y. Establishment of three-dimensional culture of neural stem/progenitor cells in collagen Type-1 Gel. *Restor Neurol Neurosci* **2007**, 25, 109–117.

Weber, C.; Freimark, D.; Pörtner, R.; Pino-Grace, P.; Pohl, S.; Wallrapp, C.; Geigle, P.; Czermak, P. Expansion of human mesenchymal stem cell in a fixed-bed bioreactor system based on a non-porous glass carrier – Part A: inoculation, cultivation and cell harvest procedures. *Int. J. Artif. Organs* **2010**, 33, 512-525.

Wendt, D.; Marsano, A.; Jakob, M.; Heberer, M.; Martin, I. Oscillating perfusion of cell suspensions through three-dimensional scaffolds enhances cell seeding efficiency and uniformity. *Biotechnol Bioeng* **2003**, 84, 205–214.

Wendt, D.; Riboldi, S.A.; Cioffi, M.; Martin, I. Bioreactors in tissue engineering: scientific challenges and clinical perspectives. *Adv Biochem Engin/Biotechnol* **2009**, 112, 1-27.

White, K.M.; Bramwell, M.E.; Harris, H. Kinetic parameters of hexose transport in hybrids between malignant and non malignant cells. *J. Cell Sci.* **1983**, 62, 49-80.

White, F.M. *Fluid Mechanics*, 7th ed., McGraw Hill, New York, NY, 2011.

Willerth, S.M.; Arendas, K.J.; Gottlieb, D.I.; Sakiyama-Elbert, S.E. Optimization of fibrin scaffolds for differentiation of murine embryonic stem cells into neural lineage cells. *Biomater* **2006**, 27, 5990–6003.

Willerth, S.M.; Sakiyama-Elbert, S.E. Combining stem cells and biomaterial scaffolds for constructing tissues and cell delivery, StemBook, ed. The Stem Cell Research Community, StemBook, doi/10.3824/stembook.1.1.1, http://www.stembook.org, 2008.

Worster, A.A.; Brower-Toland, B.D.; Fortier, L.; Bent, S.J.; Williams, J.; Nixon, A.J. Chondrocytic differentiation of mesenchymal stem cells sequentially exposed to transforming growth factor-beta1 in monolayer and insulin-like growth factor-I in a three-dimensional matrix. *J Orthop Res* **2001**, 19, 738–749.

Xie, Y.; Hardouin, P.; Zhu, Z.; Tang, T.; Dai, K.; Lu, J. Three-dimensional flow perfusion culture system for stem cell proliferation inside the critical-size β-tricalcium phosphate scaffold. *Tissue Eng* **2006**, 12, 3535–3543.

Zahm, A.M.; Bucaro, M.A.; Ayyaswamy, P.S.; Srinivas, V.; Shapiro, I.M.; Adams, C.S.; Mukundakrishnan, K. Numerical modeling of oxygen distribution in cortical and cancellous bone: Oxygen availability governs osteonal and trabecular dimensions. *Am. J. Physiol. Cell Physiol.* **2010**, *229*, C922–C929.

Zeilinger, K.; Holland, G.; Sauer, I.M.; Efimova, E.; Kardassis, D.; Obermayer, N.; Liu, M.; Neuhaus, P.; Gerlach, J.C. Time course of primary liver cell reorganization in three-dimensional high-density bioreactors for extracorporeal liver support: An immunohistochemical and ultrastructural study. *Tissue Eng*. **2004**, *10*, 1113–1124.

Zhao, F.; Ma, T. Perfusion bioreactor system for human mesenchymal stem cell tissue engineering: dynamic cell seeding and construct development. *Biotechnol. Bioeng.* **2005**, 91, 482-493.

Zhao, F.; Grayson, W.; Ma, T.; Irsigler, A. Perfusion affects the tissue developmental patterns of human mesenchymal stem cells in 3D scaffolds. *J. Cell. Physiol*. **2009**, 219, 421-429.

List of publications

Publications related to this thesis

- Donato, D.; De Napoli, I.E.; Catapano, G. Model-based optimization of scaffold geometry and operating conditions of radial flow packed-bed bioreactors for therapeutic applications. *Processes* **2014**, 2, 34-57

- Donato, D.; Falvo D'Urso Labate, G.; Debbaut, C.; Segers, P.; Catapano, G. Optimization of construct perfusion in radial packed-bed bioreactors for tissue engineering with a 2D stationary fluid dynamic model. **2015**. *Under revision*

- Donato, D.; Falvo D'Urso Labate, G.; De Napoli, I.E.; Debbaut, C.; Segers, P.; Catapano, G. Study of the effect of radial flux distribution on pericellular oxygen concentration in radial flow packed-bed bioreactors with a 2D stationary transport model. *In preparation*

Oral presentations

- Donato, D.; Falvo D'Urso Labate, G.; Debbaut, C.; Segers, P.; Catapano, G. Design criterion for radial flux uniformity in radial-flow packed bed bioreactors for bone TE based on a 2D flow model. *European Society of Artificial Organs ESAO* **2015**, Leuven, Belgium.

- Falvo D'Urso Labate, G.; Donato, D.; Segers, P.; Catapano, G. Optimization of inlet flow to obtain uniform velocity field in radial flow packed-bed biboreactors for bone tissue engineering. *International Conference on Computational and Mathematical Biomedical Engineering* **2015**, Paris, France.

- Donato, D.; De Napoli, I.E.; Debbaut, C.; Segers, P.; Catapano, G. Transport modeling of radial flow bioreactors packed with hollow cylindrical porous construct for bone tissue engineering: effect of external resistances to transport on solutes distribution. *Italian Society of Biomaterials SIB* **2014**, Palermo, Italy.

Poster presentations

- Donato, D.; Falvo D'Urso Labate, G.; Debbaut, C.; Segers, P.; Catapano, G. Study of the effect of permeability of annular porous scaffolds seeded with osteogenic cells on radial flux uniformity in radial flow packed-bed bioreactors for bone TE with a stationary 2D flow model. *Italian Society of Biomaterials SIB* **2015**, Ancona, Italy.

- Donato, D.; Falvo D'Urso Labate, G.; Debbaut, C.; Segers, P.; Catapano, G. Theoretical framework to enhance external solute transport to cells in radial flow packed-bed bioreactors for bone tissue engineering based on a stationary 2D transport model. *Tissue Engineering and Regenerative Medicine International Society TERMIS* **2015**,Boston, MA, USA.

- Donato, D.; Falvo D'Urso Labate, G.; Debbaut, C.; Segers, P.; Catapano, G. Model-based optimization of radial flow in radial-flow packed-bed bioreactors for bone tissue engineering. *National day on Biomedical Engineering* **2014**, Bruxelles, Belgium.

- Donato, D.; De Napoli, I.E.; Debbaut, C.; Segers, P.; Catapano, G. Transport model of radial-flow packed-bed bioreactors simulating natural bone vascular and interstitial fluid nutrients delivery. *Int J Artif Organs* **2014**, 37(8). *European Society of Artificial Organs ESAO* **2014**, Rome, Italy.

- Donato, D., De Napoli, I.E.; Catapano, G. Transport modeling in hollow cylindrical porous constructs for bone Tissue engineering: effect of construct properties and direction of radial perfusion flow on nutrient distribution. *Italian Society of Biomaterials SIB* **2013**, Baveno (VB), Italy.

Acknowledgements

I want to thank Prof. Gerardo Catapano of the Department of Environmental, Territory and Chemical Engineering of the University of Calabria for having encouraged my professional growth during these three years and for everything he taught me, not only from a professional, but especially from a human point of view. I am also particularly grateful to Prof. Patrick Segers of the IbiTech Institute Biomedical Technology of the Ghent University, for having welcomed me in his research group (Biommeda) during my work period at Ghent University, for the great opportunities he has given to me and for his kind availability. Furthermore, I want to express my gratitude to Eng. Giuseppe Falvo and Dr. Ilaria De Napoli, who have been older siblings during my PhD, more than simple colleagues. I want to thank all the components of the Biommeda research group for their warm welcome, particularly to my tutor Charlotte for her advices and to Alessandra and Francesco, who helped me in several occasions, especially when I arrived in Ghent for the first time. I also want to thank Ms. Saskia Classaens of the Ghent University and Dr. Eliana Zicarelli and Mr. Gabriele Pesce of the University of Calabria for their effectiveness and availability related to the administrative procedures. Furthemore, I want to thank the coordinator of my Doctoral Course, Prof. Bruno De Cindio of the University of Calabria, for his kindness and for his precious suggestions about administration problems.

In addition, I want to express my gratitude to my family for having encouraged me in the adventure of this PhD. In particular, I want to thank my uncle Franco and my aunt Ivana for their eternal kindness and my relatives from Brussels, Maria and Alain, for their generosity and availability during my stay in Belgium. Finally, a particular mention goes to my Italian “old” friends and my “club”, that, together with my family, every day give me the strength of believing in myself and in my possibility of making this world a little better than I found it. Among them, I want to express my particular gratitude to Stefano, for having made the guarantee of my laptop useless in several cases, and Vincenzo and Alessandra, for all the times they “fought” with the administration

staff of the University of Calabria in my place while I was abroad. Finally, I want to thank Ms. Franca M., for having fed me for two years without asking me nothing in exchange.